



**Università
degli Studi
di Ferrara**



**INTERNATIONAL DOCTORAL COURSE IN
"EARTH AND MARINE SCIENCES (EMAS)"**

CYCLE XXXVI

COORDINATOR Prof. Ciavola Paolo

**THERMAL CONDUCTIVITY OF UNCONSOLIDATED
MATERIALS FOR GEOTHERMAL ENERGY: THE IMPORTANCE
OF PETRO-PHYSICAL PARAMETERS AND THEIR
RELATIONSHIPS**

Scientific/Disciplinary Sector (SDS) GEO/03

Candidate

Dott. Marchetti Andrea

Supervisor

Prof. Caputo Riccardo

Co-Supervisor

Prof. Rapti Dimitra

Years 2020/2023

Acknowledgements

I would not have been able to complete such a long, fascinating, sometimes scientifically and emotionally challenging experience as my Ph.D. without the continued support of many people around me. I am grateful for that. I must express my deep gratitude to the University of Ferrara, the University of Cadiz, and the MIUR for offering me the opportunity to participate in this demanding experience, as well as for providing me with financial support.

My supervisor is the first person I thank for having faith in me. Ricardo Caputo, professor. His love and interest in Earth Sciences, along with his strong work ethic, truly guided me in tackling the new problems that arose during this research. I hope for more scientific collaborations in the future. Thanks to Dr. Rapti for being a co-supervisor. I would like to express my gratitude to both Dr. Andreotti and Dr. Neri for their invaluable assistance in setting up the laboratory, which was an essential tool for generating the data for my research. Thanks to Dr. Tessari, Dr. Ardit, and Dr. Precisvalle for technical support in granulometric and mineralogical analyses, as well as for in-depth scientific and personal exchanges. Dr. Kantzas and Dr. Fayazi, I am deeply grateful for your help with my scientific research, which has been a place and time in my life that will forever remain in my heart.

Particularly deep and heartfelt thanks go to Claudia for always being by my side, both at work and at home, and for supporting me through both the good and bad times of this experience, which we both shared. She has been a great source of anchorage, an example and a push to continue my goals, I thank her ability to support me with strength and determination, without being over the top.

Also, special thanks go to my family, my mother, father, Davide, Giulia and Joele. These people have been staples for me, sometimes far away to help me grow on my own and other times close to provide the help I needed, with sincerity and love in this doctoral program of mine.

In addition, I would like to express my gratitude to old friends, new friends, PhD students and postdocs. You have always supported and listened to me every day of this journey. You have been much more important than you can imagine; I do not want to mention you individually, but I am sure you can recognize yourselves in these figures.

Finally, I want to express my gratitude to myself for always believing in myself, at every moment.

Ringraziamenti

Non sarei stato in grado di completare un'esperienza così lunga, affascinante, a volte scientificamente ed emotivamente impegnativa come il mio dottorato di ricerca senza il continuo sostegno di molte persone intorno a me. Sono grato per questo. Devo esprimere la mia profonda gratitudine all'Università di Ferrara, all'Università di Cadice e al MIUR per avermi offerto l'opportunità di partecipare a questa esperienza formativa, nonché per avermi fornito il sostegno finanziario.

Il mio supervisore è la prima persona che ringrazio per avermi dato fiducia, professor Ricardo Caputo. Il suo profondo amore e interesse per le Scienze della Terra, insieme all'etica del lavoro, mi hanno davvero indicato come affrontare i problemi che emergevano durante questa ricerca. Spero in maggiori confronti scientifici in futuro. Grazie alla dott.ssa Rapti per essere stata co-supervisore. Mi piacerebbe esprimere la mia gratitudine sia al dottor Andreotti che alla dott.ssa Neri per la loro preziosa assistenza nella creazione del laboratorio, che è stato uno strumento essenziale per la creazione dei dati della mia ricerca. Grazie a dott. Tessari, prof. Ardit e dott. Precisvalle per il supporto tecnico nelle analisi granulometriche e mineralogiche, così come per i continui confronti scientifici e umani. Il dottor Kantzas e il dottor Fayazi li ringrazio per avermi aiutato nella mia ricerca scientifica, in un luogo e in un momento della mia vita che rimarrà per sempre nel cuore.

Un ringraziamento particolarmente profondo e sentito va a Claudia per essere sempre stata al mio fianco, sia al lavoro che a casa, e per avermi supportato sia nei momenti positivi che in quelli negativi di questa esperienza, che entrambi abbiamo condiviso. È stata una grande fonte di ancoraggio, un esempio e una spinta per proseguire i miei obiettivi, ringrazio la sua capacità di sostenermi con forza e determinazione, senza essere invadente.

Inoltre, un ringraziamento speciale va alla mia famiglia, mia madre, mio padre, Davide, Giulia e Joele. Queste persone sono state per me punti fermi, a volte lontani per aiutarmi a crescere da solo e altre volte vicini per fornire l'aiuto di cui avevo bisogno, con sincerità e amore in questo mio dottorato.

Inoltre, desidero esprimere la mia gratitudine a vecchi amici, nuovi amici, dottorandi e post-doc. Mi avete sempre sostenuto e ascoltato in ogni giorno di questo percorso. Siete stati molto più importanti di quanto possiate immaginarvi, non voglio citarvi singolarmente, ma sono certo sapete riconoscervi in queste figure.

Infine, voglio esprimere gratitudine a me stesso per averci sempre creduto, in ogni momento.

Extended abstract

Renewable energies are becoming increasingly paramount in daily life, with geothermal energy emerging as one such form that harnesses natural heat emanating from the Earth's interior. The utilization of this energy source is regarded as secure and sustainable due to its lack of direct greenhouse gas emissions or other atmospheric pollutants. The subsurface temperature remains relatively constant throughout the year, rendering it a dependable and continuous energy source. This technology can generate electricity and provide heating and cooling for buildings. The latter phenomenon is responsible for the majority of CO₂ emissions in Europe (European Commission, 2016). In this context, geothermal energy appears to be the most promising source of renewable energy, however, it remains underutilized on a global scale.

It is essential to examine the subsurface from a hydro-thermo-petrophysical perspective, particularly within the first two hundred meters, to comprehend how to harness the heat beneath the surface effectively. This study methodology can prove valuable in numerous domains, such as geology for geothermal applications and underground storage of carbon dioxide (CCUS) or heat (UTES). It can also be beneficial in other developmental areas such as engineering, ceramics, and agriculture.

The objective of this study is to emphasize the significance of certain parameters and demonstrate their interrelationships. Specifically, thermal conductivity will be considered, thought to be directly correlated with porosity, bulk density, grain size, and water content. Understanding how these factors interact and influence thermal conductivity is fundamental for designing low-enthalpy geothermal systems. To achieve this goal, we have developed a laboratory employing the Guarded Hot Plate (GHP) method to precisely measure the thermal conductivity of unconsolidated materials. This method yields reliable and replicable data, providing a solid foundation for the analysis of geological materials.

Although samples ranging from gravel to clay have been employed, the material has been categorized into specific intervals to determine and quantify the influence of grain size on thermal conductivity (Wentworth, 1922). In addition to petro-physical analysis, the samples have been tested and studied to determine the present mineralogical phases. Subsequently, the samples underwent thermal tests at various degrees of saturation. The materials under study were sourced from various regions in the Po Valley (Italy), Greece, and Canada.

The results have been processed using statistical techniques and compared with literature data and empirical equations. Identifying trends among these parameters has been a primary research objective

to facilitate the exploration of geothermal reservoirs and the extraction of heat from them. Furthermore, this work aims to enhance the use of software for subsurface modeling using specific values for each soil type, as well as to improve the scientific literature.

Riassunto esteso

Le energie rinnovabili stanno diventando sempre più importanti per la vita quotidiana, e una di queste è la geotermia, che produce energia sfruttando il calore naturale proveniente dall'interno della Terra. L'utilizzo di questa fonte di energia è considerato sicuro e sostenibile in quanto non genera direttamente emissioni di gas serra o altri inquinanti atmosferici. La temperatura del sottosuolo rimane piuttosto costante durante tutto l'anno, rendendola una fonte di energia affidabile e continua. Questa tecnologia può generare energia elettrica e calore per riscaldare e raffreddare gli edifici. Quest'ultimo fenomeno è responsabile della maggior parte delle emissioni di CO₂ in Europa (Commissione europea, 2016). In questo contesto, l'energia geotermica sembra essere la fonte più promettente di energia rinnovabile. Nonostante questi vantaggi, è comunque ancora poco sfruttata a livello globale.

È fondamentale esaminare il sottosuolo a livello idro-termo-petrofisico, in particolare nei primi duecento metri, per comprendere come utilizzare il calore sotto la superficie. Questa metodologia di studio può essere utile in molte aree, come la geologia per la geotermia e lo stoccaggio di anidride carbonica (CCUS) o di calore nel sottosuolo (UTES). Può anche essere utile in altre aree di sviluppo, come l'ingegneria, la ceramica e l'agricoltura.

L'obiettivo di questo studio è quello di evidenziare l'importanza di alcuni parametri e di mostrare come si relazionano tra loro. In particolare, si prenderà in considerazione la conducibilità termica, che si pensa sia direttamente correlata alla porosità, alla densità apparente, alla dimensione dei grani e al contenuto d'acqua. È fondamentale per la progettazione di sistemi geotermici a bassa entalpia capire come questi fattori interagiscono tra loro e come influenzano la conducibilità termica. Per raggiungere questo obiettivo, abbiamo sviluppato un laboratorio che utilizza il metodo della piastra calda protetta (Guarded Hot Plate, GHP) per misurare la conducibilità termica dei materiali non consolidati in modo estremamente preciso. È possibile ottenere dati affidabili e replicabili utilizzando questo metodo, che fornisce una base solida per l'analisi dei materiali geologici.

Sebbene siano stati utilizzati campioni che variano da ghiaia ad argilla, il materiale è stato suddiviso in intervalli specifici per determinare e quantificare l'incidenza della granulometria sulla conducibilità termica (Wentworth, 1922). Oltre all'analisi petro-fisiche, i campioni sono stati testati e studiati per determinare le fasi mineralogiche presenti. In seguito, i campioni sono stati sottoposti a prove termiche a vari gradi di saturazione. I materiali studiati provengono da una varietà di aree della Pianura Padana (in Italia), della Grecia e del Canada.

I risultati sono stati elaborati utilizzando tecniche statistiche e confrontati con dati di letteratura ed equazioni empiriche. Identificare le tendenze tra questi parametri è stato uno dei principali obiettivi della ricerca al fine di facilitare la ricerca di serbatoi geotermici e l'estrazione del calore da essi. Inoltre, questo lavoro mira a migliorare l'utilizzo di software per modellizzare il sottosuolo utilizzando valori specifici per ciascuna tipologia di terreno, oltre che a migliorare la letteratura scientifica.

Contents

Acknowledgements.....	3
Ringraziamenti.....	4
Extended abstract.....	6
Riassunto esteso.....	8
Contents.....	11
1. Introduction.....	13
2. The basics of thermophysics principles.....	16
2.1. Thermophysics principles.....	16
2.2. Conduction.....	17
2.3. Convection.....	19
2.4. Thermal conductivity.....	20
2.5. Equivalent thermal conductivity of porous media.....	21
2.6. Factors affecting thermal conductivity.....	23
3. Measuring the thermal conductivity.....	25
3.1. Thermal Response Test (TRT).....	26
3.2. Infinite line source method (ILS).....	27
3.3. Guarded hot plate method (GHP).....	30
3.4. Other methods (e.g. TPS).....	34
4. Laboratory set-up.....	36

4.1.	State of the art	36
4.2.	GeoTh laboratory	41
4.3.	Experimental procedure	61
4.4.	Samples selection and preparation	65
5.	Experimental results and discussions	73
5.1.	Porosity and bulk density	73
5.2.	Lambda vs grain size.....	74
5.2.1.	Results and discussion	77
5.3.	Lambda vs Mineralogy	80
5.3.1.	XRD analysis	81
5.3.2.	Results and discussions	84
5.3.3.	Glass beads.....	85
5.4.	Lambda vs Water saturation	88
5.4.1.	Prediction equations review	90
5.4.2.	Results and discussion	99
6.	Concluding remarks.....	100
	References.....	104
	Appendix A.....	110
	Appendix B	128

1. Introduction

The term “geothermal” is derived from the greek “geos” = earth and “thermos” = heat, from which the literal meaning is “Heat of the Earth”. Therefore geothermal energy means the one contained as heat in the ground, and whose only manifestation is temperature.

There are various types of geothermal systems, that is defined as any underground resource which it can exchange heat. Initially they were considered only the hydrothermal ones, with a thermal tank represented by subsoil in which the heat is propagated by convection because of the convective motions of the fluids contained. It can be water dominant (with lower energy content, in that case there is also conduction) or vapor-dominated (with very high energy content). The systems with a temperature higher than 150°C are called “high-enthalpy” and are exploited for the production of electricity: the first exploitation of the Earth's heat to generate electricity took place in Larderello in Tuscany by Prince Piero Ginori Conti in the years 1904-05, and the first commercial geothermal power plant was installed there in 1911. Medium-enthalpy systems have a temperature lower than 150°C. Instead low-enthalpy have a temperature lower than 90°C and are used mainly for the heating and cooling of buildings (Legislative Decree 22/2010). The soil, because of its moderate thermal inertia, even at low depth is less influenced by the daily and seasonal temperature fluctuations. Below 15 m of depth its temperature can be considered constant throughout the year, due to the balance between the heat flow that comes from the Earth's mantle and core, the contribution of solar energy to the earth's surface, and sometimes the contribution of the available energy from groundwater. In the framework of low-enthalpy field, the thermal properties of the ground can be exploited could be used to cool building in summer and warm them in winter. This heat energy may be tapped either by: i) pumping groundwater from a borehole and extracting heat from it via a heat pump. This method is best suited to permeable rocks and wells with a high yield (open loop); ii) circulating a fluid through a closed hose system down the borehole. The fluid is warmed to the temperature of the rocks and, on its return to the surface, may be sent through a heat pump (closed loop). In most Italian regions, regardless of the type of rock, the geological structure and stratigraphy, at about 15 m depth the available temperature is between 12°C and 16°C, while below the temperature increases by an average of 3°C per 100 m, according to the geothermal gradient. In addition, subsoil can be used as a thermal storage to store heat during the summer for winter house heating. Different types of rocks and soils have different behaviours in accumulating heat; in the thesis the thermal properties of some types soils are studied, however, we focused on a few fundamental parameters for the study of thermophysics aspect of the soils, thermal conductivity being one of these parameters.

Thermal conductivity finds application in a variety of sectors, the most common and widespread of which is low-enthalpy geothermal energy. In recent years, there has been an increase in the application of this methodology with the installation of thermal pumps. Thermal conductivity plays a primary role here, being a fundamental parameter in both the preliminary and application phases. Thermal conductivity is one of the most important properties needed in the design or control of an agricultural material storage equipment and treatment system. This is also fundamental for engineering studies of buildings, sometimes analyses are done before the construction of buildings, to minimise initial construction costs, the pipes can be cast into the foundations, eliminating the need to make further excavations. Ground source heat pump (GSHP) systems provide a viable alternative to conventional heating and cooling systems in the move towards sustainable building solutions. Heat is transferred between the ground and the building by means of a refrigerant which is pumped through a series of pipes buried in the ground. These systems are known as energy or thermal foundations. This work can also be of relevance for large-scale subsurface research such as Underground Thermal Energy Storage (UTES) system or Carbon Capture and Storage (CCUS)

Soil thermal conductivity is an important factor in other ground heat exchanger systems. It can be determined by a field thermal response test (TRT), which is both costly and time consuming, but tests a large volume of soil. Alternatively, cheaper and quicker laboratory test methods may be applied to smaller soil samples.

The aims of the work is both the construction of a new laboratory and the construction of a database of data acquired on unconsolidated natural samples, then an experimental phase and subsequently, once the guidelines for measuring the various hydro-thermo-petro-physical parameters have been outlined, the identification of possible trends between correlations of these, so the processing phase will be equally important to the previous ones.

The work of this thesis began with a literature study, to understand the state of the art in these matters, to understand the instrumentation used to reproduce the data generated, and to take inspiration and understand the best setup for the new laboratory under construction. Having done this, we created from new a low-cost laboratory but with highly efficient and accurate sensors, GeoTh is the name of the new laboratory (Rapti et al. 2022). At this stage, we outlined the best setting to make the measurements. We then chose the sampling area on which to measure the previously chosen parameters; using not only sands but also silts, clays and gravels, covering all the grain sizes present in the Po Valley. The aim of the tests was to verify qualitatively, and statistically, any correlations between thermal conductivity and intrinsic properties of the selected natural materials. This method

was also performed in order to discriminate the properties that are most correlated with thermal conductivity, at least in this project. This approach is highly innovative, as there is no work in the literature that relates the different relationships in such high detail.

The first chapters then discuss the theoretical principles of applied thermophysics on which the PhD project is based. Initially, the basic theoretical concepts are set out, which are fundamental to the understanding of the choice of (natural unconsolidated) materials, and the motivation for the creation of this type of laboratory using a specific method, which is already scientifically accepted in the literature. The principles of thermal conductivity were then expressed, both from a mathematical and applicative point of view, always bearing in mind that the field of study is geology and the materials studied are loose sediments. We also investigated parameters closely related to conductivity, the relationships between which are well known from scientific studies, such as porosity, bulk density, mineralogy and moisture. The description of the samples tested and the preparation of the materials for analysis are set out in the following chapters in which the provenance of the sediments examined and the sampling method are also specified. This chapter also provides a general explanation of the geology of the Po Valley, the area of provenance of the samples.

The data generated is the most important part of this thesis, we decided to have obtained from intact materials, different grain sizes, in order to be able to compare the thermal conductivity data with the grain size, primarily. In the tests, however, we had the possibility of calculating and obtaining other parameters mentioned above, which allowed us to better characterise the material used. The comparison of all the data was essential to understand how the different parameters affect the thermal conductivity value.

All the results obtained can be considered a confirmation of the scientific literature, but some of them also unpublished results that deserve further investigation. Finally, the last chapter contains conclusions in which, referring to the results, some final unpublished considerations are also expressed.

2. The basics of thermophysics principles

Thermophysics is a branch of physics that deals with the study of thermal and heat transfer phenomena. Some key principles of thermophysics include thermal equilibrium, heat transfer, temperature, specific heat, thermal expansion, heat capacity, heat conduction, and heat convection. These principles are used to understand how heat flows and how it affects the properties of materials. Thermophysics principles are applicable in many areas of science and engineering, including materials science, energy systems, and climate science. For example, in materials science, thermophysics principles can be used to understand the thermal properties of materials and how they behave under different temperatures. In energy systems, thermophysics principles are used to design and optimize energy conversion processes, such as heat engines and power plants.

2.1. Thermophysics principles

The flow of heat is a fundamental phenomenon in many fields, such as thermal and mechanical engineering, physics, chemistry, energy, and others. A material's ability to transfer heat depends on its structure and thermal properties, such as thermal conductivity and thermal diffusivity.

In solid materials, heat transfer occurs through conduction, where the material particles conduct heat energy through the crystal structure. In fluids, heat transfer occurs through convection, where fluid motion carries heat from a hot region to a cold region. This process is also influenced by the thermal conductivity of the fluid and flow velocity. In the case of porous materials, heat transfer occurs through a combination of conduction, convection, and radiation. The amount of heat transferred depends on the porous material structure and the thermal properties of the solid and fluid components. It is important to note that heat transfer is not always unidirectional, as thermal conditions can change over time, and heat can be transferred from a hot region to a cold region and vice versa. It is also important to consider a material's ability to transfer heat within a thermodynamic system.

In summary, heat transfer is a complex and multi-factorial phenomenon that must be carefully studied and understood for optimal design in many applications.

Therefore, the flow of heat is defined as the exchange of energy with the surrounding environment that occurs during a transition from one equilibrium state to another. The transfer of heat can vary based on the phase of the material under examination: in gases and liquids, it occurs through

molecular collisions, while in solids, it occurs through vibrations of the molecules within the crystal structure. The amount of heat exchanged depends on several factors, including the geometry of the body, the temperature difference, and the thermal conductivity, which is the material's ability to transfer heat. In solid materials, heat transfer is primarily governed by conduction, while in fluids, it primarily occurs through convection, which also involves mass transport in addition to conduction. The transfer of heat in porous media is a combination of conduction, convection, and radiation (Figure 2-1). The focus of our tests is primarily on conduction and convection (Cocchi, 1998).

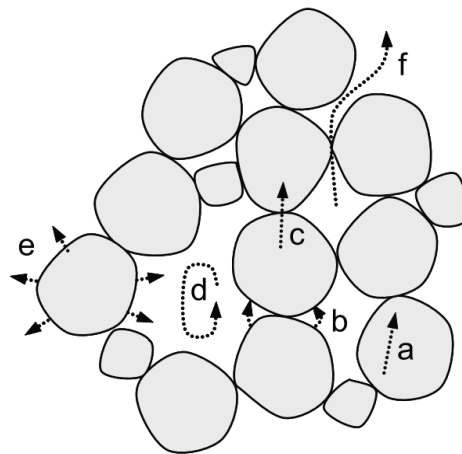


Figure 2-1: Primary particle-level heat transport processes in granular materials. (a) Conduction along the mineral, (b) particle-fluid-particle conduction across the fluid near contacts, (c) particle-to-particle conduction across contacts, (d) fluid convection within large pores, (e) particlefluid conduction, and (f) conduction along the pore fluid within the pore space (Cortes et al., 2009).

2.2. Conduction

Conduction is the transfer of heat or electricity through a material without any movement of the material itself. It occurs when there is a temperature difference between two points in a material, and heat is transferred from the hotter area to the cooler area. This transfer of heat occurs through the collision of atoms and molecules in the material, with the energy being transferred from particle to particle until it reaches the other end.

The process of conduction can be modelled using the equation of heat flow, which describes the amount of heat that is transferred through a material per unit of time. This equation depends on several factors, including the temperature difference, the thermal conductivity of the material, and the surface area through which the heat is flowing. The thermal conductivity of a material is a measure of its ability to conduct heat. It is determined by the nature of the material, including its structure and chemical composition. Some materials, such as metals, are good conductors of heat because they have a large number of free electrons that can carry energy from one end of the material to the other. On the other hand, insulators have very few free electrons, and therefore have low thermal conductivity.

Conduction is the primary method of heat transfer in solids, and it is also a significant factor in liquids and gases. In solids, conduction occurs primarily through the movement of lattice vibrations and the transfer of energy from one atom to another. In liquids and gases, conduction occurs through the movement of individual particles. It is important in many industrial applications, including the design and operation of heating and cooling systems, the transfer of heat in cooking and food processing, and the design of insulation materials. It is also important in the natural world, for example in the transfer of heat from the Earth's interior to its surface.

It should be noted that conduction consists of an exchange of heat between bodies that are in contact with each other.

In particular, the following law describes the passage of heat:

$$\frac{Q}{\Delta t} = \lambda \cdot A \cdot \frac{\Delta T}{d}$$

Equation 2-1

where Q indicates the heat that is transferred, and Δt the time interval taken for this transfer. The ratio $Q/\Delta t$ gives information on how quickly heat is transferred through the layer of matter. λ , called the thermal conductivity coefficient, depends on the particular substance the layer of matter is made of, the coefficient can vary with temperature and pressure. A denotes the area of the surface involved,

ΔT the temperature difference before and after the passage of heat, and d the thickness of the body. In particular, the degree of conductivity of a body depends on the coefficient: the bodies that transmit heat most easily, i.e. good conductors, are those that have high values of λ ; on the contrary, bodies that have low values of λ tend not to diffuse heat inside them particularly well. For example, metals in general have high λ -values, and are good conductors of heat; wood and plastics, on the other hand, usually have low λ -values, and heat is prepared more slowly through them.

Furthermore, it can be seen experimentally that thermal conductivity is influenced by many factors. For example, substances in the solid state have a higher thermal conductivity than their liquid-phase counterparts, and similarly, those in the liquid phase conduct better than their gas-phase counterparts. The various parameters affecting thermal conductivity are discussed in the following chapters (Bergman et al., 2011).

2.3. Convection

Convection is a method of heat transfer that occurs when a fluid in motion carries heat from one region to another. This method of heat transfer is distinct from conduction, which occurs when heat is transferred through a solid material without the movement of the material itself. In a convection system, the temperature of a fluid is altered due to contact with a hot or cold surface. The hotter fluid expands and becomes less dense compared to the colder fluid, causing it to rise. Conversely, the colder fluid will contract and become denser, causing it to fall. This process creates a convection current cycle that continuously moves heat from one region to another.

There are two types of convection: natural and forced. Natural convection occurs when the fluid's motion is caused by a difference in density, without the intervention of an external force. Forced convection occurs when an external force, such as a fan or pump, causes the fluid's motion. Convection is highly important in many industrial applications, such as heating homes and commercial buildings, cooling machinery, and generating electrical power in thermal power plants.

2.4. Thermal conductivity

Knowledge of the thermal properties of the soil is fundamental to the design of a geo-exchange system. To thermally characterise the soil, it is first necessary to know the soil's ability to transfer heat. The 'conductivity' or 'thermal conductivity' indicates precisely this aptitude and is defined as the amount of heat transferred in a direction perpendicular to a surface of unit area, due to a temperature gradient, in the unit of time and under stable conditions. Thermal conductivity (λ) describes how much heat flows across a unit cross-section of a material along a unit distance per unit temperature decrease per unit time; in other words, the ability of a material to transmit heat. Its dimension is $W/m K$ (Watt / meter Kelvin).

The first to study heat transfer by conduction was Fourier, who through experiments on a cylindrical element with different temperatures at the end, he was able to formulate the law describing the phenomenon (Cocchi, 1998)

Considering a homogeneous and isotropic medium to which a heat source is applied, the thermal conductivity process is given by Fourier's law:

$$q = \lambda \cdot \frac{A}{L} \cdot (T_1 - T_2)$$

Equation 2-2

$$\frac{\Delta Q}{\Delta t} = \lambda \cdot \frac{A}{L} \cdot (T_1 - T_2)$$

Equation 2-3

$$\frac{\Delta Q}{\Delta t} = Q_{rate} = \text{heat flow over time} \left[\frac{J}{s} = \text{Watt} \right]$$

$$\lambda = \text{thermal conductivity} [W/m K]$$

A = surface [m^2]

L = length of the medium section [m^2]

T_n = temperature [K] ($T_1 > T_2$)

Thermal conductivity is then given by the following equation:

$$\lambda = \frac{Q_{rate} \cdot L}{A \cdot (T_1 - T_2)}$$

Equation 2-4

2.5. Equivalent thermal conductivity of porous media

The heat transfer through conduction in porous materials primarily depends on the structure of the solid matrix and the thermal conductivity of each present phase. One of the fundamental and also the most complicated aspects of thermal analysis through porous materials is the creation of the structure model. This is because the representative elementary volume is generally three-dimensional and porous materials have very complex structures. The macroscopic analysis of the problem of conduction through heterogeneous materials is based on the definition of equivalent thermal conductivity. The two fundamental properties are density ρ and thermal conductivity λ .

A generic porous material (Figure 2-1) consists of a solid matrix with pores filled with a generic fluid (air and/or water); the pores can have various geometric shapes. Before any determination of thermal conductivity, both experimentally and numerically, a correct definition of the nomenclature must be reached. The medium is assumed to be homogeneous and isotropic with the phases in local thermodynamic equilibrium. Therefore, given the coexistence of different species and different phases within the same sample, it is not correct to simply talk about a measurement of thermal conductivity, but rather of equivalent or effective thermal conductivity (Smith et al., 2013).

Heat transfer, furthermore, by conduction through porous materials depends primarily on the structure of the solid matrix and the thermal conductivity of each present phase.

Considering the soil as a multiphase system, to determine the main method of thermal propagation, it is possible to determine it through the Peclet number (Pe), which is expressed by the relationship (Domenico and Schwartz, 1990):

$$Pe = \frac{\rho_1 \cdot c_1 \cdot qL}{\lambda_{eff}}$$

Equation 2-5

Where $\rho_1 c_1$ is the volumetric heat capacity of water (J/m^3K), L is the length or geometry of the system (m), q is the flow of water in the pores of the sample (m/s) and λ_{eff} is the average conductivity of the soil (W/mK). If the Peclet number is greater than 1, convection prevails, while if it is smaller, conduction prevails (Domenico e Schwartz, 1990).

Because the water movement is zero because the system is not supplied, the value of Pe is unquestionably zero; nevertheless, convective motion can occur during heating if the pores are big. Conduction dominates in porous bodies in clays and silts, while convection dominates in sands and gravels, except in this case due to precautions taken. During our tests, we placed aluminum disks to break convective motion, as discussed in later chapters. Conduction is often considered the principal phenomenon in laboratory measurements due to the constrained dimensions of the materials on which the tests are performed (Bergman et al., 2011).

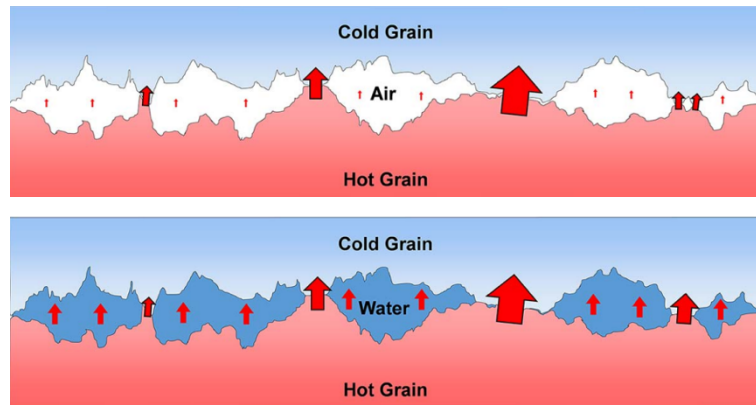


Figure 2-2: Contact-scale heat conduction pathways for (a) dry; and (b) water-saturated conditions. Arrows indicate the magnitude of heat transfer through touching asperities and interstitial fluids (Roshankhah et al., 2021)

2.6. Factors affecting thermal conductivity

In this thesis, we exclusively focus on unconsolidated materials, referred to as soil. Soils are composed of particles separated by pores that can contain air or water. The particles can consist of one or more minerals, with no presence of organic material as it is selected soil. Water can exist in a liquid or gaseous state. All these components constitute the soil structure, and each of them needs to be considered in the phenomenon of thermal conductivity. The four main factors influencing the thermal conductivity of sedimentary rocks and soils are porosity, mineralogy, water saturation, and grain size (Brigaud and Vasseur, 1989; Farouki, 1981). Among these factors, texture is the most challenging to account for as it is the most complex. Grain size and grain size distribution are important factors controlling the texture of sedimentary soils. For this reason, scientific literature does not extensively cover this scientific window, but it is one of the factors on which this work has focused, as the shape, size, and distribution of grains and pores affect thermal conductivity. For example, coarse sand with spherical and well-connected grains will have higher thermal conductivity compared to fine sand with irregular grains and poor connectivity.

Porosity is the fraction of volume occupied by empty spaces between material grains. Mineralogy is the study of minerals that compose the material and their physical and chemical properties. These two factors influence the amount and type of contact between grains, the presence and movement of fluids in pores, and the material's ability to transfer heat through conduction, convection, or radiation (Brigaud and Vasseur, 1989). In general, the higher the porosity of an unconsolidated material, the

lower its thermal conductivity, as the pores are filled with air or water, which have lower thermal conductivity than solids.

Mineralogy also plays an important role, although not of primary order, in the thermal conductivity of unconsolidated materials, as different minerals have different thermal properties. For example, silicate minerals have higher thermal conductivity than carbonate minerals. Additionally, the chemical composition and degree of crystallinity of minerals can influence their thermal conductivity. For instance, quartz has higher thermal conductivity than calcite.

The relationship between thermal conductivity and water content is necessary for the quantitative study of heat and water transfer processes in saturated and unsaturated soils. In these analyses, we initially focused on the thermal conductivity versus grain size relationship and later on the water content. There are few works in the literature that consider grain size (Midttømme and Roaldset, 1998), and none of them address it in the same way we have, by dividing it into small grain size ranges.

3. Measuring the thermal conductivity

The most common methods of measuring thermal conductivity can be categorized into different types depending on their nature. They can be absolute measurements or comparative measurements, depending on whether the body being considered is measured directly or compared to a standard object. They can be direct or indirect, depending on whether the parameters are measured or mathematically derived. There are various laboratory techniques available for measuring the thermal conductivity of soil (Farouki, 1981). These techniques can be categorized into two main groups: steady state and transient methods. In steady state methods, a unidirectional heat flow is applied to a soil specimen in the laboratory, and the power input and temperature difference across the specimen are measured once a steady state is reached. Using Fourier's Law, the thermal conductivity is then directly calculated based on these measurements. On the other hand, transient methods involve applying heat to the soil specimen and monitoring the resulting temperature changes over a period of time. The collected transient data is then used to determine the thermal conductivity, often by employing an analytical solution to the heat diffusion equation. Both steady state and transient methods offer valuable insights into the thermal conductivity of soil, each with its own advantages and considerations.

The thermal cell and needle probe are currently industry recommended laboratory methods (ASTM D5334-08 2014). No standard laboratory tests to measure thermal conductivity of soils have been identified, though a number of tests exist for the measurement of thermal conductivity of building materials. Tests include the comparative method (ASTM 1997c), the guarded hot plate method (ASTM 1997b), the hot wire method (ASTM 1997a), the thermal needle test (ASTM 1997d) and the unguarded hot plate method described in the (BS 874-2.2 1988). The GHP method is generally regarded as accurate. However, it is usually quite time consuming. The hot wire and the probe methods require much less time but without high precision data (Hamuda et al., 2011). By employing these laboratory techniques, researchers and scientists can obtain crucial information about the heat transfer properties of soil, which is essential for various applications in fields such as geotechnical engineering, environmental sciences, and agriculture.

3.1. Thermal Response Test (TRT)

The TRT, also known as the Thermal Response Test, is an advanced methodology used to assess the performance of a Ground Source Heat Pump (GSHP) system and determine the thermal conductivity of the surrounding soil. This test provides crucial information for the design, optimization, and evaluation of the energy efficiency of a GSHP system. During a TRT, a ground heat exchanger system is installed, consisting of a series of buried pipes in the soil. These pipes are connected to a heat pump that transfers heat between the ground and the building, depending on the thermal needs. The test is conducted by applying a constant thermal power to the ground heat exchanger system and monitoring temperature variations over time. One of the key features of the TRT is its ability to assess the long-term thermal behavior of the soil. During the test, the inlet and outlet temperatures of the heat transfer fluid circulating in the ground heat exchanger pipes are measured. These data are then analyzed to determine the thermal response of the soil, including its thermal conductivity.

The analysis of TRT data relies on mathematical models and computer simulations that consider various factors, including the geometry of the heat exchanger system, thermal properties of the soil, heat flow conditions, and the presence of any external influences such as interaction with groundwater. Through this analysis, precise estimates of the soil's thermal conductivity and other relevant thermal properties can be obtained. The TRT offers several advantages over other techniques for measuring soil thermal conductivity. Since it involves a real-scale ground heat exchanger system, the TRT takes into account complex factors that can affect heat transfer in the soil, such as soil stratification, groundwater presence, and seasonal variations in environmental conditions. This allows for more accurate assessments of soil thermal conductivity and GSHP system performance in the specific context of a given site.

Furthermore, the TRT provides information on the long-term thermal characteristics of the soil, enabling more precise system design and optimization of GSHP systems. This information can be used to correctly size the ground heat exchanger, determine the required heating and cooling capacity, and evaluate the overall energy efficiency of the system. Its advanced analysis techniques and consideration of complex factors make it a valuable tool for designing and optimizing energy-efficient GSHP systems (Sass and Lehr, 2011; Signorelli et al., 2007).

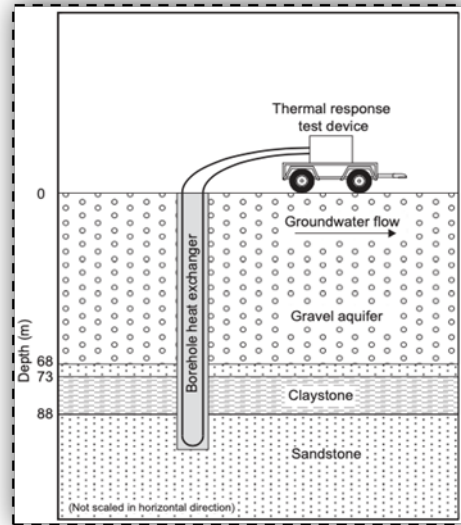


Figure 3-1: Simplified image of the TRT instrument and schematic cross section of the stratified geological units, not in scale. (Wagner et al., 2014)

3.2. Infinite line source method (ILS)

The temperature increase of a heat source within a material depends on the thermal conductivity of the material itself. In a solid (and unconsolidated) material, this method can be applied by incorporating a linear heat source into the material for which thermal conductivity is to be measured. There are two types of methods that utilize the infinite line source principle: dynamic or non-steady-state methods (Carslaw and Jaeger, 1959). The temperature distribution throughout the sample varies with time, thus requiring the complete differential equation of heat flow. If the experimental time is short, heat losses have a minor influence on the measurement compared to steady-state methods. Dynamic methods can be divided into two categories: transient or periodic, depending on whether thermal energy is supplied to the sample as a single step function (constant source) or with a fixed period modulation. Consequently, temperature variations in the sample are transient or periodic. The latter is challenging to implement. The transient method, on the other hand, starts from a condition of thermal equilibrium, where the heat source is excited and heats the sample with a constant power. The thermal response of the sample is a function of its thermal properties, and thermal conductivity is calculated based on the observed temperature increase in the sample. After a short transient period,

the temperature versus natural logarithm of time graph becomes linear, as shown in Figure 1 (linear region between times t_1 and t_2 and temperatures T_1 and T_2). The slope of the linear region is used to calculate the thermal conductivity of the material under examination. (Low et al., 2015; Low et al., 2013; Daw et al., 2010).

The needle probe method is based on the theory of an infinite line heat source embedded within a semi-infinite solid. In this configuration, the thermal response is detected by a sensor (such as a thermocouple) located a finite distance from the heat source. The probe is designed such that the heat source and thermocouple are both located within the probe. A schematic diagram showing components of a thermal conductivity needle probe is shown in (Figure 3-2).

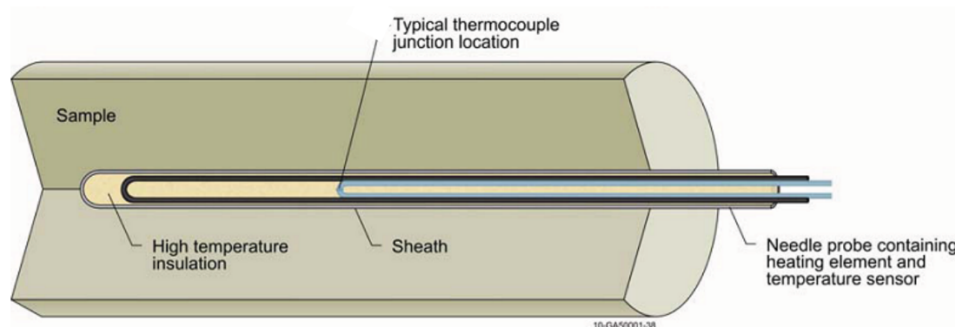


Figure 3-2: Schematic diagram of thermal conductivity needle probe (Daw et al., 2010).

The thermal conductivity of the sample material is derived from the slope of the thermal transient using the following relation from the ASTM needle probe testing standard Equation 3-3

where λ is the thermal conductivity, C is a calibration factor, Q is power dissipated by the heater, L is the heater length, and S is the slope of the linear portion of the transient response.

$$\lambda = \frac{C Q}{4\pi L S}$$

Equation 3-1

Note that for a small probe (less than 2.5 mm in diameter) C may be neglected. As discussed previously Figure 3-3, the slope of the linear section of the transient response is given by:

$$S = \frac{T_2 - T_1}{\ln \frac{t_2}{t_1}}$$

Equation 3-2

Then the thermal conductivity is estimated according to the relationship:

$$\lambda = \frac{Q}{4\pi} \frac{\ln(t_2/t_1)}{T_2 - T_1}$$

Equation 3-3

This is a method used for measurements on liquids, unconsolidated materials or rocks when previously drilled and filled with conductive paste (Roshankhah et al., 2021).

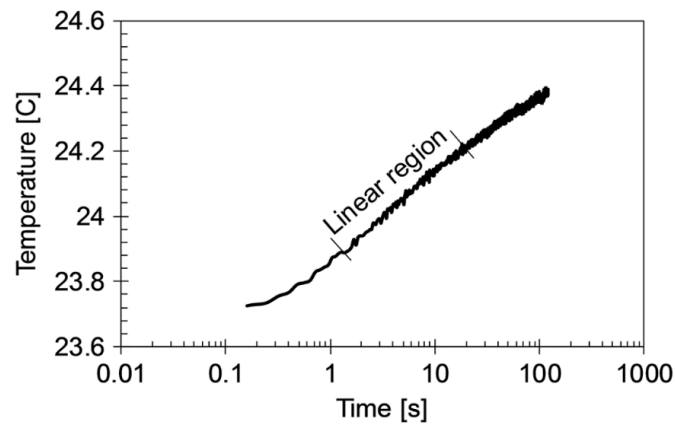


Figure 3-3 Typical raw data from needle probe measurements Roshankhah et al., 2021.

3.3. Guarded hot plate method (GHP)

The Guarded Hot Plate (GHP) method is a commonly used laboratory technique for measuring thermal conductivity. It involves the use of a specially designed apparatus called a guarded hot plate, which consists of a sample holder sandwiched between two temperature-controlled plates. In this method, the sample material with known dimensions and thickness is placed between the hot plate and the cold plate. The hot plate is maintained at a constant temperature, while the cold plate is kept at a lower temperature. The temperature difference between the plates creates a heat flow through the sample material. To minimize heat losses to the surrounding environment, the hot plate and the cold plate are surrounded by insulation, forming a guarded region. This helps to ensure that most of the heat flow occurs through the sample material rather than through the edges or the surroundings. Temperature sensors are placed at known locations on the hot plate and the cold plate to measure the temperature profiles. The heat flow rate is determined by measuring the power input to the hot plate and monitoring the temperature difference across the sample.

The thermal conductivity of the sample material is calculated using Fourier's law of heat conduction, which relates the heat flow rate to the temperature gradient and the dimensions of the sample. By accurately measuring the temperature gradient and knowing the dimensions of the sample, the thermal conductivity can be determined. The GHP method offers several advantages. It provides a direct measurement of thermal conductivity and is applicable to a wide range of solid materials, including both isotropic and anisotropic materials. It is also a steady-state method, meaning that the temperature difference across the sample reaches a constant value, allowing for accurate measurements (Low et al., 2015; Low et al., 2013).

However, the GHP method also has some limitations. It requires precise control of temperature and insulation to minimize heat losses, and any errors in temperature measurements or heat losses can affect the accuracy of the results. Additionally, the GHP method is generally limited to materials with low to moderate thermal conductivities. Overall, the Guarded Hot Plate method is a reliable and widely used technique for determining thermal conductivity in laboratory settings. Its accurate measurements and direct approach make it a valuable tool for understanding the thermal properties of various materials (ASTM C177-13 2017; Zhao et al., 2016; Dubois e Lebeau 2015). Figure 3-4 illustrates some of the most common techniques: the absolute technique and the comparative technique.

- In the absolute method (a), the sample is positioned between a heat source and a heat sink. The heat source generates a heat flux, from which the parasitic heat losses must be subtracted, including losses due to propagation in the surrounding environment and losses through the probe itself. These factors make it challenging to estimate the actual heat flux that crosses the body, which is why measurements are sometimes conducted under vacuum conditions. Once thermal steadiness is reached, the temperature gradient is measured at the ends of the body, of which the dimensions and input heat flux are known (Fourier's law; Bergman et al., 2011).

$$\lambda = \frac{Q_{rate} \cdot L}{A \cdot (T_1 - T_2)}$$

Equation 3-4

- The comparative technique (b). The primary challenge of the absolute technique lies in precisely determining the heat flow through the sample. However, if a standard material is available with a known thermal conductivity, the equation differs from the previous case. At least two temperature sensors must be present on each rod. Since the amount of heat flow through the standard material is equal to the heat flow through the measuring sample, the thermal conductivity of the measuring sample is given by:

$$\lambda_{sample} = \lambda_{ref} * \left(\frac{T_2 - T_3}{L_{ref}} \right) * \left(\frac{L_s}{T_1 - T_2} \right)$$

Equation 3-5

λ_{ref} = Thermal conductivity of the reference material

L_{ref} = Length of the reference material

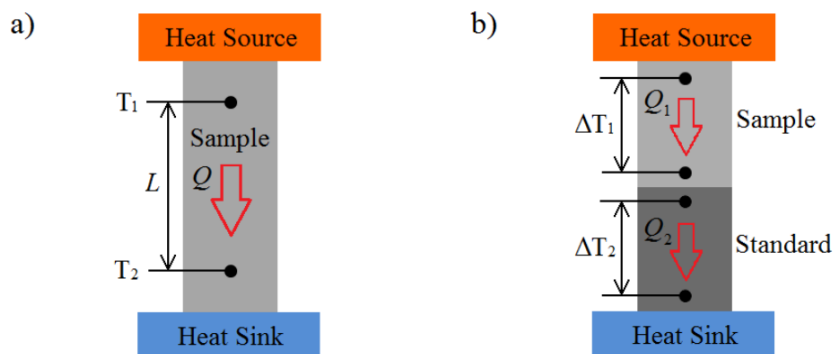


Figure 3-4: Schematic of steady-state methods commonly used for measuring the thermal conductivity of bulk materials. (a) Absolute technique; (b) Comparative technique (Zhao et al., 2016).

This particular method presents two primary disadvantages that warrant further discussion. Firstly, it demands a considerable amount of time to achieve the desired level of thermal steady state (

Figure 3-5). This requirement often entails several hours of waiting before the system reaches equilibrium. Additionally, the measurement process itself is quite time-consuming, further prolonging the overall experimental duration. However, these time-related aspects have a direct impact on the accuracy of the results due to the potential influence of moisture migration during the extended measurement period. It is worth noting, though, that through our own investigations in the chapter 4.2 we have demonstrated that conducting tests on identical materials over consecutive days does not yield significant variations in the thermal conductivity value. This finding serves to underscore the fact that the presence of moisture within the sample, using our specific setup, does not substantially affect the outcome of the measurements.

In light of these considerations, our selection of the GHP method was a carefully made decision. We were well aware that one crucial factor to be taken into account could be the contact resistance between the sensors and the individual grains within the material being tested. However, the advantages of utilizing the GHP method outweighed this potential drawback. Specifically, the precision of the data obtained through this method was enhanced by the meticulous construction of a dedicated laboratory, purposefully designed to facilitate accurate thermal measurements. We employed highly precise thermal probes and took extensive measures to minimize heat losses by employing effective insulation materials in the surrounding environment. The comprehensive details of this experimental setup and its associated considerations are thoroughly explained in the dedicated chapter 4.2.

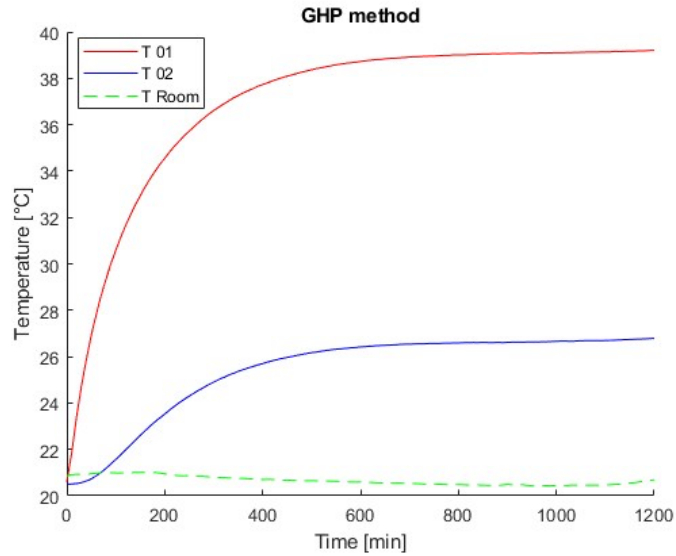


Figure 3-5: Stationary phase of two sensors and ambient temperature during a test using GeoTh.

3.4. Other methods (e.g. TPS)

There are several alternative methodologies for measuring the thermal conductivity of rock samples. These methods generally require a flat surface, sometimes coated with a thin graphite film, to ensure uniform and stable contact during measurements.

One of the most commonly used methods is the Transient Plane Source (TPS) method. This technique involves using a metallic disk as a flat and continuous heat source, along with a temperature sensor for data recording. The metallic disk is electrically insulated and placed between two thin plates of the rock sample. All other parts of the sample are appropriately thermally insulated to prevent heat losses. During measurements, a small current is applied to the metallic disk, allowing for the monitoring of temperature increase over time. Through the analysis of the obtained data, it is possible to determine the thermal properties of the sample, including thermal conductivity (Zheng et al., 2020; Zhao et al., 2016).

The laser source method, on the other hand, addresses the contact resistance issues that occur in all the methods described so far. This technique harnesses the principle of thermal diffusion, utilizing a laser as the heat source and measuring the response with a detector. The sample on which the

measurements are conducted is typically planar in shape and is positioned between the laser source and the detector. The sample is prepared with a thin layer of graphite on both sides, allowing one side to absorb and the other side to emit infrared radiation.

In this method, the laser beam is directed onto one side of the sample, causing localized heating. As the heat diffuses through the sample, the temperature distribution changes, and this thermal response is detected by the detector on the other side of the sample. By analysing the thermal response, including the rate of temperature change and the temperature distribution, the thermal properties of the sample, such as thermal conductivity, can be determined.

The use of a laser as the heat source offers several advantages. It provides a focused and controlled heat input, allowing for precise and localized heating of the sample. The use of graphite coatings on the sample surfaces enhances the absorption and emission of infrared radiation, improving the accuracy of the measurements. Additionally, since the laser source is non-contact, it eliminates any contact resistance issues that may arise in other measurement methods.

Overall, the laser source method offers a reliable and accurate approach to measuring thermal properties, mitigating the limitations associated with contact resistance. It is particularly suitable for planar samples and provides valuable insights into the thermal behaviour of materials (Zhao et al., 2016).

Every method used to measure the thermal conductivity of rocky or loose samples has specific advantages and limitations, but it is through these methods that fundamental information about the thermophysical properties of such samples can be obtained. This information is of great importance in various scientific fields and enables a deeper understanding of these materials and their applications.

4. Laboratory set-up

4.1. State of the art

As mentioned in the explanation of the two thermal conductivity investigation techniques, there are different currents of thought, and different laboratories and scales are used in testing. There are research groups that deal with large-scale laboratories, using ILS method (Wagner, et al. 2014). uses a TRT tank with dimensions of 9 meters (m) length and 6 m width and 4.5 m depth to recreate real-life-like stratification and an artificial aquifer. In the setup, he also uses 0.1 m diameter and 4.3 m depth probes, recreating a length-to-width ratio of 21.5. The whole is filled with sand of three different grain sizes, fine, medium and coarse, also creating a groundwater flow. The work done uses large amounts of material and the same tool used in the field, but the result is an average of the thermal conductivity value of all the layers crossed. In this way, it takes several days to receive a constant K figure, and there is no knowledge of what lithologies were crossed by the probes. In addition, it takes 4 to 5 days to return to initial system conditions.

The work of Beier (Beier et al., 2011) also uses a very large laboratory with a great deal of material. The technique is the same and uses a hydraulic pump and heater to do tests similar to U-Tube borehole heat exchanger. The sandbox is 18 meters long, and the vertical cross section of the box is a square with 1.8 m sides. The frame was built of wood to hold the sand material. A plastic insert separates the sand from the wooden frame to prevent water from escaping from the sand, and a wooden lid placed over the box. A hole 18 m long centred horizontally along the length of the box was drilled inside. An aluminium tube with an inner diameter of 12.6 cm serves as the wall of the hole. A test of heating by heat transfer fluid requires tens of hours. This test represents a well-controlled test to determine the thermal conductivity of the soil and the thermal resistance of the borehole. In addition to the usual field test measurements, the data sets include temperature measurements on the borehole wall and surrounding soil. This work therefore focuses only on one type of soil and one type of material in the borehole wall, with very long tests.

Katsura (Katsura et al., 2006) instead created a smaller system, but the laboratory is still considered large scale. The apparatus consists of an acrylic cylinder with an inner diameter of 3 meters, contains a 2 meter silica sand layer with an average grain size of 0.2 mm. This layer is in contact with water through nonwoven fabrics and perforated acrylic panels. The whole thing was constructed to mimic the constant groundwater flow in a sand layer and understand its thermal response by linear (or cylindrical) method. The probe was buried in the middle of the sand layer. Composition of the thermal

probe a line and the Pt-100 sensor are covered by a steel pipe a stainless steel pipe 2 meters long and 3.2 mm outside diameter. The temperature sensor is attached to the centre of the probe, where the representative point is located. The whole system is thermally controlled by measuring temperatures using thermocouples. Using this technique, the thermal responses and data taken into account are derived in a few seconds, on the order of 2 – 3 hours. The amount of material used and tested, and the amount of water used unfortunately allows a very small case study to be analysed. Similar structure was exposed in the article by Kramer et al., 2014. A precast concrete pile with a diameter of 0.1 meter and a length of 1.38 meters, with a depth of 1.17 meters, was used for the thermal experiments described in the paper. A U-shaped PVC circulation pipe was inserted into the concrete to allow circulation of the heat transfer fluid within the pile. The circulation pipe was connected to a temperature-controlled fluid circulation bath, which maintained a constant fluid temperature at the fluid entry point. The soil tank has a square cross section of 1.83 m x 1.83 m and consists of a base portion 1.22 m high and an upper portion with a height of 0.91 m. The upper half of the tank fits directly over the lower portion of the tank and has bolted connections around the circumference of the tank. Standard F50 Ottawa sand (silica sand with average grain size $D_{50} = 0.25$ mm) was placed inside the tank. The use of materials similar to geothermal probes is an advantage for this work, but the use of a single, small-sized material, compared to the real thing, and does not help in generating accurate data. In addition, only one type of material is studied. (Di Sipio e Bertermann 2017) use the soil as an open-air laboratory but insert different types of unconsolidated natural material into portions of the soil. The sands used are different grain sizes of sand and sand plus bentonite. The heat sources are 5 helical manifolds placed in different sectors. As for the hydraulic system, the five helices are paired by Tichelmann method, each showing the same flow rate over 24 hours, and are connected to an absorber, which can stress the working condition. The measurement system allows recording every 15 minutes in a data logger, via dedicated sensors. Unfortunately, this system is optimal for ultra-shallow geothermal system but the ground temperature is too much affected by daily and seasonal ambient temperature.

The sensors used were included for most of these papers to calculate how much the natural material would heat up as heat transfer fluids passed through similar tubes in geothermal probes. In contrast, other papers expose the same issues but with the use of commercial needle probe instruments, obviously with smaller laboratory scales.

One of these works is Cortes (2009), interested in analysing the performance of different parameters such as grain size, mineralogy, water content, density, and packing effects. Thermal conductivity was measured in hydrated sediments with different mineral grain sizes and subjected to different vertical

effective stresses. The sediments are confined within a cylindrical stainless steel cell (inner diameter 63.5 mm, height 187.95 mm) to impose zero lateral deformation conditions. The top side is free to move; measuring the vertical displacement of the cap calculates the instantaneous porosity. Excess pore fluid is allowed to drain freely. The sample is subjected to the effective vertical stress (0.05; 0.1; 0.25; 0.5 or 1 MPa), corresponding to depths up to 100 m below the surface. In this laboratory, however, a needle-shaped assembled system with a thermocouple and heating wire inside is used. The system is useful for being able to measure thermal conductivity in a short time (a few seconds), at the expense of data accuracy.

Another work that uses a very similar technique is Roshankhah et al., (2021) that measures thermal conductivity using a thermal needle probe. This device inserted in the middle part of the specimen imposes a constant heat flow along its entire length for 120 s. The specimens are tested under zero lateral deformation conditions. Thermal measurements are taken along the centre line of the cylindrical specimens (with a diameter of 7.2 cm and a depth of 7.6 cm). The sandy-silt material is inserted through a scoop a few centimetres at a time to compact it. Once the dry density is calculated, the thermal conductivity at different stress conditions is measured. Then the few seconds of heating the material is analysed, using formula Equation 3-3. The purpose of this good work is to understand the influence of some factors such as the amount of fine material in the tested material, the percentage of water in it, the influence of density and packing. Unfortunately, using this instrumentation does not provide absolute accuracy of data, but certainly good reproducibility.

Di Sipio and Bertermann (2017) presented the same problem with an instrumentation for measuring thermal conductivity similar to the previous work, but used a different media for the samples. A key challenge of this work is to understand how the thermal properties of different soil types change under the same environmental conditions. The parameters considered are quartz content, amount of fine material, bulk density and different saturation conditions. The material used is sand and fine sand as well as silty sand, mixing the natural materials with bentonite or clay powder in different percentages (8, 15, 30 %). Soil moisture is calculated by time domain reflectometry (TDR). In addition to moisture, electrical resistivity is also measured using special sensors. The disadvantage of this work is the use of rectangular plastic trays (less than one meter in size) as sample holders that can be affected by ambient temperature and alter the final values, or not make the saturated material homogeneous at different sizes or even have edge effects, in addition to the use of a commercial instrument for research purposes.

To measure thermal conductivity on unconsolidated inert natural materials, there is not only the needle technique, but there is the possibility of exploiting the physical principles of GHP (chapter 3.3). This methodology may seem disadvantageous in some aspects, especially in terms of timing because the tests take several hours, but the special feature is the accuracy of the data if the instrumentation used has high accuracies. The protected hot plate makes it possible to have thermal conductivity values even for materials of particular grain size that are impossible to measure with needle instrumentation, such as gravel. Gravel was tested with this methodology by Dalla Santa (et al. 2017). Direct measurements of the thermal properties of gravel are quite challenging, mainly because of technical problems related to the very coarse size of sediments, which prevents adequate physical contact between the material and conventional measurement sensors. In addition, the variability of the mineralogical composition of polygenic samples in many cases requires the involvement of a rather large volume of geologic material in the measurement procedure to obtain representative values of thermal properties. However, adequate physical contact between the sediment and the sensor is required, which, in the case of gravel, is not achieved due to the coarse size of the clasts. The samples tested in this work consisted of a carbonate sample, a granitic sample and rhyolitic lava clasts. Obviously, the latter sample had a higher porosity (about 0.7) than the others (both around 0.5). It can be seen in the article that a commercial instrumentation (Taurus Instruments TLP 800) was used, again to be able to test gravel samples (and more) even though it is usually used to test building material. The instrument consists of two 0,8 x 0,8 m measuring plates. However, to carry out this type of testing, the original instrument was modified with a 0,5 x 0,5 x 0,06 m plexiglas box. It works by imposing and maintaining a constant temperature difference, usually 10 °C, between two parallel plates, with the cold one at the top (usually 15 °C) and the hot one at the bottom (usually 25 °C). The material to be tested is placed in between. Having the described part of the instrument completely insulated, a unidirectional heat flow is established through the sample, and the thermal conductivity is measured every minute. The test is stopped when thermal equilibrium is reached and the thermal conductivity values measured thereafter are stable; at a given temperature, the series of measurements needed to obtain the validated value of measurements needed to obtain the validated value takes about 6-7 hours. The result may also be good, but modifications were made to a commercial instrumentation. In addition, materials such as sandy gravel were tested, which may have some critical issues.

Hamdhan and Clarke (2010) instead, they reproduced a laboratory like the one explained in our thesis. Tests to determine thermal conductivity are based on measuring the power required to create a constant temperature difference or applying constant power and measuring the resulting temperature

difference, or monitoring the temperature as it changes. Their system (about ten centimetres in size) consists of a thermal cell, a temperature control unit, a data logger, and a personal computer (PC) and an array of temperature sensors (thermocouples). In detail, it is designed to use a cylindrical specimen. The flat ends of the specimen are held at different temperatures and heat is flowed axially through the specimen. The cylindrical soil specimen is surrounded by a jacket of insulating material (for axial flow) and is placed between two plates. The plates contain heating elements (a cartridge heater is used) but also seal the specimen by preventing any change in water content. Temperatures inside the bottom plate, at the base of the specimen, at the top of the specimen, and in the air above the top plate, along with energy consumption, are measured throughout the test. The test is performed in air, so currents must be minimized, and the procedure involves a heating phase, a stationary temperature phase, and a cooling phase for the system. The problem is that data is calculated every 5 minutes, so there is not much accuracy if sudden voltage drops or unexpected air shifts occur. In addition, only four types of sand (coarse sand 0.5 to 2 mm dry and saturated, fine sand 0.062 to 0.3 mm dry and saturated) were tested to ensure the validity of the data.

Hamuda et al., (2011) They have set up a system to simultaneously measure two samples using the GHP technique. The purpose of the thermal cell apparatus is to characterize the thermal properties of soil. The sample has a diameter of 103 mm and is placed at the center of a double-walled cylinder, which is used to contain the samples, the heat source, and the dissipation plates in order to limit radial heat losses and create one-dimensional flow conditions. To achieve a uniform temperature at one end of the sample, a heat source with the same cross-section as the sample is used. At the other end of the sample, an aluminium disk with good thermal conductivity is used to dissipate the heat. In order to reduce radial heat losses during this test, the samples are isolated with a low thermal conductivity material, in addition to the double wall of the thermal cell that allows air circulation. Their instrument has been specifically designed to measure the thermal conductivity of two simultaneous unconsolidated natural samples. To obtain accurate results, they conducted a series of experiments using different types of sands characterized by varying particle sizes, both in dry and saturated conditions. The results obtained from these experiments were employed within this thesis to carry out a detailed and comprehensive comparison.

Also Haraisha et al., 2019's work is focused on finding the effective thermal conductivity coefficient of the soil, studying the effect of porosity and particle arrangement (density) and water content on the thermal conductivity of sand using a specially designed instrument, with the steady-state method. A thermal cell apparatus is used, where a heating disk is placed between the two samples to generate a unidirectional gradient towards the sample. Heat is generated within the disk by a cartridge heater

inserted through a hole in the aluminium disk. Two aluminium disks are positioned at the non-heated ends of the samples to dissipate heat from the outer ends. The heating disk, the outer disks, and the samples all have the same diameter (84 mm). The temperature sensor was pushed longitudinally through the holes at the centre of the samples in the two cylinders of the cell to reach depths of 0, 35, 65, and 100 mm from the heater. Another temperature sensor was used to control and monitor the temperature of the heating disk. The system temperature is measured and monitored using a temperature control system and a data acquisition unit, with a system temperature sampling every 20 seconds. The main body of the cell is made of PVC, whose low thermal conductivity helps minimize radial heat loss, and its rigidity allows for sample compaction during preparation, if necessary.

4.2. GeoTh laboratory

The scientific paper by Rapti et al., (2022) entitled GeoTh: An Experimental Laboratory Set-Up for the Measurement of the Thermal Conductivity of Granular Materials is a study conducted by our research team in which a new experimental system for measuring the thermal conductivity of granular materials, particularly soils, is explained. The system, called GeoTh, uses the stationary heat flow method and a series of highly accurate measuring instruments to obtain reliable thermal conductivity data.

Objectives and laboratory

The main objective of the GeoTh laboratory was to obtain all the necessary parameters to calculate the thermal conductivity of unconsolidated natural materials, such as soils, and to measure all values with minimal error using the GHP (Geothermal Heat Pump) method. To achieve this goal, we drew inspiration from the state of the art in these topics and tried to understand the best method for the type of material to be tested. The laboratory was specifically created for the doctoral project with the aim of being cost-effective, yet highly functional and efficient in sample preparation and data acquisition. We assembled the laboratory using common materials that allowed us to create a system capable of generating constant heat, adjustable through software specifically developed for this tool, using Python. These materials had to be durable, affordable, easy to use and assemble, sometimes thermally conductive and sometimes thermally resistive. GeoTh was developed to overcome some of the

limitations of traditional measurement methods, which often produce unreliable data or require expensive and complex equipment.

The overall scheme of the apparatus is represented in Figure 4-1. The system is composed of some basic parts among which are the casing for the samples thermally isolated and equipped with several sensors, a heating system with adjustable power supply, and a governing hardware and software system, including the data-logger and the general management.

Sample casing

During the initial experimental phase, the sample casing was calibrated to test a quantity of material comparable to a portion of a core, measuring around 10-20 cm in length and approximately 10 cm in diameter. To minimize edge effects, cylindrical sample holders made of polyvinyl chloride (PVC) with a thermal conductivity of 0.159 W/m K were chosen. Some cylinders were used (Figure 4-1), with internal and external diameters of 8.6 and 9.0 cm, respectively, and a length of 10 cm during this preliminary phase. The cylinders were closed at the base with a 3 mm-thick aluminium disk with a thermal conductivity of 200 W/m K , which was sealed with a high-temperature-resistant conductive paste to make the casing water-resistant.

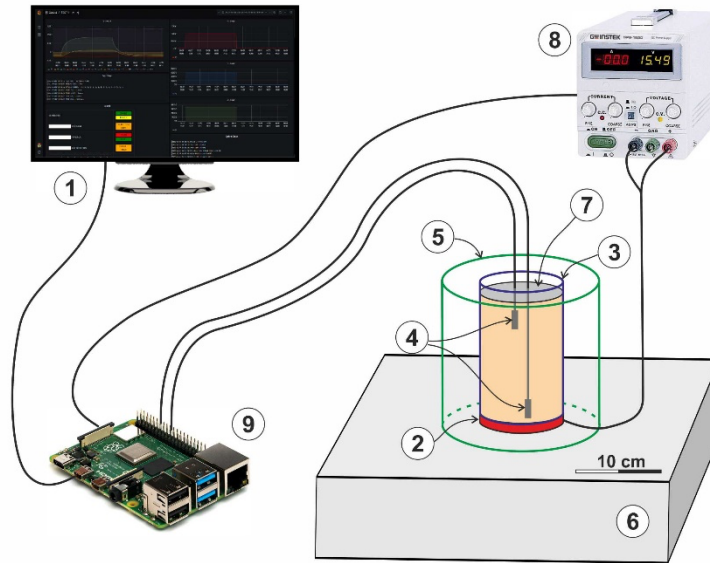


Figure 4-1: Schematic representation of the apparatus described in the present paper. (1) Graphical user interface; (2) disk-shape heat source; (3) sample casing; (4) temperature probes (PT100); (5) lateral polyurethane foam ring; (6) bottom polystyrene layer; (7) aluminum film; (8) power supply; (9) single board computer (Raspberry PI) for data acquisition, processing and storage.

During the tests, each casing was placed in direct contact with a discoidal electrical resistor that matched the diameter of the cylinder as shown as component number 2 in Figure 4-1. The entire setup was placed on top of a 10 cm-thick layer of polystyrene (with a thermal conductivity of 0.034 W/m K) serve as an insulator. Additionally, polyurethane foam (with a thermal conductivity of 0.022 W/m K) was fixed all around and in direct contact with the PVC cylinder for further insulation (as shown as component number 5 in Figure 4-1).

Once the casing was filled with the material to be tested, an aluminium film was placed on top to prevent water evaporation during the wet tests resulting from the heat generated by the electrical resistor. The film has high conductivity and minimal thickness, which negligibly affects the heat flux from the sample to the air and hence does not alter the test results.

The hardware components

The hardware components of the system consist of a master device single board computer, a power supply for the heater with two independent channels, and a custom-made electronic motherboard that

accommodates thirty-two commercial daughter-cards for temperature measurements. Communication between the master device and power supply is based on the standard SCPI protocol via a USB interface, while the temperature measurements are acquired from the daughter-cards using SPI communication with multiplexed technique implemented on the motherboard. Figure 4-2 illustrates a representative schematic of the hardware components and their connections.

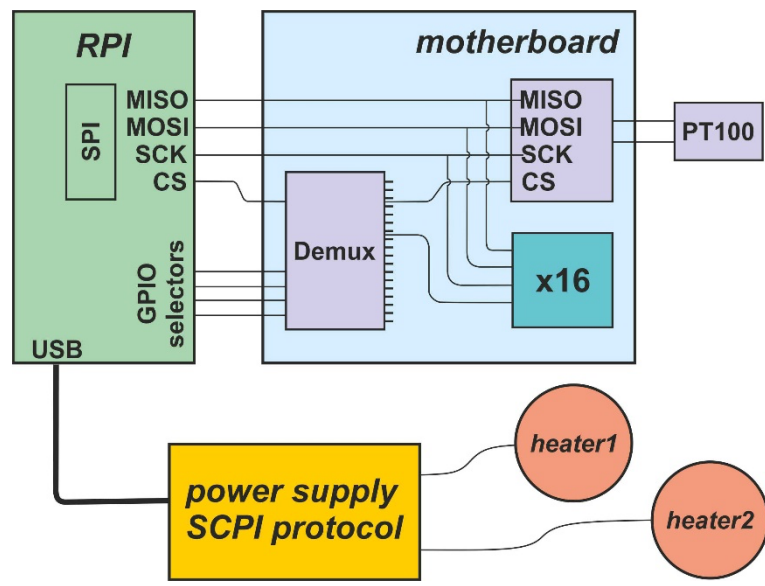


Figure 4-2: Schematic overview of the hardware components.

For governing the whole apparatus, a commercial Raspberry PI single board computer (Figure 4-1) has been exploited as a master system, because the hardware peripherals equipment, e.g., USB and SPI interfaces, is ready to use for this scope. Moreover, the Linux operating system running on the Raspberry PI allows the highly reliable implementation of custom software, it has high flexibility for low level diagnosis and configuration, various free license extensions, and a lot of information is available from the Raspberry community that could contribute to the development of custom applications. Additionally, low-cost hardware components, such as the ones we used, allow us to have a backup system or an entire replica with a very low economic impact. For this project, a Raspberry

PI 4 model B with 4 GB RAM and 32 GB SD card and official raspbian OS has been selected. The OS is installed on the SD card, but in order to prevent the possible loss of integrity, as a good practice for long term applications, two USB-disks have been configured for data storage. One linux file system formatted disk is dedicated to the database local storage, while the second one Ex-FAT file system is used as backup of the database and for pre-processed data. In the following they will be referred to as DB-DISK and BACKUP-DISK, respectively. The linux file system format for DB-DISK was set up for easy management of permissions and for security reasons, while the Ex-FAT format for BACKUP-DISK has been preferred for allowing users to have an alternatively easy way to retrieve data on different operating systems PCs. In order to reach as constant as possible heating power during the first phase of tests and with the aim to have as low as possible economic impact factor on the system, a low-cost commercial power supply has been identified in the DC programmable Power Supply model RSPD3303X provided by RS Components SRL. This model comes out in two versions: 10 mV/10 mA and 1 mV/1 mA voltage and current precisions, respectively. Typical heating power needed for the tests is of the order of few watts. A convenient way to heat samples is the use of commercial 75 Ohm heating resistors. From these considerations, the second version of Power Supply allows to obtain a power precision of about 15 mW, while the first one shows one order of magnitude higher precision, which is not necessary for this aim. For precision temperature sensing, Platinum Resistance Temperature Detectors (RTDs), with a resistance of 100 Ohm at 0 °C, have been chosen as temperature sensors, i.e., the so-called PT100 (n. 4 in Figure 4-1). These have been used for many years to measure temperature in laboratory and industrial processes, and have developed a reputation for accuracy, repeatability, and stability in time. Because these elements are usually quite fragile and our test conditions could be hard, the acquired PT100 probes are sheathed and protected by a thin film which assures a short response time due to the bare measuring resistance and a reduced thermal capacity. In order to get precision and accuracy out of the PT100 RTD, the Adafruit MAX31865 module has been used, this being very suitable for the precise measuring of extremely high and low temperatures. Indeed, the MAX31865 IC is an easy-to-use, resistance-to-digital converter optimized for platinum RTDs. It features an amplifier which is designed to read the low resistance and can automatically adjust and compensate for the resistance of the connecting wires, together with a 15-bit ADC converter providing a nominal resolution of ± 0.03125 °C. In Figure 4-3, results from a test performed on a PT100 probe kept at constant temperature for about half an hour are shown. Temperature as a function of time and its distribution show a resolution of 0.03382 °C, which is comparable to the nominal value within nonlinearity effects. An external resistor sets the sensitivity for the RTD being used and a precision Δ

ADC converts the ratio of the RTD resistance to the reference resistance into digital form. In this project, a R_{ref} of 430 Ohm was chosen.

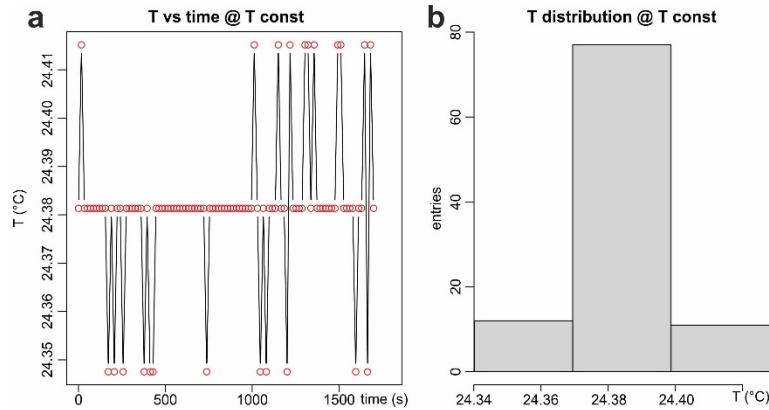


Figure 4-3: a) Constant temperature versus time. b) Measured temperature values distribution.

Since temperature probes could show different values due to intrinsic fabrication and due to effective R_{ref} values, a calibration was carried out to correct temperature measurements for each sensor. As reference temperature, the mean value of all sixteen probes was assumed, while all single measurements were corrected to fit the same values.

There are four screw terminals on the Adafruit MAX31865 module, so different PT100 probe types can be used with this design. Moreover, it can work with 2-, 3-, or 4-wire PT100 probe types. Since the 4-wire probe connection eliminates errors due to cable resistance, for very precise readings of low resistance values, 4-wire measurement were carried out. With the aim to realize the whole temperature system, a printed circuit board was designed and produced at the INFN Electronics Design Service at Physics and Earth Science Department (Ferrara, Italy). The motherboard hosts the Raspberry PI and 16 Adafruit MAX31865 resistance-to-digital converter modules which communicate through SPI interface with the main controller. In order to reduce the number of chip select signals on board of the Raspberry PI, a 1-to-16 demultiplexer (74HC154) was mounted on the electronic motherboard. This allows the user to select up to 16 modules, meaning that ‘contemporaneous’ measurements of up to 16 temperature values can be achieved.

The calibration

We performed the calibration of the probes to ensure accurate data analysis. All probes were calibrated simultaneously to avoid systematic errors. The tests were conducted for several hours using a calorimeter and a water stirrer, varying the power of the system to change the temperature. The probes were connected and inserted into the system when it was in a steady state, with a constant ambient temperature. Subsequently, we introduced heat into the system and maintained a certain temperature for at least 10 minutes for each interval, always with water in motion. The raw and corrected data are presented in Figure 4-4.

From the results, we can observe that before calibration, the maximum temperature differences between the probes were 0.407, 0.442, 0.408, 0.477, and 0.547°C, respectively, at the steps of 33, 44, 48, 53, and 62°C. After data processing, the temperature difference between the maximum and minimum values is 0.097, 0.098, 0.053, 0.063, and 0.091°C.

We conducted a test where the temperatures measured by the probes were increased at intervals while keeping the desired temperature constant. During the test, we recorded the data every 10 seconds to obtain a significant number of values over time. For each probe, we calculated the average value during the steady or pseudo-steady phase. Subsequently, we obtained 32 average values and calculated the mean of the means to obtain a representative value for that period and at that temperature. Afterwards, we calculated the difference between each probe and the reference value (mean of the means). This calculation was possible because all probes remained stable at the desired temperature.

Although a slight slope was observed at temperatures below 45°C, calculations have shown that the value of the slope of a possible correction line is approximately 1 as the temperature varies, making it negligible.

$$y = mx + q$$

Equation 4-1

Assuming a generic equation for a line as Equation 4-1, we observed and calculated how the 32 probes deviated from the line. We considered the average of the means as the reference equation, with a negligible value of m . To achieve this, we calculated the difference (q) and added it to the probe under examination, effectively shifting the line towards the reference line. By doing this, we obtained a value of q for each probe, resulting in 32 q values for each stable temperature step. To have a consistent value at each temperature, we decided to calculate the average value of q for each individual probe, giving us a single value that could be used as a corrective factor for the temperature data during subsequent tests. This was possible by further controlling the q values, comparing each q for each step with all 32 probes and observing that the order was always the same.

To analyze how much the 32 probes deviated from the reference line, we assumed a generic equation for a line, referred to as Equation 4-1. Considering the average of the means as the reference value and with the negligible value of m , we calculated the difference (q) between each probe and the reference line. Subsequently, we added this difference to the respective probe to shift the line towards the reference line.

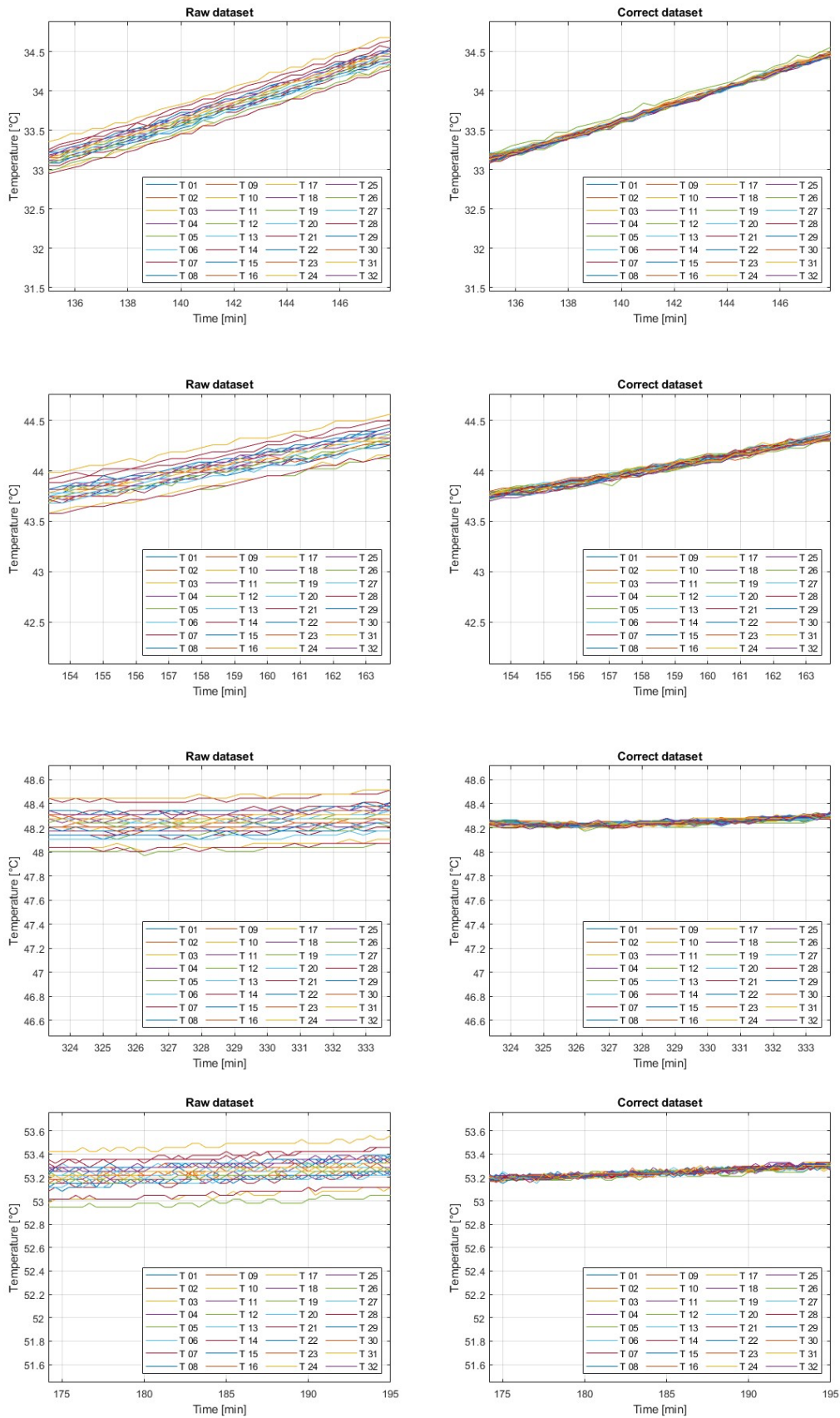


Figure 4-4: different steps during the calibration test of the 32 sensors used in the laboratory and the respective graphs with the calibrated values

Software and user interface

The control and monitoring system is based on a main master script, in the following called Master Script, which interfaces with hardware (power supply and motherboard; n. 7 and 8 in Figure 4-1) and with a dedicated database for an organized data storage. In the same database, the single board computer monitor status is stored by a secondary script called RPImon Script. Master Script and RPImon Script are based on python3 (<https://www.python.org>, accessed on 10 November 2022) and run on the Raspberry as two independent daemons. In order to avoid the loss of data, two linux cron jobs have been configured to provide local and remote time scheduled data backup. Data and test configuration as well as the monitoring status are saved on the time series Influx database (<https://www.influxdata.com>, accessed on 10 November 2022), which is organized in six main sections, as it will be described later. User interface and data visualization are realized with Grafana (<https://grafana.com>, accessed on 10 November 2022) tools which interface with the Influx-DB. In Figure 4-5, a schematic overview of the script and used software tools is shown.

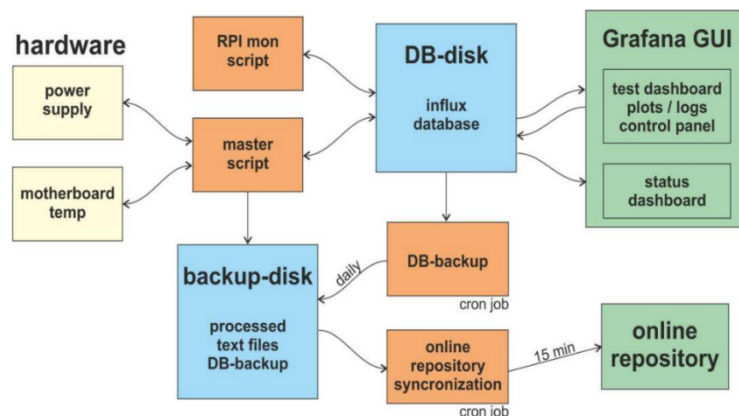


Figure 4-5: Schematic overview of software components, data fluxes and hardware interfaces.

A detailed description of each software component is reported in the following. In order to help readers to understand data and command fluxes, we start describing the database configuration. In order to have a complete view of data and system status, all information has been organized in a time series influx database configured with the following dedicated sections.

1. Raspberry PI System Monitor section contains diagnostics of the single board computer, e.g., CPU temperature and usage, RAM usage and disk usage. This information allows users to investigate possible system failure.
2. 2. Daq Log database section contains all runtime information about operations executed by Master Script. This information allows users to check test configuration, correctness of hardware and database accesses, and view history of test operations.
3. 3. Temperature section contains all sixteen temperatures measured with a default time sampling interval of about twenty seconds.
4. 4. Tests Configuration section contains all details of test configuration, e.g., test name, enabling test, enabled temperature probes, heating power, enabling power, single measurements time sampling, and time interval for recording temperature average for raw data file.
5. 5. Tests Data section contains related enabled temperatures and power measurements details.
6. 6. Run State section contains information on changes of test configuration and Raspberry shutdown request. Changes on test configuration by user interface are recorded on a single flag in this section and this will trigger Master Script to reconfigure the test with the new set-up.

For data storage and management, all sections have read/write access from Main Script and RPImon Script. For data visualization, sections 1, 2, 3, and 5 have only read access from Grafana user interface. Meanwhile, in order to allow users to control tests, Sections 4 and 6 have write access from a dedicated panel on Grafana user interface. Main Script is designed to have full control of involved hardware and to manage data and test configuration. The script is based on five concurrent processes, each dedicated to a specific task, while a main independent process checks the running status of all tasks. Main Script processes can be summarized with the following list:

- Main controller process checks running status of all other five processes, sends infos to Daq Log database section and provides a restart of Main Script in case of failure;
- Daq process is dedicated to temperature measurements and control of the heating power system through the power supply. If at least one of the two possible tests is enabled, all sixteen temperatures and the two channels power supply parameters are acquired at a defined sampling rate and stored in the Temperature section of the database; temperatures are acquired by daughter-cards with SPI protocol with a

multiplexed technique driven by GPIO of Raspberry PI; monitor and control of power supply are provided with standard SCPI protocol via USB interface.

- DataProcessing process provides a data remap to related tests and fills the corresponding Tests Data database section.
- DataMean process provides average measurements on a user defined time interval and produces raw data text files.
- CheckConf process checks changes in configuration requested by users, then provides a reconfiguration of tests when required.
- CheckPowerSupply process checks the correctness of connection with the power supply for the heating system.

RPImon Script is a simple single threaded process which is demanded to log into database infos about Raspberry system status. In detail, system functionality is monitored by looking at CPU temperature and usage, RAM, DB-DISK and BACKUP-DISK usage. Infos are checked and stored every minute. Local storage into database performed by Master Script and RPImon Script is located on the external USB disk (DB-DISK). A secondary external USB disk, named BACKUP-DISK, contains processed data and daily updated database backup produced by a dedicated linux cron job running influxdb backup commands. In order to enforce integrity and safety of data, a second linux cron job running every fifteen minutes takes care of the synchronisation between BACKUP-DISK and an online data repository. A locally installed, open-source version of the Grafana framework has been used to create the GUI (graphical user interface) for the system. GUI is composed of three dashboards, two dedicated for independent tests and one used for the status overview visualisation. GUI dashboards are connected to the influx database used for data archive. Test dashboards show plots of enabled temperatures, heating power, applied voltage and heating resistance values versus. Time interval visualisation can be changed by users. A text panel shows the actual test configuration and status. A second text panel shows log messages from Master Script. In addition, an html panel based on a javascript is dedicated to control the system. From this control panel, it is possible to configure the test and to control its execution. Javascript is used to send configurations to the Test Configuration and Run Status database sections. The control and monitoring temperature system is designed to calibrate the power directed to the heater(s) and to measure and store the temperatures from the sensors. The system is capable of operating up to two independent sets of tests by driving two independent sets of heaters and to monitor up to sixteen temperatures. The system could be completely controlled remotely, and the online monitor allows to check the status of tests and diagnosis of the whole system in real time.

Tests for the reliability of the results

Following several tests for checking all components of the apparatus and validation of the whole experimental set-up, including a smooth laboratory procedure, we performed numerous further tests for verifying the reliability of the measurements and of the overall results. In particular, we verified the possible effect of the ambient temperature on the measurements, the need and the positive impact of properly insulating the sample casing, the reproducibility of the obtained measurements, and the calculated thermal conductivity values, and finally compared a set of our preliminary results with literature data.

As mentioned above, the whole apparatus was purposely created to test different loose granular materials in various boundary conditions. One of these conditions is represented by the ambient temperature, which is continuously measured during the experiments by two distinct sensors. This issue was analysed to recognize a possible impact on the final thermal conductivity values. Accordingly, several tests were performed under nearly identical thermo-physical conditions (grain size in the range 0.5 to 0.25 mm, porosity in the range 40–44%, and a bulk density of 1450 kg/m³), but at two different ambient temperatures of +25 °C and –5 °C. For the former conditions, the daily temperature change in the laboratory is typically ± 0.5 °C, while within the insulated chamber of the refrigerator temperature variability is limited to ± 0.25 °C. Within each tested sample, two sensors are installed at 7 cm and positioned in correspondence with the cylinder axis, with one sensor at distance of 1.5 cm from the casing bottom and the other sensor in the upper part of the sample, but remaining buried 1.5 cm from the top surface. After a few hours following their placement within the sample and before heating, the installed sensors reach a thermal equilibrium showing a temperature difference of less than 0.07 °C, thus confirming the lack of heat flux inside the insulated sample casing in both ambient temperature settings.

Lateral insulation tests

In order to verify the need and the efficiency of the lateral thermal insulation and hence the occurrence of a unidirectional (upwards) heat flux across the sample, we set-up some tests with and without a thermally resistant coating. For this purpose, we measured the temperature variation during time at two different sensors located respectively near the top (TA) and the bottom (TB) of the sample casing. Experiments were carried out within the refrigerator because of the more stable ambient temperature

leaving the samples after a heating test to homogenize with the ambient temperature of circa $-4\text{ }^{\circ}\text{C}$. The results from one of such double tests are shown in Figure 6, representing the curves of the temperature versus time for the two sensors, which are characterized by initial cooling phase temperatures of ca. 17 and $2\text{ }^{\circ}\text{C}$, respectively.

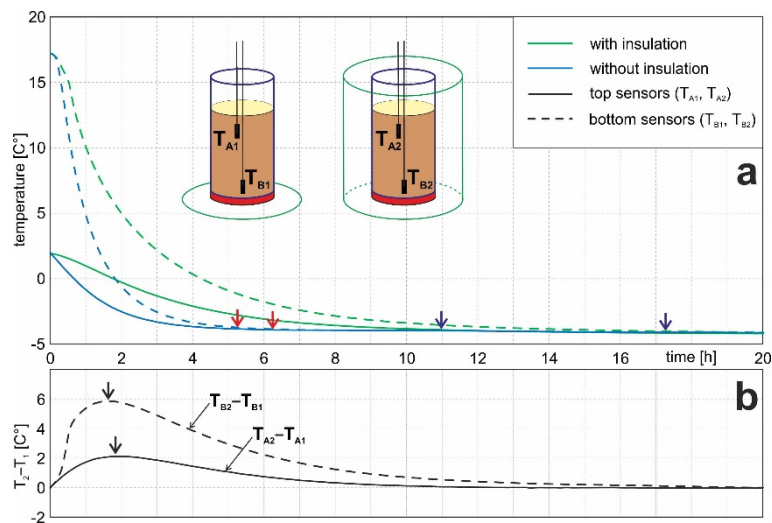


Figure 4-6: a) Temperature versus time at two sensors posed at the top and bottom of the sample during the cooling phase with and without lateral thermal insulation of the casing. Arrows indicate the approximate timing for reaching the environment temperature. b) Temperature difference between the two measurements versus time. Black arrows indicate the timing of the maximum differential temperature between the two sensors.

Independent from their initial thermal conditions and hence the differential temperature with the environment (at ca. $-4\text{ }^{\circ}\text{C}$), both sensors in the experiments without the lateral thermal insulation clearly document a much larger rate of temperature drop, while ambient values are approached within few hours (red arrows in Figure 4-6). Moreover, notwithstanding the different position of the sensors, with TB being much deeper and more thermally protected within the sample, the maximum difference is similarly observed after 1–2 h (black arrows in Figure 4-6), therefore confirming the occurrence of comparable phenomena of lateral heat dispersion in the experiments lacking the lateral insulation. In contrast, when the sample case is laterally isolated in a proper way, heat dispersion occurs only vertically, and the temperature drop is much slower. The efficiency of the lateral insulation was also

analyzed by means of a thermal camera (model FLIR C5, visual camera 5 MP; thermal sensitivity < 70 mK), allowing to observe the heat distribution on the top surface of the casing and the lateral isolation material. An example of these tests is represented in Figure 7 clearly showing the quite homogeneous temperature on the top surface of the sample and the very high temperature gradient immediately outside the casing, where the temperature on the top surface of the insulation material sharply fades into the ambient temperature (Figure 4-7). In conclusion, the performed tests satisfactorily confirm the efficiency of the designed and adopted thermal insulation strategy, both lateral and at the bottom of the casing, in order to assure a unidirectional heat flux across the samples during the experiments.

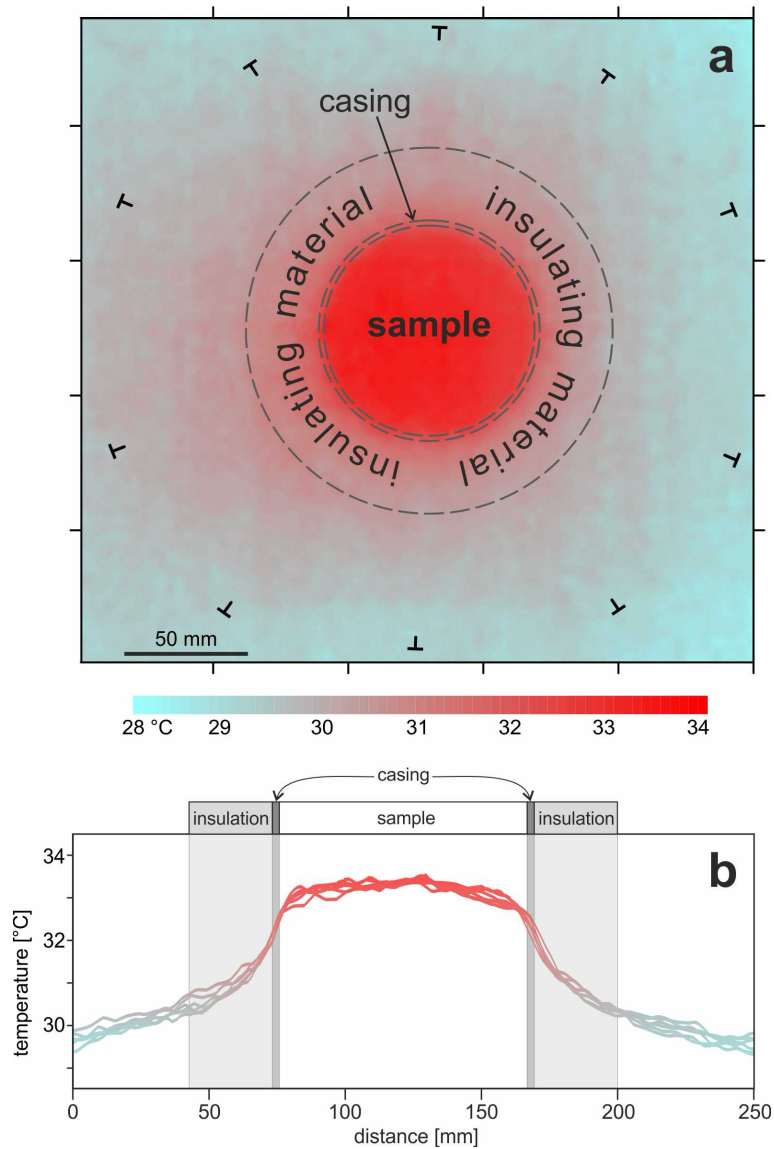


Figure 4-7: a) Thermal image (top view) obtained during a test and some thermal profiles. b) The uniform temperature on the sample surface and the strong gradient outside the casing is evident, confirming the effective insulation and assuring the unidirectional heat flux during the experiments.

The following is an explanation of the heat diffusion in this system, which is composed of basal and lateral insulation materials with a thermal conductivity coefficient below $0,034 \text{ W/m K}$. This allows the heat generated by the electric resistances to be directed in a single direction and towards a single direction. To confirm this theory, we conducted a test using 17 thermal probes placed at different distances from the center of the cylinder and at different heights from the base of the cylinder. The PT100 probes were placed both inside the PVC and inside the cup, as well as outside the entire system.

The results were shown in Figure 4-8 and Figure 4-9 for dry and saturated conditions, respectively. The results were carefully examined and we found that the greatest heat is concentrated inside the cylinder and the flow is mainly unidirectional. This effectively demonstrates the efficiency of the system and the validity of the theory. This test also highlights the importance of proper system installation and the selection of materials with the appropriate thermal conductivity coefficient.

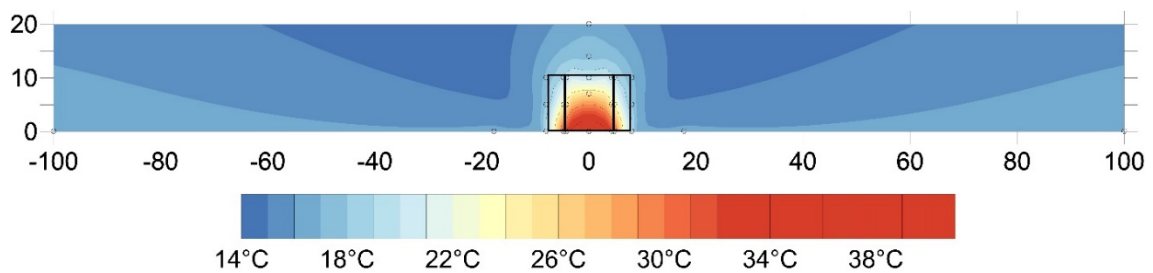


Figure 4-8: Thermal section in dry condition. The dimensional unit of the image axes is the centimeter (cm).

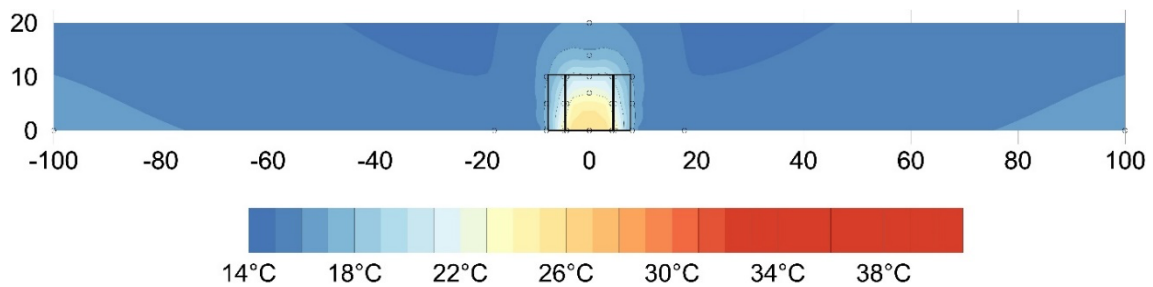


Figure 4-9: Thermal section in fully saturated condition. The dimensional unit of the image axes is the centimeter (cm).

Reproducibility test

A central issue in custom-built apparatuses is represented by the reproducibility of the results when several tests are performed with the very same material and thermal conditions. In order to verify this crucial aspect, we tested several times identical set-up conditions in terms of mineral composition, texture, porosity, water content, and heating power. The only difference observed during the diverse tests was the ambient temperature showing slight variations from test to test of 1–2 degrees (Figure 4-10).

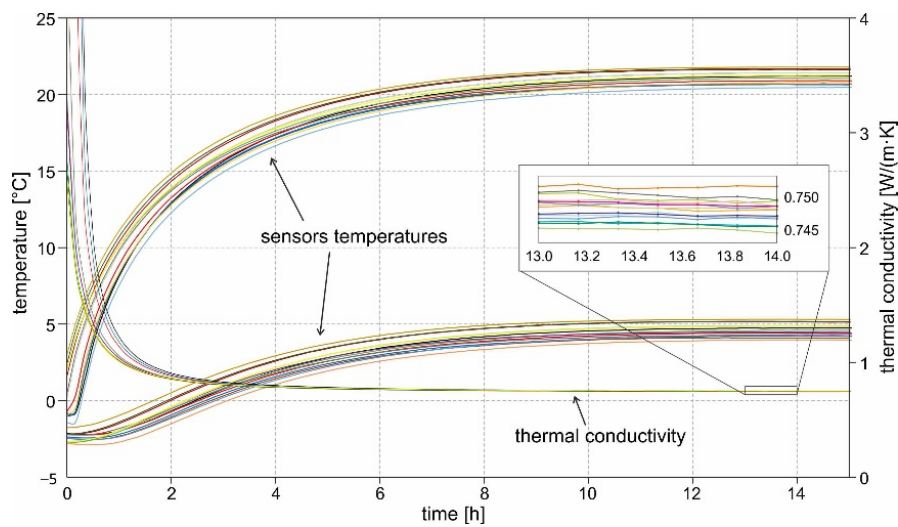


Figure 4-10: Measured temperatures (top and bottom sensors, left axis) and thermal conductivity (right axis calculated from 15 experiments carried out for verifying the repeatability of the obtained values and hence the reliability of the built apparatus. See text for discussion.

Notwithstanding these operative variations during the different experiments, the thermal conductivity calculated by means of Equation 3-4

is spectacularly stable for all the tests (Figure 4-10). This is clearly evident from the curves represented in the inset of Figure 4-10. Indeed, the enlarged graphs of the calculated thermal conductivity show that during the steady-state regime, the obtained values of the investigated parameter could vary at the third decimal representative number (± 0.002 W/m K), therefore documenting the repeatability of the measurements and the reliability of the created apparatus.

Comparison with literature data

Beyond the previously discussed tests, we also performed several other experiments for comparing the thermal conductivity values obtained from our apparatus with other published results of comparable materials. For this purpose, we selected from the literature laboratory experiments which have been carried out on sandy and silty-clayey sediments, in both dry and fully saturated conditions (Roshankhah, 2021; Barry-Macaulay et al., 2013; Chen, 2008; Lu, et al. 2007; Côté and Konrad 2005; Abu-Hamdeh and Reeder, 2000; Kersten, 1949; Farouki, 1981; Johansen, 1977) For the two granulometric classes, different authors commonly provide a range of values for the calculated thermal conductivity as represented in Figure 4-11a. The available information about mineralogical and textural characteristics are reported in the Supplementary Material. As can be observed, the results we obtained nicely fit the ranges of the λ values proposed by different authors. Slight differences or wider ranges by some authors are due to the different tested material either in terms of mineralogy and/or texture as well as sometimes on the different technique applied for drying the samples. For the aims of this paper, the results of the comparison are certainly satisfactory to confirm the reliability of the obtained thermal conductivity values. We also performed several tests by varying the water content for sandy samples. In this case, we compared our results with some empirical relationships proposed in the literature correlating thermal conductivity to the degree of water saturation. Moreover, in this case, the results obtained with our apparatus with different percentage of water content are in perfect agreement with the proposed curves Figure 4-11b.

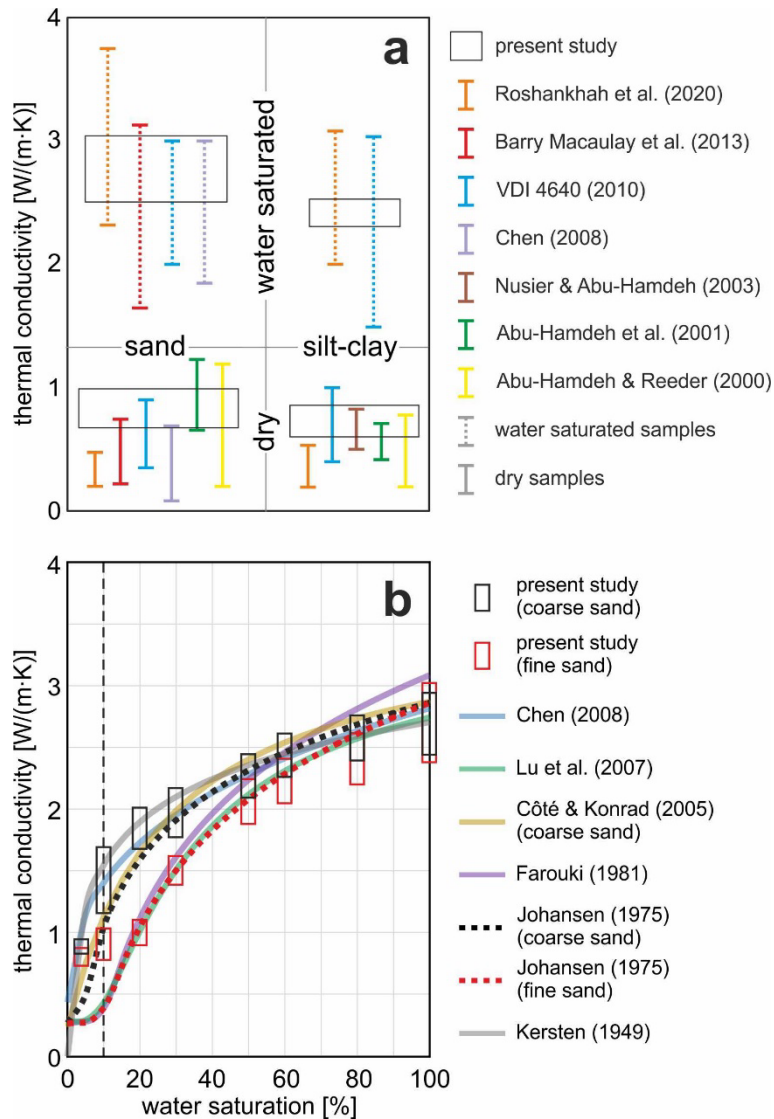


Figure 4-11: (a) Comparison of thermal conductivity values proposed in the literature for sandy (left) and silty-clayey (right) materials with some preliminary results obtained from our laboratory apparatus (Roshankhah, 2021; Barry-Macaulay et al., 2013; Chen, 2008). (b) Comparison between empirical relationships correlating thermal conductivity with water saturation in sands proposed in the literature and some of our preliminary tests on sands carried out with different water content (Lu, et al. 2007; Côté and Konrad 2005; Kersten, 1949, Farouki, 1981 Johansen, 1977). The information provided by the different authors about the mineralogical and textural characteristics of the materials tested for thermal conductivity measurements are reported during next chapters.

The GeoTh laboratory has been tested on various soil samples, demonstrating the validity of the proposed method and its effectiveness in determining the thermal conductivity of granular materials. The results of the conducted tests have been analysed and presented in detail in the article (Rapti et al., 2022).

4.3. Experimental procedure

Here is a detailed procedure for filling a cylinder described in (Rapti et al., 2022), and conducting a test to obtain the thermal conductivity under dry and saturated conditions, as well as the density and porosity of the material:

To prepare the cylinder, first ensure that the PVC cylinder with a metal base is free of dust, debris, and holes in the joint seam. Then, place the cylinder in a stable vertical position on a flat surface. Next, position two PT100 temperature probes at the centre of the cylinder, spaced 7 centimetres apart along the vertical axis and securely fastened together. It's worth noting that we have tried positioning the probes horizontally, but this has not yielded any significant variation in results. After the probes are in place, fill the cylinder with the screened material, adding a layer every 3 centimetres. To aid in the compaction of the material, tap the cylinder laterally with a rubber mallet after each layer is added, and compress the material from above if necessary. As you add material, insert three evenly spaced aluminium film discs per sample to reduce convective motion of fluids within the pores. Once the cylinder is completely filled, add another layer of aluminium film to the surface of the material to minimize convective surface motion and water evaporation during saturation tests. To calculate the bulk density of the material, weigh the cylinder. Then, seal the cylinder with a layer of expanding polyurethane foam around the PVC and place it on the circular resistance covering 90% of the metal base. Start the test by running the dedicated software with 1 watt of power per resistance (Rapti et al., 2022). Wait for the steady-state condition to be reached, which usually occurs after 12-15 hours of heating, depending on the type of material. After 20-24 hours of testing, remove the aluminum film layer on top of the material to add water. Fill the cylinder with water to the brim to prevent air bubbles from forming within the material. This technique allows us to obtain both dry bulk density and porosity data for the same material under both dry and saturated conditions. After the necessary amount of water has been added to saturate the sample, replace the aluminum film layer on top of the material, and wait for steady-state conditions to be reached again during saturation testing. Finally, the test can be considered complete after 20-24 hours of saturation testing

A problem that emerged during data observation is the variability of thermal conductivity with power. This phenomenon has different consequences for different granulometries. It is particularly evident for gravels, where there are wide ranges of values both at low and high power, while for sands, it is less pronounced and it does not occur for silt. Presumably, water at certain temperatures and with

large pores (gravel) has enough space to create convective movements, so that the value of thermal conductivity is influenced not only by conduction, but also by convection. Conversely, in sand and silt, there is not enough space to generate convective motion. Additionally, at low power, the ambient temperature seems to have a significant impact on the value of thermal conductivity, leading to increased uncertainty and range (Figure 4-12a). To overcome this issue, it was decided to insert three layers of conductive aluminium with a thickness of 0.1 mm at different heights inside the cylinder, in order to reduce convective movements between the pores of the materia (Figure 4-12b).

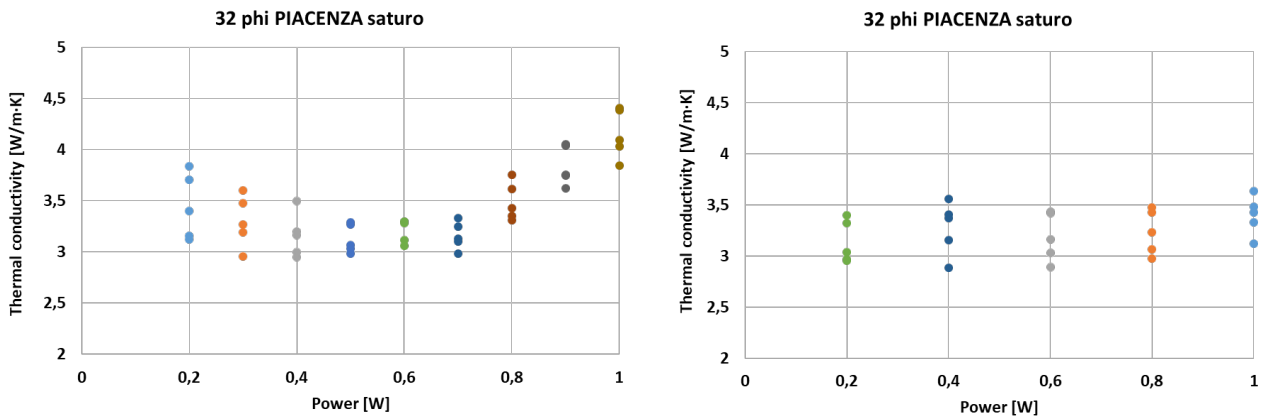


Figure 4-12 : Several test with and without layers.

A good quantity of the sieved material was prepared for reducing systematic errors in the system (such as voltage drops, variations in the cylinder filling procedure of the tester, etc.). To achieve this, some testers were simultaneously tested, each filled with identical material, using the same timing and power parameters

Another factor we analyzed is the influence of temperature on the thermal conductivity value. We conducted several multi-day tests, one of which is shown in Figure 4-13. In this particular test, lasting over 10 days, the ambient temperature fluctuated within ± 0.25 °C, with an average value (during the steady-state phase) of 17.834 °C. Lambda fluctuates with the same frequency as the ambient

temperature, however, the latter has a very limited impact on the final value. The average value is 3.214, while the maximum calculated value is 3.248 and the minimum value is 3.180 $W/m K$.

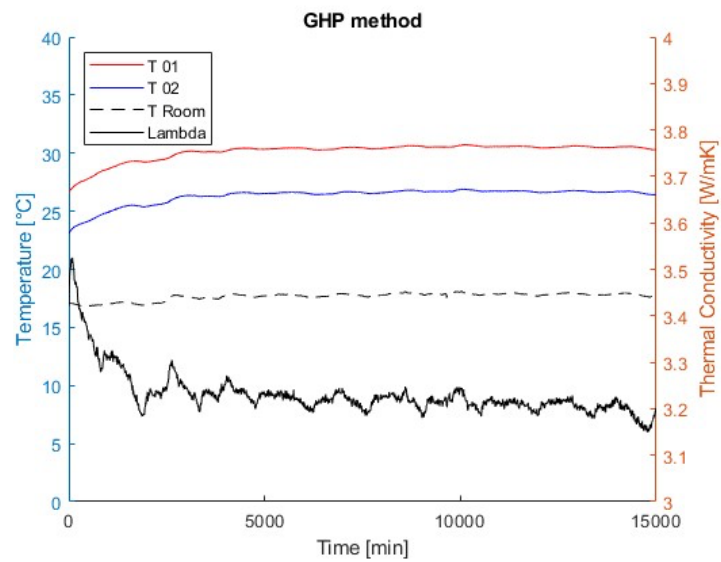


Figure 4-13: Graph representing a test over several days. It depicts T01, T02 T room and the instantaneous thermal conductivity value.

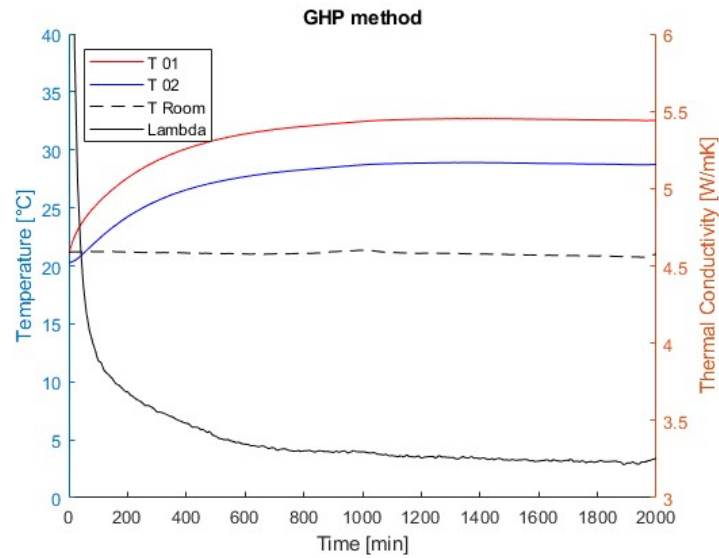


Figure 4-14: Representative graph of a test in the GeoTh laboratory, lasting more than 30 hours.

Moreover, tests typically have a duration of 24 hours in order to minimize the impact of ambient temperature. The power turn on in the morning, allowing the heat flow to reach a steady-state condition overnight, thereby mitigating temperature fluctuations. The attainment of the steady-state phase occurs approximately 800-1000 minutes after the initiation of the test, as corroborated by Figure 4-14. Examining the curve derived from instantaneous thermal conductivity values, it becomes evident that an initial phase ensues, wherein the introduced heat propagates through the test material, resulting in temperature elevations and an exponential decline in thermal conductivity. Subsequently, the slope of the thermal conductivity curve tends to approach a more horizontal orientation, typically after the initial two hours of the experiment, culminating in the establishment of a steady-state regime concurrent with the stabilization of temperatures as measured by the thermal sensors. To yield the most accurate representation, an average value is computed from the commencement of the steady-

state phase until the termination of the test, prior to the influence of subsequent-day heat on the system.

4.4. Samples selection and preparation

Particle size is relevant to many aspects of engineering, petroleum, carbon capture, subsurface research and agriculture industries (e.g., controls on aquifer porosity and permeability in petroleum and groundwater studies). Providing a definition for a ‘particle’ is not an easy task. According to the In the second edition of dictionary of geological terms (The American Geological Institute 1984), a particle is “a general term, used without restriction as to shape, composition, or internal structure, for a separable or distinct unit of rock e.g. a fragment or grain.” This differs slightly from ‘clasts,’ which are defined as “an individual constituent grain, or fragment of a detrital sediment or sedimentary rock, produced by the physical disintegration of a larger rock mass” by the same source. A comprehensive text edited by (Syvitski, 1991), shows that although there are many methods for grain size, none have been adopted as a comprehensive standard in sedimentology and geomorphology. One could argue that the use of protocols of the International Standards Organization (ISO s.d.) or American Society for Testing and Materials (ASTM s.d). are comprehensive standards.

The Udden–Wentworth scale Figure 4-15 has a relatively simple geometric progression of sizes that are based on a logarithmic scale (phi (ϕ) scale) developed by (Krumbein e Pettijohn, 1961). The ϕ scale uses the (negative) logarithm to the base 2 of the grain diameter (d , in millimeters).

The Greek symbols ϕ (lower case) or Φ (upper case) are numerically defined by:

$$\phi = -\log_2 d$$

Equation 4-2

Conversely,

$$d = 2^{-\phi}$$

Equation 4-3

ϕ	PHI - mm CONVERSION $\phi = \log_2 (d \text{ in mm})$ $1 \mu\text{m} = 0.001 \text{ mm}$		SIZE TERMS (after Wentworth, 1922)	SIEVE SIZES		Intermediate diameters of natural grains equivalent to sieve size	Number of grains per mg		Settling Velocity (Quartz, 20°C) cm/sec	Threshold Velocity for traction cm/sec	
	mm	Fractional mm and Decimal inches		ASTM No. (U.S. Standard)	Tyler Mesh No.		Quartz spheres	Natural sand			
-8	256	10.1"	BOULDERS (> -8 ϕ) COBBLES								
-7	128	5.04"									
-6	64.0	2.52"	PEBBLES	2 1/2"	2"					200	
-5	53.9			very coarse	2.12"	2"					150
-4	45.3			coarse	1 1/2"	1 1/2"					100
-3	33.1				1 1/4"	1.06"					
-2	32.0	1.26"		medium	3/4"	.742"					50
-1	26.9				5/8"	.525"					
0	22.6	0.63"		fine	1/2"	.371"					30
-1	17.0				7/16"						
-2	16.0	0.32"		very fine	5/16"	.265"					10
-3	13.4				3/8"						
-4	11.3	0.16"	Granules	4	4					5	
-5	9.52			6	6						4
-6	8.00	0.08"	SAND	7	7					3	
-7	6.73			8	8						2
-8	5.66			10	10	1.2	.72	1.5	10	10	2
-9	4.76			very coarse	12	12	.86	2.0	1.5	8	1
-10	4.00	0.157"		coarse	14	14	.59	5.6	4.5	7	0.5
-11	3.36				16	16				6	0.3
-12	2.83	1/2		medium	18	18	.42	15	13	5	0.2
-13	2.38				20	20				4	0.15
-14	2.00	1/4		fine	25	25	.30	43	35	3	0.1
-15	1.63				30	30				2	0.07
-16	1.41	1/8	very fine	35	35	.215	120	91	2	0.05	
-17	1.19			40	40				1	0.03	
-18	1.00	1/16	coarse	45	45	.155	350	240	1	0.02	
-19	.840			50	50				0.5	0.01	
-20	.707	1/32	medium	60	60	.080	2900	1700	0.329	0.005	
-21	.545			70	70				0.1	0.002	
-22	.500	1/4	fine	80	80				0.023	0.001	
-23	.420			100	100				0.0057	0.00036	
-24	.354	1/8	very fine	120	120				0.0014	0.0001	
-25	.297			140	140				0.00036	0.0001	
-26	.250	1/4	coarse	170	170						
-27	.210			200	200						
-28	.177	1/16	medium	250	250						
-29	.149			325	325						
-30	.125	1/32	fine	400	400						
-31	.105										
-32	.088	1/64	very fine								
-33	.074										
-34	.062	1/128	coarse								
-35	.053										
-36	.044	1/256	medium								
-37	.037										
-38	.031	1/32	fine								
-39	.026										
-40	.021	1/64	very fine								
-41	.016										
-42	.011	1/128	coarse								
-43	.008										
-44	.005	1/256	medium								
-45	.004										
-46	.003	1/512	fine								
-47	.002										
-48	.001	1/1024	very fine								
-49	.001										

Figure 4-15: Comprehensive correlation table showing the relationships between phi sizes, millimetre diameters, size classifications (Wentworth, 1922), and ASTM and Tyler sieve sizes. The table also shows the corresponding intermediate diameters, grains per milligram, settling velocities, and threshold velocities for traction.

The decision to take unconsolidated natural materials for testing is related due to the thesis focuses on low-enthalpy geothermal energy, so it seeks to measure thermo-physical parameters of materials that are predominantly found in the first few hundred metres in the Po Valley.

The unselected material was taken from various quarries or fields in the Po Valley area like: Piacenza, Parma, Reggio Emilia, Ferrara but also in Preveza (Greece). The grain-size characteristics of each sample were determined using the standard sieving technique as described by Switzer (2013), Tanner e Balsillie (1995) and ASTM. These sediments were analysed at granulometric level by means of dry sieves, sedimentation balance and X-ray sedigraph. Commonly, a combination of methods is needed and no particular technique can be considered 'more accurate' or 'more precise' than another.

Geomorphological investigations of landforms composed primarily of sand, silt, and clay material, generally require the routine application of PSA (see reviews of Syvitski 1991a and b).

Analysis procedure

The sample is collected and prepared by removing impurities and reducing the material to usable dimensions for granulometric analysis.

Gravel and sandy material

The sample before sieving was carefully analysed to remove organic material and any marine material (such as shells), except for samples from Greece. This step is only used for the separation of the largest particles, usually larger than 63 micrometres. Sieve analysis is likely the oldest and most conventional technique utilized for the analysis of sand and gravel-sized materials (Krumbein e Pettijohn, 1961). By employing a proper set of sieves, as shown in Figure 4-17, particles ranging from 0.002 to 250 mm in size can be separated into regular size classes. While silt particles can also be sieved, this technique is primarily employed to determine the size of sand-sized materials or larger (McManus, 1988). Sieve screens employed for dry sieving are typically composed of sturdy wire mesh, made of stainless steel or brass, with finer wire meshes employed for smaller particles. In contrast, wet sieving equipment is typically made of stainless steel or plastic, with nylon sieves.

In the realm of particle analysis, the term "particle sieve size" may be defined as either the smallest sieve size that a particle is able to pass through (D_{pass}), or alternatively as the largest sieve size that retains the particle (D_{ret}). The number of sieves employed in the analysis indicates the number of size fractions considered, thereby reflecting the level of analytical resolution. Following sample preparation, the sieve stack is typically subjected to mechanical agitation via a shaker for a fixed time period, typically 15 to 20 minute to reduce the errors (Figure 4-17). The material retained on each sieve is then carefully removed and collected on a sheet of paper. This is achieved by gently tapping the sieve in a diagonal direction, and utilizing specialized brushes to release any particles that may be trapped within the mesh (McManus, 1988). Each fraction of the sediment obtained is subsequently

weighed, often with a precision of 0.01 grams. From these measurements, sieve mesh sizes, raw weights, weight percentages, and cumulative percentages of finer or coarser particles may be calculated.

Sedimentation balance: The sieved sample is mixed with water and a dispersing agent to create a suspension. The suspension is placed in a sedimentation cylinder, where the particles settle based on their sedimentation velocity. The weight of the particles that settle on the bottom of the cylinder is measured using a sedimentation balance, from which the granulometric distribution of the material can be determined using a dedicated software (Figure 4-16).



Figure 4-16: Sedimentation balance Physics and Earth Sciences Department at University of Ferrara (ITALY)

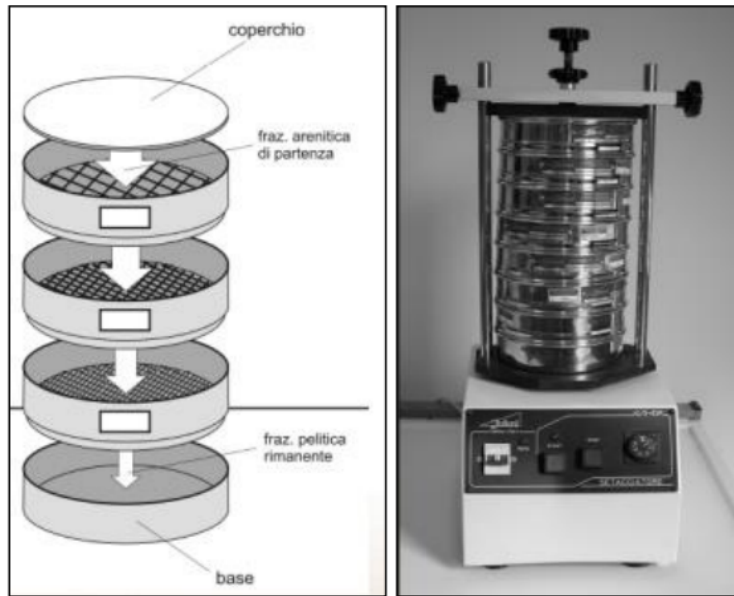


Figure 4-17: Sieve stack and mechanical sieving instrument.

Loamy and clayey material

Prior to the introduction of laser-based particle-size analysis, the determination of grain size in silts and clays relied heavily on indirect calculations of particle diameters. These calculations were based on observations of grain behaviour in fluids, or the impact of grains on fluid displacement. Such methods are commonly referred to as sedimentation methods and rely on the rate at which particles settle through fluids. By utilizing this information, settling velocities can be determined and equivalent grain diameters subsequently calculated.

The calculation of equivalent diameters from settling velocities of particles is grounded in Stokes' Law of settling, which assumes that sediment particles are predominately spheres of uniform density. This assumption is unlikely to be true for most natural sediments. Stokes' Law is premised on the principle that a particle settling in static water will do so at a consistent velocity, during which the gravitational force exerted on the particle is balanced by fluid resistances characterized by viscosity and the particle-drag coefficient. This balance is typically expressed mathematically through the use of an equation:

$$V_s = \frac{D^2(\rho_s - \rho)g}{18\mu}$$

Equation 4-4

In this equation, V_s denotes the settling velocity of the particle, D refers to the particle diameter in millimetres, ρ_s and ρ represent the densities of the particle and water, respectively, g is the gravitational acceleration, and μ signifies the dynamic viscosity of the fluid. The particle size can be determined by rearranging the equation as follows:

$$D = \sqrt{\frac{18\mu V_s}{(\rho_s - \rho)g}}$$

Equation 4-5

For the analysis of our samples we used the Micromeritics Sedigraph 5100, which uses an X-ray beam to measure the size of the grains and their quantity. The X-ray sedimentation technique is a reliable method for determining the relative mass distribution of a sample according to particle size. This technique is rooted in two fundamental physical principles: sedimentation theory and the absorption of X-radiation. These principles are embodied in an analytical instrument known as the SediGraph, in fact. Any particle settling in a liquid will achieve a terminal velocity when the forces of buoyancy, drag, and gravity are balanced. This velocity is dependent on the size and density of the particle, as well as the density and viscosity of the liquid. A beam of photons, such as X-rays, passing through a medium is attenuated in proportion to the length of the path through the medium, the concentration of the medium, and the extinction coefficient (Switzer, 2010).

By employing Stokes and Beer-Lambert laws, raw data can be interpreted to establish the correlation between fundamental measurements and the reported size distribution. This interpretation is necessary to comprehend the complex relationships between particle size and other physical properties of the sample.

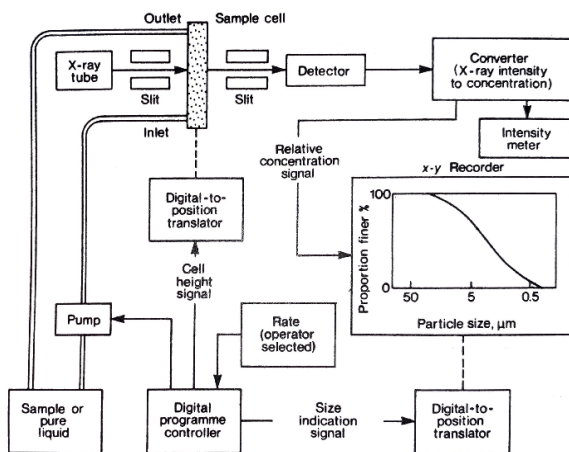


Figure 4-18: Left) Simplified schematic diagram of the X-ray Sedigraph instrument (Syvitski, 1991); Right) Micromeritics Sedigraph 5100 at Physics and Earth Sciences Department at University of Ferrara (ITALY).

The process of sieving sandy materials according to the (ASTM s.d) with sedimentation balance and X-ray sedigraph is more precise and accurate than simple manual sieving, and we used these method to measure the cumulative curve of grain size of our unselected materials.

Our materials and innovative aspect

Unconsolidated sedimentary particles range in size from boulders (e.g., glacially produced products) to colloids (Wentworth, 1922). This work deals with quartzose sediment sizes ranging from about -6

ϕ (64 mm) to about 10 ϕ (0,001 mm), that is, those sediments are gravelly, sandy, silty and clayey materials.

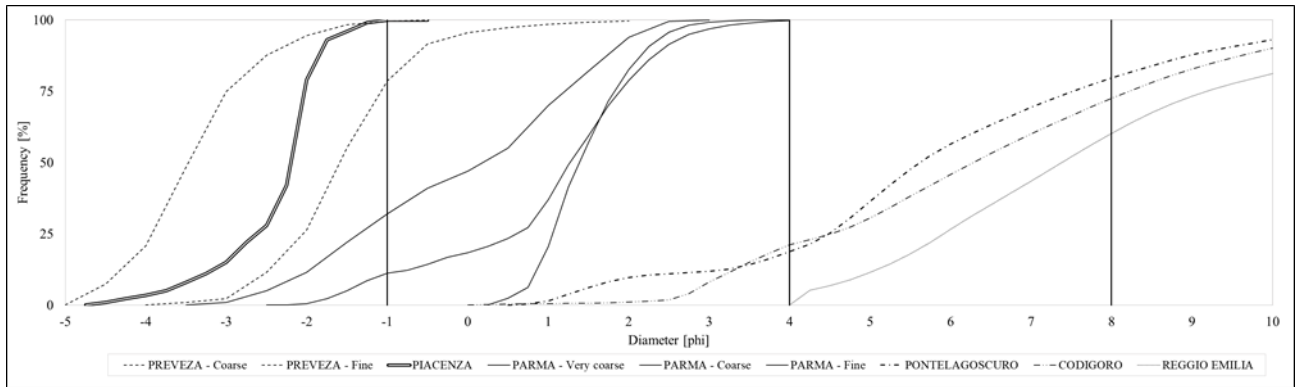


Figure 4-19: Grain size results of unselected samples

Each sample was cleaned and dried in an oven at 80 °C (105°C for gravel and coarse sand) for about 24 h.

For this project, it was decided to take an innovative step for the literature, i.e. not to use only unselected materials taken from the field, but to sieve them in the Phi range. The sieves used were selected to divide the material into range of one phi, as fine pebbles (-3/-2 ϕ), very fine pebbles (-2/-1 ϕ), very coarse sand (-1/0 ϕ), coarse sand 0/1 ϕ , medium sand (1/2 ϕ), fine sand (2/3 ϕ), very fine sand (3/4 ϕ), coarse silt(4/5 ϕ), medium silt (5/6 ϕ), clayey silty (6/11 ϕ). Subsequently, the individual ranges will be defined without the 'slash' in the text, i.e. 32 ϕ to mean fine pebbles.

5. Experimental results and discussions

More than a thousand different tests were conducted, all with common purposes, including the comparison of thermal conductivity variation with grain size. We consistently took into account several other factors mentioned earlier. There are few works in the literature concerning this topic (Gori et al., 2001; Midttømme and Roaldset 1998; Inaba 1986), and none of them addresses the approach we have taken, which involves dividing the materials into small and specific grain size ranges. The study of several grain sizes is derived for the consociated variability of thermal conductivity with this factor, but that has not been analysed in the specific for geological purposes.

In general, a compact material without fractures exhibits higher conductivity compared to one with fractures. The case of quartz serves as an example: quartz without fractures has a conductivity of 7,8 $W/m K$, while quartz with few fractures is approximately 5 $W/m K$. As fractures increase and grains form, materials with larger grains tend to have higher thermal conductivity compared to those with smaller grains. This phenomenon is attributed to the presence of more empty space between larger grains, which act as more efficient thermal conductors, facilitating smoother heat transfer through the material. In other words, the presence of void spaces between grains allows for greater heat transfer.

On the other hand, materials with smaller grains have a higher specific surface area compared to those with larger grains. This implies a greater amount of contact surface between the grains, which can hinder heat flow. Smaller particles tend to adhere more tightly to each other, reducing the amount of empty space and increasing resistance to heat transfer. Consequently, materials with smaller grains generally exhibit lower thermal conductivity than those with larger grains. Therefore, it is important to underline that thermal conductivity also depends on other factors, such as the chemical composition of the loose materials and the degree of water saturation. However, grain size remains a determining factor in the relationship between thermal conductivity and loose materials such as sand and silt. (Dalla Santa et al. 2020; Bertermann et al., 2018; Tarnawski et al., 2011; Hamuda et al., 2011; Gori et al., 2001; Inaba, 1986)

5.1. Porosity and bulk density

Our materials differ in nature and origin, but both sieved and no-sieved materials fall within a narrow enough range of porosity and bulk density values that it was not deemed appropriate to study the

performance of these two factors, which were nevertheless considered important in characterising the samples used for testing (Marchetti et al., submitted).

5.2. Lambda vs grain size

The relationship between thermal conductivity and grain size in unconsolidated natural materials is a topic of great interest in geotechnical materials science. Several studies have investigated the relationship between thermal conductivity and grain size in natural unconsolidated materials, aiming to understand how grain size influences the heat conduction capacity. Below, we will review some of the most relevant works concerning this relationship.

Midttømme and Roaldset (1998) investigated thermal conductivity on fragmented quartzose materials. They argue that the grain size influences the size, shape, and distribution of pores, and that with the same porosity but different pore sizes, heat transfer varies significantly. They conducted tests on shards of nearly pure quartz materials with different particle size ranges, which they compacted to create 30 cm³ cubes. Two theories arise from the results: (i) grain size affects porosity, thereby altering thermal conductivity, or (ii) porosity itself is the determining factor. In any case, this work demonstrates the influence of particle size on thermal conductivity, even though the tests were performed on crushed quartz materials and thus differ greatly from real soils. It's understandable how a study of particle size distribution could be essential for better understanding and applying the identified relationships.

In the work of Dalla Santa et al. (2020) a new database of thermal properties for unconsolidated sediments and rocks was developed using literature data and over 400 direct measurements. Attempting to directly measure the thermal properties of gravel samples proved to be challenging, particularly due to technical issues associated with the extremely coarse grain sizes of the sediments. These sizes prevent sufficient physical contact between the tested material and traditional thermal measurement sensors. For instance, in dry gravel, they obtained a thermal conductivity value of 0,55 W/mK. After compiling literature data and using their own measurements, in agreement with the literature, they argue that the relationship between thermal conductivity values and characteristics of unconsolidated sediments (fine and coarse), such as particle size, porosity, mineralogical composition, and water content, still needs to be clearly understood, but well-defined relationships exist among some of these factors. For example, the fundamental role of water saturation.

Additionally, from their direct tests, it is evident that saturated gravel has a lower value than saturated sands.

Brigaud and Vasseur (1989) base their interpretation on laboratory measurements of conductivity, porosity, and mineralogy conducted on small volumes (around 100 cm³) of water-saturated, moist, and air-saturated samples. This is to estimate the thermal conductivity of major non-clay and clay sedimentary minerals, particularly focusing on clay minerals. They conducted various tests, analysing the quantity of quartz from 10% to 90% and the clay mineral content from 30% to 80% in the samples, stating that mineralogy doesn't have as much influence as porosity, which is a key factor instead. Later on, we will see that our theory also relies on the fact that mineralogy does not significantly influence the lambda value.

Another significant study by Bertermann et al. (2018) explains in the paper the thermal conductivity as a fundamental property for assessing the geothermal potential of very shallow geothermal systems. Lambda was analysed and measured using a commercial device, also studying other parameters (bulk density, water content, and porosity) determined for a wide range of different textural soil classes. In this case, they used the USDA soil texture classification, thus employing a triangular diagram with natural unconsolidated materials. Their data confirms that coarse materials exhibited higher thermal conductivity values compared to fine materials. Specifically, clay has the lowest values (0,9 W/m K), while loamy sand and sandy loam displayed very high thermal conductivities (2,5 W/m K). Therefore, in general, they mainly examined the particle size curve and bulk density; under saturation conditions, the higher the amount of sand or quartz grains, the higher the soil's thermal conductivity. Furthermore, high bulk density also significantly enhances thermal conductivity.

Tarnawski et al., (2011) focused on the thermal conductivity of sandy deposits with variable particle size distributions, primarily using sands with high quartz content and a transient thermal probe for measurements. The thermal conductivities of fully saturated sand increase as porosity decreases; this is just one of the results presented in this article. The results also indicated that well-sorted deposits with a uniform particle size distribution exhibit higher thermal conductivity compared to those with an irregular particle size distribution. The text also discusses temperature variations; however, we did not include this parameter in the study as it pertains to research focused on shallow geothermal systems. Ultimately, this work concludes that both dry and saturated lambda values strongly depend on porosity, water saturation, solid phase thermal conductivity, and to a lesser extent, the heat conduction pathway through solid contacts.

Hamuda et al., (2011) created a device for testing dry and wet soils in order to examine the impact of porosity and particle size distribution on effective thermal conductivity. They studied four types of sand were used. The sands ranged from coarse to fine in particle size, including coarse sand, medium-grain sand, fine sand, and a sand mixture. Various soil samples were also tested under fully saturated conditions. The porosity range was between 30% and 40%. The instrument can accommodate two samples for testing, each with a heater at the middle. The results confirmed the significance of water saturation and revealed that larger particle sizes exhibit higher lambda values. The effective thermal conductivity of the tested soils depends on the volumetric proportions of components, particle sizes and arrangement within the soil, and interface relationships.

Tavman 1996's laboratory investigation showed comparable results. The results of experiments on construction sand of variable grain size and porosity in air at atmospheric pressure are compared to theoretical models. The effective thermal conductivity dropped as the effective particle size decreased. The reduction in effective thermal conductivity with smaller grain size can be explained by the need for more particles for the same porosity, which results in increased thermal resistance between particles.

Additionally, the works of Gori et al., 2001 and Inaba (1986) investigated thermal conductivity, focusing on the relationship between lambda and grain size while eliminating variables such as grain roughness or mineralogy by using glass spheres. Their studies examined gravel and sand, yielding results consistent with the trends identified in our research. In the subsequent chapters, we will further explore these significant studies and reference their results to support our conclusions.

Through our study, we have contributed to a deeper understanding of the relationship between granulometry and thermal conductivity of materials (Marchetti et al., submitted). Our findings clearly indicate that grain size plays a significant role in determining the thermal properties of materials. Particle size and gradation heat flux between particles is proportional to the radius of the particles. Larger particles and fewer contacts in a given volume result in higher thermal conductivity. Well-graded soil exhibits higher heat transfer as small particles fill the interstitial pore space and increases the inter-particle coordination (Dong et al., 2015).

Generally, different software and different calculations are used in applications to create and investigate feasibility studies for geothermal plants. When analysing the subsurface, very approximate and too general values for thermal conductivity are used. Such values may be those commonly accepted and extrapolated from (VDI, 2010)

Sediment category	Thermal conductivity [W/mK]		Recommended value
	Min-value	Max-value	
Gravel dry	0,4	0,9	0,4
Gravel water-saturation	1,6	2,5	1,8
Sand dry	0,3	0,9	0,4
Sand moist	1	1,9	1,4
Sand water-saturated	2	3	2,4
Clay / silt dry	0,4	1	0,5
Clay / silt water-saturated	1,1	3,1	1,8
Till / loam	1,1	2,9	2,4
Peat, soft lignite	0,2	0,7	0,4

Table 5-1: Thermal conductivity reference from VDI 2010.

We therefore first tested some materials comparable with those used in VDI 2010, trying to investigate all the parameters mentioned and then focusing on thermal conductivity. After investigating these aspects, we did the same with materials sieved in specific ranges, the same results are published in Marchetti et al., submitted.

5.2.1. Results and discussion

The materials initially tested were no-sieved from Parma. These materials have a particle size distribution shown in (Figure 4-19), with over 80% sand and 0, 10 and 20% gravel content within fine Parma material (F-PA), coarse Parma material (C-PA) and very coarse Parma material (VC-PA) respectively. The most relevant results are shown in Table 5-2. It can be observed that the porosity range is very similar, while the apparent density increases with the increase of coarser material within the sample. The mineralogy is very similar, with quartz content never exceeding 60%, but VC-PA has about 25% carbonate minerals (mainly calcite and dolomite). Their thermal conductivity values in dry conditions range between 0,84-1,08; 0,84-0,98 and 1,08-1,43 W/mK , respectively. In saturated conditions, their thermal conductivity values range between 2.87-3.31, 2.53-3.23 and 3,02-

3,72 W/m K. The mean values and the porosity values calculated by the Missimer and Lopez (2018) are also in the Table 5-2.

	Porosity	Bulk density	Mineralogy	Mean thermal conductivity	Grain Size
	[%]	[kg / m ³]	Qz / Pl / K-Feld / Carb [%]	Dry / Sat [W/mK]	Gravel / Sand / Silt / Clay [%]
Very coarse	23 - 27	2015 - 2100	45 / 12 / 2 / 25	1,2 / 3,3	35 / 65 / 0 / 0
Coarse	33 - 36	1630 - 1660	60 / 11 / 7 / 7	0,9 / 2,9	10 / 90 / 0 / 0
Fine	33 - 35	1455 - 1555	60 / 16 / 5 / 5	0,9 / 3,1	0 / 100 / 0 / 0

Table 5-2: Main parameters of unselected materials from Parma.

The same parameters were investigated on sieved materials (1 phi range). For this purpose, we obtained materials from Parma (PA), Piacenza (PI), and Preveza (Greece, GR) for gravel and sand particle sizes. For silt particle size the samples were taken from Reggio Emilia (4/5 phi, 5/6 phi and 6/10 phi, RE), Pontelagoscuro (after sieved, 98% of the grain size distribution curve within the silt range, 4/8 phi, PO) and Codigoro (where the material had over 78% silt and clay content, 4/10 phi, CO).

The results relative to the sieved materials are reported in Table 5-3, divided by grain size. In general, porosity data do not show large variations with grain size, settling from 40 to 43% (the average values for samples from Greece is 35%). In fact, we hypothesized that porosity has less importance in varying thermal conductivity data than other parameters such as water content, grain size and mineralogy. The average value of bulk density is 1500 kg/m³ for sandy ranges, while lower values are recorded for silty and clayey materials, from 1000 to 1300 kg/m³. Thermal conductivity results were divided into two rows, one for the dry condition and one for the saturated condition. This was done because the thermal conductivity value for the same grain size range can increase by over 300% when all pores are filled with water. Lambda in dry conditions has an overall range between 0,81 and 1,02 W/m K. Instead, with the addition of water, variability increases and the overall range varies between 1,75 (6/10 phi) and 3,24 (-3/-2 phi) W/m K. In Figure 5-1, the range of thermal conductivity

and the average value for each grain size range can be observed. Overall, the data obtained from the experiments are over a thousand. Individual phi ranges have been tested dozens of times to get good statistics of the data.

Grain size range	Thermal conductivity dry [W / mK]	Thermal conductivity sat [W / mK]	Bulk density [kg / m ³]	Porosity [%]
-3/-2 φ	1,02	3,24	1534	41
-2/-1φ	0,94	2,81	1545	43
-1/0 φ	0,88	2,79	1553	43
0/1φ	0,88	3,06	1499	41
1/2 φ	0,86	2,99	1455	40
2/3 φ	0,81	2,68	1430	41
4/5 φ	0,95	2,70	1584	
4/8 φ	0,81	2,34	1288	
5/6 φ	0,88	2,59	1347	
4/10 φ	0,82	2,19	1174	
6/10 φ□		1,67	1017	

Table 5-3: Main parameters of sieved samples

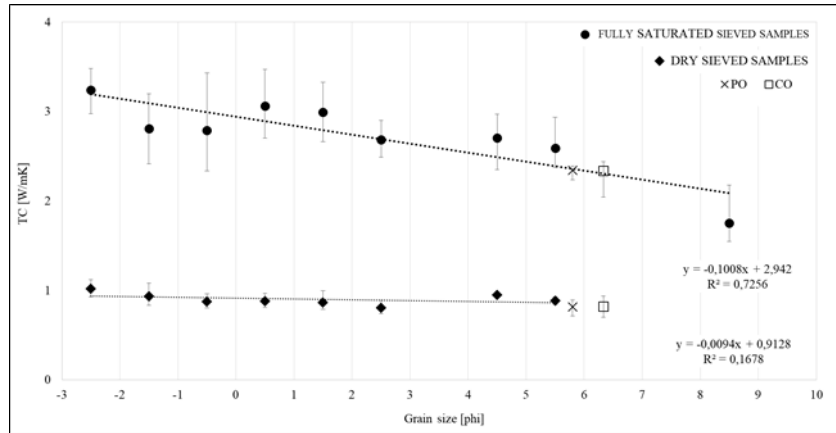


Figure 5-1: Comparison data of thermal conductivity mean value versus grain size. The dashed lines are the trend lines.

Regarding thermal conductivity, by also including data from the RE, PO, and CO samples, it can be observed from the Figure 5-1 that the maximum and minimum mean values under dry conditions from $-3/-2 \varphi$ to $4/10 \varphi$ are 1.04 and 0.81, respectively, with a difference between the maximum and minimum value for each range no greater than $\pm 0.12 \text{ W/mK}$ ($-2/-1 \varphi$). In fully saturated conditions, for the same grain sizes and a range of very fine material ($6/10 \varphi$), the overall maximum mean value is 3.24 and the minimum is 1.75 for $-3/-2 \varphi$ and $6/10 \varphi$. In this case, there is a variability of $\pm 0.54 \text{ W/mK}$ ($-1/0 \varphi$). In the two ranges where the highest uncertainty values have been detected, it can be observed that in relation to the continuous linear decrease in thermal conductivity values with grain size, at $-2/-1 \varphi$ and $-1/0 \varphi$, then in dry and saturated conditions (more evident), there is a slight negative peak in the trend. These two ranges are also those that show a higher average porosity and bulk density and a lower quantity of quartz (more evident in the samples from Parma). However, these two ranges belong to the gravelly class, and the thermal conductivity values of gravel are slightly lower than sand, as shown by the studies of Hamuda et al., (2011) and Gori et al., (2001).

5.3. Lambda vs Mineralogy

In addition to grain size, we investigated the significance of mineralogy. The most effective technique for examining the presence of minerals and identifying them in soils is undoubtedly X-ray diffraction

(XRD). Through a specific procedure outlined below, along with specialized software for qualitative and quantitative analysis, the percentages of minerals present in the tested samples can be derived.

5.3.1. XRD analysis

X-ray Powder Diffraction (XRPD) measurements of polycrystalline samples require specific sample preparation and instrumentation. Coarse powders need to be reduced to a grain size suitable for XRPD. In the specific case, approximately two grams of material, as representative as possible, are extracted from the initial sample after two series of quartering. The sample is then ground in an agate mortar until it reaches a particle size below ten microns. Once reduced to powder, the sample is loaded in polymethyl methacrylate (PMMA) sample holders. These holders consist of a plate to be fitted into the corresponding space in the diffractometer. They have a cavity to accommodate the powder, and upon sample loading, it is necessary to fill the cavity in order to achieve sample surface aligned with the top holder surface. This must be done without inducing any preferential orientation to the microcrystalline structure, especially in the case of clays. The diffraction measurements were performed on a Bruker D8 Advance DaVinci diffractometer equipped with a copper tube X-ray source equipped with a Si(Li) solid-state detector available at the Diffraction Lab of the Physics and Earth Science Department of the University of Ferrara. X-ray diffraction pattern was collected in continuous mode from 3–80 °2 θ , with step size of 0.02 °2 θ and a counting time of 5 s per step. The measured XRD patterns (intensity vs. 2-theta angle) are reported in several Figures (Appendix A). It is important to note that if a mineral phase is present in a weight fraction less than one percent, depending on the mineral phase, it might go undetected. Pattern fitting and quantitative phase analysis (QPA), performed through the Rietveld method, took advantage of the Profex version 4.3.6 (BGMN) software. Some representative fits are reported in Appendix B.

The measured patterns has been analysed with Profex (BGMN) software (v. 4.3.6). First, it has been done the mineral phases identification with Profex internal database and COD database; then pattern fitting based on the Rietveld method has been used for quantitative phase analysis (QPA) by the same software.

Generally, mineralogy is related to grain size in sedimentary facies. There is typically a significant correlation between mineralogy and grain size. Most of the materials used contain large amounts of quartz, which exhibits high thermal conductivity ($\lambda_{\text{QUARTZ}} = 7,8 \text{ W/m K}$). The presence of clay minerals is a characteristic property of claystones. Clay minerals have low thermal conductivities

($\lambda_{\text{ILLITE}} = 1,8 \text{ W/m K}$; $\lambda_{\text{SMECTITE}} = 1,9 \text{ W/m K}$; $\lambda_{\text{KAOLINITE}} = 2,8 \text{ W/m K}$ (values from Brigaud and Vasseur 1989; Horai 1971)).

Mineral	Thermal conductivity W/m·K
Quartz	7.8
Calcite	3.4
Dolomite	5.1
Anhydrite	6.4
Pyrite	19.2
Siderite	3.0
K-feldspar	2.3
Albite	2.3
Mica	2.3
Halite	6.5
Kaolinite	2.8
Illite	1.8
Mixed layer I/S	1.9

Figure 5-2: Thermal conductivity of common minerals in sediments rock.

Test performed on monominerals in double-distilled water (Horai, 1971).

In our specific case, we conducted XRD analysis on all the samples used and tested to understand how the increased presence of certain minerals could affect the thermal conductivity value. Since the materials from which we obtained the individual ranges have different origins, particularly for the sandy and gravelly ones, we performed both mineralogical (Table 5-4) and thermal (Table 5-6) analyses on the individual groups.

[%]	PARMA [%]								PIACENZA [%]								GREECE [%]			
	Plagioclase	Clay mineral	Quartz	Mica	Carbonate	Serpentine	K-Feld	Others	Plagioclase	Clay mineral	Quartz	Mica	Carbonate	Serpentine	K-Feld	Others	Plagioclase	Quartz	Carbonate	Pyroxene
-4/-3 φ	4	2	20	5	53	6	9	2	9	10	42	2	28	2	7	1	9	90	0	
-3/-2 φ	5	4	25	4	58	3	2	2	8	10	54	5	16	1	4	1	10	89	0	
-2/-1 φ	6	4	24	8	45	2	6	5	14	11	41	5	19	1	9	1	9	90	1	
-1/0 φ	5	3	21	27	36	1	3	4	10	6	56	7	13	2	7	1	9	90	0	
0/1 φ	12	3	59	4	15	2	5		15	9	64	3	3	1	7					
1/2 φ	16	5	51	8	6	3	6	4	18	7	57	5	2	1	8	2				
2/3 φ	13	4	43	7	14	1	9	8												
3/4 φ	7	8	36	7	17	1	16	9												
4/5 φ	10	6	37	20	21	1	5													
5/6 φ	11	20	33	14	19	0	3													
6/11 φ	4	22	18	26	18	12	0													

REGGIO EMILIA [%]

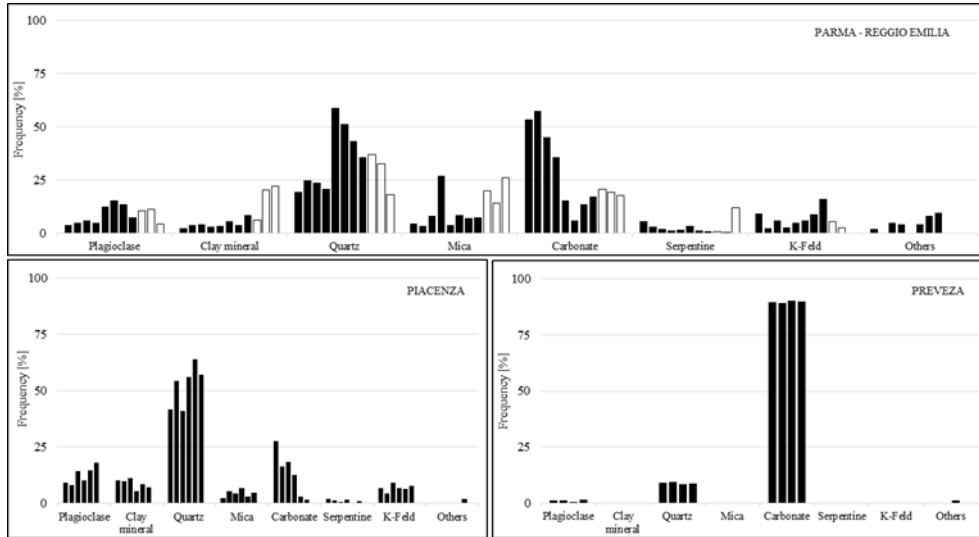


Table 5-4: Results of mineralogical analysis of sieved materials by XRD. From left to right, the particle size decreases. The first left column is -4/-3 φ.

[%]	Plagioclase	Clay Mineral	Quartz	Mica	K-Feld	Carbonate	Serpentine	K-Feld
Very coarse	12	8	43	8	0	25	3	2
Coarse	11	4	59	4	5	15	1	2
Fine	16	7	60	5	3	6	0	2

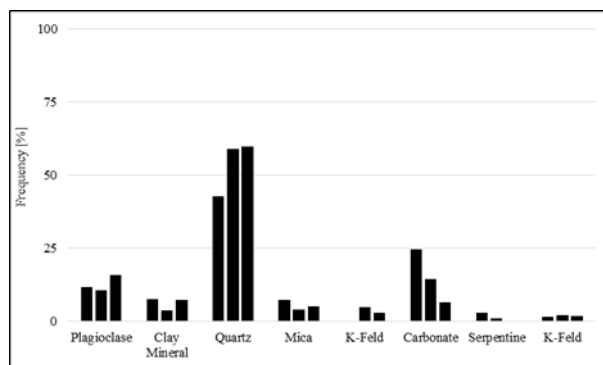


Table 5-5: Results of mineralogical analysis by XRD of not-sieved materials from Parma. From left to right, the particle size decreases. The first left column is "Very coarse".

	Thermal conductivity dry [W / mK]			Thermal conductivity sat [W / mK]			Porosity [%]			Bulk density [kg / m ³]			Quartz [%]			Carbonate [%]		
	PA	PI	GR	PA	PI	GR	PA	PI	GR	PA	PI	GR	PA	PI	GR	PA	PI	GR
-3/-2 φ	1,1	1,0	0,9	3,2	3,3	3,1	42	40	35	1580	1544	1505	25	54	10	53	28	90
-2/-1 φ	0,9	1,0	0,9	2,8	2,9	2,8	43	41	35	1595	1515	1653	24	41	9	58	16	89
-1/0 φ	0,9	0,9	0,8	2,8	3,1	2,4	43	40		1631	1477		21	56	9	45	19	90
0/1 φ	0,9	0,9		3,1	3,0		40	40		1499	1477		59	64		36	13	
1/2 φ	0,9	0,8		3,0	3,0		39	40		1460	1442		51	57		15	3	
2/3 φ	0,8			2,7			42			1427			43			6		

Table 5-6: Parameter data divided by range size and provenance.

5.3.2. Results and discussions

The data in Table 5-4 reveal that quartz and carbonates (calcite and dolomite) are the most common minerals. In the Parma no-sieved samples Table 5-5, the amount of quartz fluctuates between 20 and 25% in the gravel and very coarse sand classes, whereas as the granulometry drops from 0/1φ, the amount of quartz steadily reduces (58, 51, and 43%). The percentage of the same mineral in the Piacenza samples is around 50%, with no variance across the classes. The proportion of quartz amount in Greek samples, on the other hand, seldom reaches 10% (in the absence of trends). In terms of carbonate minerals, the Parma samples show a steady decrease in percentage from 27% to 3%. The same pattern may be seen in Piacenza samples ranging from 55% to 6%. For Preveza samples, the value is consistent at around 90%.

In terms of carbonate minerals, the Parma samples show a steady decrease in percentage from 27% to 3%. The same pattern could be seen in Piacenza samples ranging from 55% to 6%. While the quantity of quartz in Greek samples is consistent at roughly 90%. In Figure 5, the amount of carbonate minerals are plotted versus thermal conductivity for verifying possible effects on the parameter, both in dry and saturated conditions together. No correlation is observed between lambda and the percentage of quartz and carbonate minerals observed individually (Figure 5-3A and B). The similar value of lambda can be obtained with different amount of quartz, from 10 to 60%. The same goes for carbonate minerals, confirming (Brigaud and Vasseur, 1989).

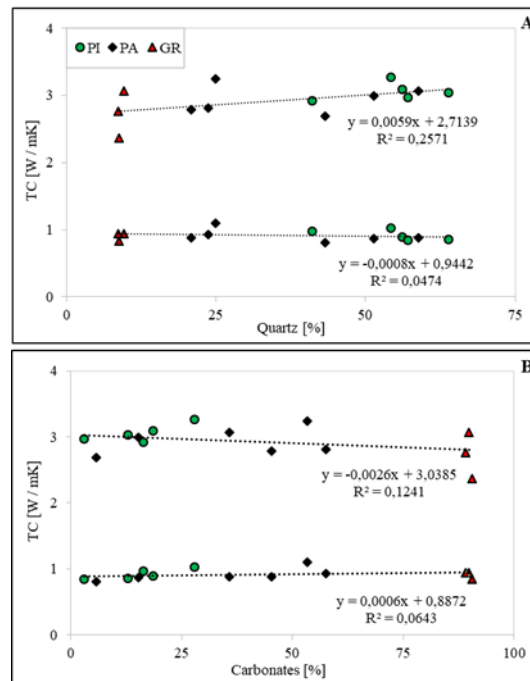


Figure 5-3: The graphs show the variation in thermal conductivity values under dry and fully saturated conditions versus mineralogy. PA: Parma, PI: Piacenza, GR: Greece (Preveza). **A)** Thermal conductivity vs. quartz content; **B)** Thermal conductivity vs. carbonate mineral content

5.3.3. Glass beads

In addition, we wanted to test the glass beads since they have the ability to adjust numerous aspects such as rounding, roughness, and texture aspect. Indeed, over the years, the study of glass spheres has frequently been employed in several sectors to simplify a situation and explain its core notions.

Gori et al. (2001) are the leading exponents in this subject of thermal conductivity. The influence of spherical grain size on thermal conductivity is examined using a needle probe (ILS technique) in this work. Of course, the value of lambda is smaller than that of natural soil, but it is feasible to compare the statistics published in the article to those presented in this thesis.

To validate the validity of the literature data, we performed tests on glass beads with the GHP system, although in a different configuration from that shown in the previous chapters. In Alberta, Canada, we used a laboratory at the University of Calgary. Figure 5-4 depicts the instrument configuration. Unlike the apparatus described in Rapti, et al. (2022), this one included a reference material with a

known thermal conductivity value. The addition of this reference material reduced the number of required tests because the precision and quality of the obtained results were confirmed by the reference material's known thermal conductivity value. As a result, the thermal conductivity of the material under test, with an unknown λ , was measured concurrently. An illustration of heat flow uniformity inside the device during a test is shown in Figure 5-5.

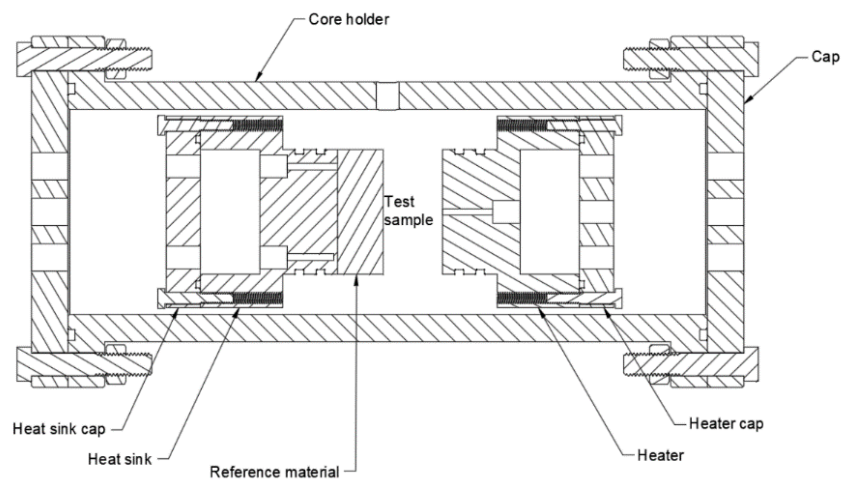


Figure 5-4: Thermal conductivity setup of University of Calgary

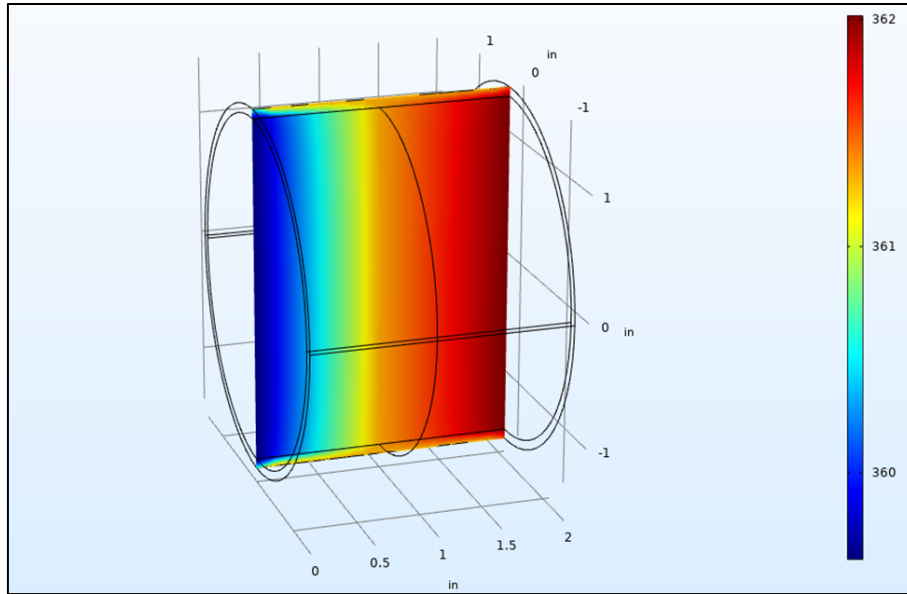


Figure 5-5: Example of simulation of the heat transfer profile by COMSOL software for the saturated case.

The temperature unit is Kelvin.

$$\lambda_{sample} = \lambda_{ref} * \left(\frac{T_2 - T_3}{L_{ref}} \right) * \left(\frac{L_s}{T_1 - T_2} \right)$$

Equation 5-1

The calculation of the thermal conductivity of the material under test, as well as the value of the thermal conductivity (λ) of the reference material (λ_{ref}), is expressed in Equation 5-1. Also important is the inclusion of the thickness of the reference material (L_{ref}) and the thickness of the test sample (L_s). The other parameters are the temperature between test sample and reference material (T_2) and the temperature between reference material and the heat sink (T_3).

Figure 5-6 shows how, under dry conditions, a nearly steady trend in the grain size range of $-3/2 \phi$ to $3/4 \phi$ is observed, similar to that shown in natural materials alone. When the glassy materials are fully saturated, a positive trend from $-3/2 \phi$ particle size range to $0/1 \phi$ particle size range is observed, reaching a maximum peak. From grain size $0/1 \phi$ to $3/4 \phi$, the trend reverses and

becomes negative. This pattern matches exactly what was discovered in the natural samples studied throughout this thesis at the GeoTh laboratory.

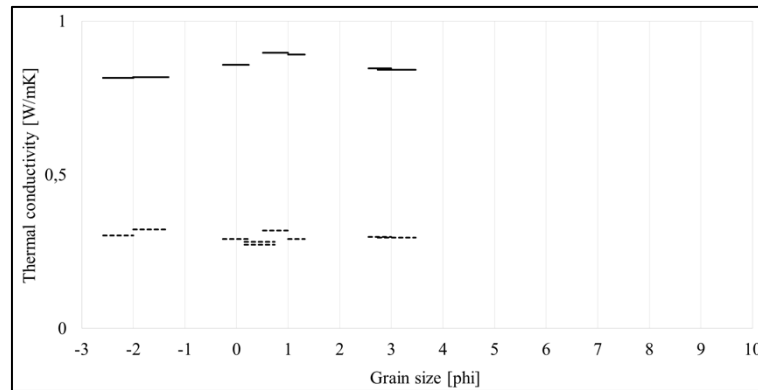


Figure 5-6: Dataset of glass beads tested

Great uncertainty exists with grain sizes bigger than -2 phi, because coarser material could not be tested using the University of Calgary system, whereas with GeoTh, the diameter of PT100 (D) could not exceed the diameter of the grains (d) to be tested. The D/d ratio must be greater than one. This can have a significant role in raising the uncertainty of measured data during testing (Inaba, 1986).

5.4. Lambda vs Water saturation

Water saturation (W_s), is a percentage of the total volume of pores in a substance that measures the amount of water contained in the soil or another porous material. In other words, it represents the amount of porous space filled with water in relation to the maximum filling capacity. W_s influences the thermal conductivity of porous materials such as soil, according to scientific literature and study. Thermal conductivity increases when the soil is completely saturated with water. Because water is a good conductor of heat, the presence of more water inside the soil enhances heat transfer through the

porous medium. Thermal conductivity diminishes when the soil is partially or fully dry (low water saturation). This is because air, which has a poorer thermal conductivity than water, can occupy the vacuum spaces between soil particles and impede heat transport. Understanding how thermal conductivity varies with water saturation is critical for researching heat exchange phenomena in soil, water infiltration, and moisture transportation in the ground, as well as constructing thermal insulation systems and groundwater management.

It was discovered that the difference between dry and saturated values vary by up to 300%. Thus, in partially saturated soils, the volume percentage of fluid water content is a dominating determinant for thermal conductivity. The addition of tiny amounts of water boosts thermal conduction considerably in the region of residual water content (Figure 5-7). The rise in thermal conductivity with increased water content in unsaturated soils shows that porous fluid conduction plays an essential role (Roshankhah et al., 2021; Di Sipio and Bertermann, 2017; Dong et al., 2015). The link between thermal conductivity and water saturation is important in many scientific and practical fields, including geology, hydrology, geotechnical engineering, and building temperature control.

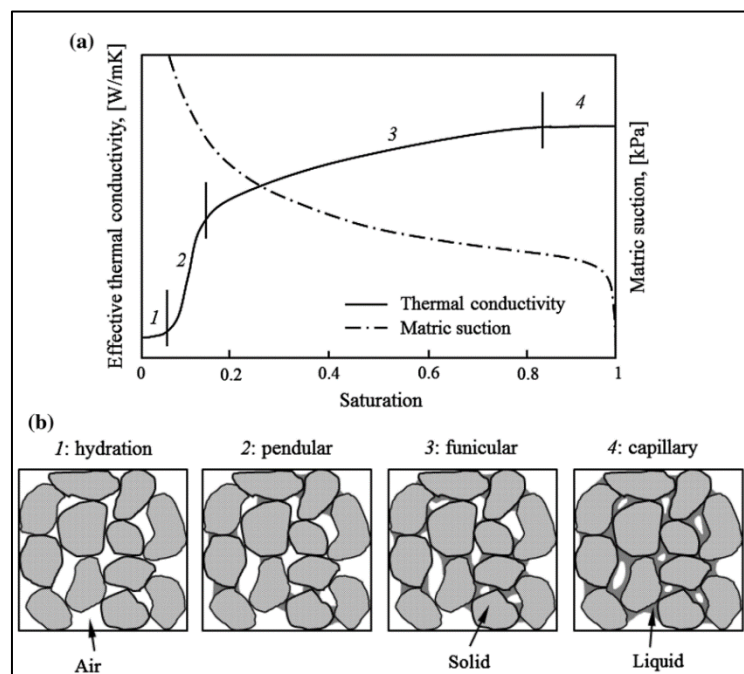


Figure 5-7: Conceptual model of thermal conductivity: a thermal conductivity and soil–water retention, and b regimes of pore-water distribution (Dong et al., 2015).

5.4.1. Prediction equations review

In the past, equations were developed to predict the thermophysical value in proportion to the percentage of water contained in the porous media. The majority of these equations are based on sandy materials because their content has a large effect on heat conductivity. Various analytical models for determining effective thermal conductivity (λ_{eff} [W/m K]) have been presented in recent years by various experts.

Kersten, 1949

One of the most widely used is based on (Kersten, 1949) empirical formula, which proposed an empirical relationship between thermal conductivity and moisture content and dry density based on laboratory experiments on five soil types.

The following are Kersten's formulas for coarse soils (with 10% silty and clayey material) and fine grain soils (with more than 50% fine material (Johansen, 1977; Kersten, 1949). There are no sample mineralogy factors given (Lee, et al. 2016; Kersten, 1949). It is obvious from analyzing Kersten's equations that the thermal conductivity value of the soil is substantially impacted by its moisture content. In reality, the presence of water or air in soil porosities has a significant impact on the thermal conductivity value, since water has a thermal conductivity 20 times that of air.

The geometric mean equation can be used to calculate the thermal conductivity of saturated soil materials when the quartz concentration and volumetric compositions are known (roughly 30 - 60% quartz). This comparison clearly reveals that the particle conductivity differences between the two soil material groups are significant. The coarse materials equation yields an average particle conductivity of roughly 5 W/m K, while the fine grain soil equation yields about 3 W/m K for samples from Norway.

$$\lambda_{Fine\ soils} = 0,1442 \cdot (0,9 \cdot \log W_s - 0,2) \cdot 10^{0,6243\rho}$$

Equation 5-2

$$\lambda_{Coarse\ soils} = 0,1442 \cdot (0,7 \cdot \log W_s + 0,4) \cdot 10^{0,6243\rho}$$

Equation 5-3

Johansen, 1977

He investigated soils with quartz contents ranging from 10% to 100%, with an average of roughly 50%, and suggested a normalized thermal conductivity equation to study the impacts of soil type, porosity, degree of saturation, and mineral component. The relevance of lambda values as a function of mineral composition and packing density was also underlined in the paper. He opted to incorporate Kersten, 1949 prediction equations into mathematical models, with mineral- and structure-dependent elements serving as parameters. The mathematical model can be expressed as a main equation representing the conductivity of the soil material as a function of the degrees of packing and saturation, as well as normalized conductivity values (Kersten number), also employing the soil material conductivities (Lu et al. 2007; Johansen, 1977)

These variables can be determined using data on the texture of the soil material, the degrees of packing and saturation, and the mineral composition (quartz content) affecting particle conductivity.

He expressed an unsaturated soil's thermal conductivity as a function of its thermal conductivity in the dry (λ_{dry}) and saturated (λ_{sat}) states at the same dry density. This was accomplished by establishing a normalized thermal conductivity known as Kersten's number K_e , which is given by Equation 5-4

Based on trends in mineral composition in diverse soils, a mathematical model for particle conductivity was built, with the dominating minerals being quartz, feldspar, and mica. Quartz has the highest conductivity (7,8 W/m K). Horai, (1971) whereas feldspar and mica have nearly comparable conductivities (2,0 W/m K). Using these data, particle conductivity can be calculated using a two-component model in which quartz content is important (Johansen, 1977).

These equations can only be used beyond 5% (or 10%) saturation, because the sensitivity declines and the uncertainty in the data grows, resulting in a 45% inaccuracy (Farouki, 1981)

$$\lambda = (\lambda_{sat} - \lambda_{dry}) \cdot K_e + \lambda_{dry}$$

Equation 5-4

$$\lambda_{sat} = \lambda_{solid}^{1-n} \cdot \lambda_{water}^n$$

Equation 5-5

$$\lambda_{dry} = \frac{0,137 \rho + 64,7}{2700 - 0,947 \rho}$$

Equation 5-6

$$K_e = 0,7 \cdot \log W_s + 1 \quad \text{Coarse grain soil } (S_r > 0,05)$$

Equation 5-7

$$K_e = \log W_s + 1 \quad \text{Fine grain soil } (S_r > 0,1)$$

Equation 5-8

Farouki (1981)

Farouki used Johansen (1977) equation to estimate the thermal conductivity of dry soils (Equation 5-6). He did, however, make certain changes to the computation procedure under saturated conditions. Instead of utilizing quartz content to evaluate mineral soil thermal conductivity, he looked at sand and clay content.

The Farouki (1981) scheme is simple to use, and the essential inputs, such as the contents of sand, clay and gravel, can be obtained directly from soil property databases. To measure the mass thermal conductivity of soil solids, he computed a value using the volumetric weighted arithmetic average of all soil components (Dai et al., 2015). Accordingly, the saturated thermal conductivity (λ_{sat}) was calculated empirically as Equation 5-5. This method was utilized to generate a more accurate estimation of saturated soil thermal conductivity by directly considering the particular sand and clay components rather than the overall quartz concentration. “%sand” and “%clay” in Equation 5-10 reflect the gravimetric fractions of sand and clay in the mineral soil, respectively. Farouki (1981) simplified the Ke-Sr connection further by neglecting the impacts of soil particle size distribution Equation 5-8 for all soil types (not only fine grain soils).

$$\lambda_{sat} = (f_{minerals} \cdot \lambda_{minerals_{dry}} + f_{om} \cdot \lambda_{om_{dry}} + f_{gravel} \cdot \lambda_{gravel})^{1-W_s} \cdot \lambda_w^{W_s}$$

Equation 5-9

$$\lambda_{mineral_{wet}} = \frac{8,8 \%_{sand} + 2,92\%_{clay}}{\%_{sand} + \%_{clay}}$$

Equation 5-10

Côté e Konrad, 2005

Côté and Konrad investigated soil and building material thermal conductivity further in 2005 (especially for fine and medium sands including crushed rock particles). They examined a large data set of dry thermal conductivities and discovered that the connection between dry thermal conductivity and porosity was substantially dependent on porosity. demonstrated that the connection between dry thermal conductivity and porosity was highly influenced by soil shape and particle size. Johansen (1977) approach does not account for soil shape and grain size. Furthermore, in order to simplify and increase the quality of data fitting, they modified Johansen (1977) equation by removing logarithmic functions to determine Ke and replacing them with a soil texture-dependent component, k . The k

values chosen were 4,60, 3,55, 1,90 and 0,60 for gravel and coarse sand, medium sand and fine sand, silty and clayey soils, and fibrous organic soils, respectively Equation 5-12).

In addition, Côté and Konrad (2005) proposed a new empirical equation to represent the dependence of λ_{dry} on soil porosity (n), where χ ($W/m K$) and η are parameters that account for the effects of particle shape. The values of χ and η were 1,70 $W/m K$ and 1.80 for crushed rocks, 0,75 $W/m K$ and 1,20 for mineral soils, and 0,30 $W/m K$ and 0,87 for fibrous organic soils (Dai et al., 2015; Lu et al., 2007).

Côté and Konrad utilized the Johansen Equation 5-5 to calculate saturated thermal conductivity. However, because the calculation is based on the geometric mean approach, which takes into account the thermal conductivity and volumetric proportion of the minerals forming the sample, a complete mineralogical composition of the sample was required to calculate λ_{soild} .

$$\lambda_{dry} = \chi \cdot 10^{-\eta n}$$

Equation 5-11

$$K_e = \frac{K \cdot W_s}{1 + (K - 1) \cdot W_s}$$

Equation 5-12

Lu et al., 2007

Lu et al. (2007) conducted a series of thermo-temporal reflectometry (TDR) tests on twelve natural soils ranging from sand to loam or clay loam and presented a thermal conductivity model through a new connection over a broad range of soil moisture conditions. According to Lu et al.'s analysis of laboratory tests and earlier scientific formulae, the increase in thermal conductivity at low percentages of W_s is not abrupt because the first water that enters the porous media travels to the edges of the

particles, forming a film. The thickness of the water films grows in this domain as W_s and λ gradually but not dramatically increase. With further increases in W_s , water bridges begin to form between the solid soil particles, and λ begins to increase rapidly due to the improved contact between the particles.

Until the majority of the solid particles (20–50% W_s) are not attached to one another, this process continues. They altered the Kersten number equation as a result. They also presented a straightforward linear function, where a and b are empirical values, to describe the relationship between λ_{dry} and n for mineral soils. They used the same method as Johansen (1977) to determine λ_{sat} , but since we did not assess the quartz content of our soils, they made the assumption that the quartz content was equivalent to the sand content.

$$\lambda_{dry} = -an + b$$

Equation 5-13

$$K_e = \exp \{ \alpha [1 - W_s^{\alpha-1,33}] \}$$

Equation 5-14

Chen, 2008

Developed a thermal conductivity model for sands (four different grain size curves) with extremely high quartz content. Chen (2008) presented a database of thermal conductivity measurements of four different soils, each tested at four void ratios and five saturation ratios. The resulting set of 80 thermal conductivity values were used to study the ability of this mathematical method to predict the thermal conductivity of soils. The soils included in the work are all quartz sands. The proposed equation for estimating the thermal conductivity of sands involves a linear relationship between λ and n , and the slope of the line, a function of the degree of saturation W_s . Therefore, the following equation can be

used to describe the thermal conductivity of sandy soils (Equation 5-15). As for the calculation of thermal conductivity in the saturated phase, the equation is the same as that of Johansen (1977).

$$\lambda_{(n,W_s)} = \lambda_0^{1-n} \cdot \lambda_{water}^n \cdot [(1 - b)S_r + b]^{cn}$$

Equation 5-15

$$\lambda_{(n,W_s)} = 7,5^{1-n} \cdot 0,613^n \cdot [(1 - 0,0022)W_s + 0,0022]^{0,78n}$$

Equation 5-16

Haigh (2012) attempted to investigate actual thermal conductivity by a theoretical analysis based on conduction through a simple soil element with three phases: soil particles, pore water, and air. Simple equations may be derived from this model to estimate soil thermal conductivity, which will be evaluated against the findings of thermal conductivity tests given in the literature for a variety of sandy soils.

NOTATION

λ_{dry} = Thermal conductivity in dry condition [$W/m K$]

λ_{sat} = Thermal conductivity in saturated condition [$W/m K$]

ρ = Bulk density [Kg/cm^3]

W_s = Water saturation [%]

K_e = Kersten's number

n = Porosity [%]

λ_{solid} = $\lambda_{quartz}^\alpha \cdot \lambda_o^{1-\alpha}$ [$W/m K$]

λ_{quartz} = $7,8 W \cdot m^{-1} \cdot K^{-1}$ (Horai, 1971)

λ_{water} = $0,6096 W \cdot m^{-1} \cdot K^{-1}$ (Ramires et al., 1995)

λ_o = Lambda of minerals [$W \cdot m^{-1} \cdot K^{-1}$]

α = soil texture dependent parameter, 0,96 (Lu, et al. 2007; Lee, et al. 2016)

a and b = empirical parameters, respectively, 0,56 and 0,51 (Lu, et al. 2007; Lee, et al. 2016)

d = $\lambda_{water} / \lambda_o$

K = 4,7 (Côté and Konrad, 2005)

<i>Kersten (1949)</i>	$\lambda_{eff\ fine} = 0,1442 \cdot (0,9 \cdot \log W_s - 0,2) \cdot 10^{0,6243\rho}$ $\lambda_{eff\ coarse} = 0,1442 \cdot (0,7 \cdot \log W_s + 0,4) \cdot 10^{0,6243\rho}$
<i>Johansen (1975)</i>	$\lambda = (\lambda_{sat} - \lambda_{dry}) \cdot K_e + \lambda_{dry}$ $\lambda_{sat} = \lambda_0^{1-n} \cdot \lambda_w^n$ $\lambda_{dry} = \frac{0,137\rho + 64,7}{2700 - 0,947\rho}$ $K_e \text{ Coarse soils} = 0,7 \cdot \log W_s + 1$ $K_e \text{ Fine soils} = \log W_s + 1$
<i>Farouki (1981)</i>	$\lambda_{dry} = \frac{0,137\rho + 64,7}{2700 - 0,947\rho}$ $\lambda_{sat} = (f_{minerals} \cdot \lambda_{minerals\ dry} + f_{om} \cdot \lambda_{om\ dry} + f_{gravel} \cdot \lambda_{gravel})^{1-W_s} \cdot \lambda_w^{W_s}$
<i>Côté and Konrad (2005)</i>	$\lambda_{dry} = \chi \cdot 10^{-\eta n}$ $\lambda_{sat} = \lambda_0^{1-n} \cdot \lambda_{water}^n$ $K_e = \frac{K \cdot W_s}{1 + (K - 1) \cdot W_s}$
<i>Lu et al. (2007)</i>	$\lambda_{dry} = -an + b$ $\lambda_{sat} = \lambda_0^{1-n} \cdot \lambda_{water}^n$ $K_e = \exp \{ \alpha [1 - W_s^{\alpha-1,33}] \}$
<i>Chen (2008)</i>	$\lambda_{(n,W_s)} = \lambda_0^{1-n} \cdot \lambda_{water}^n [(1-b)S_r + b]^{cn}$

5.4.2. Results and discussion

Some equations have been developed to predict the thermophysical properties in relation to the percentage of water content within the porous medium. Many studies have utilized the parameters mentioned in this thesis, such as water saturation, porosity, bulk density, and quartz content. The proposed equations have been compared with our experimental results (see Figure 5-8).

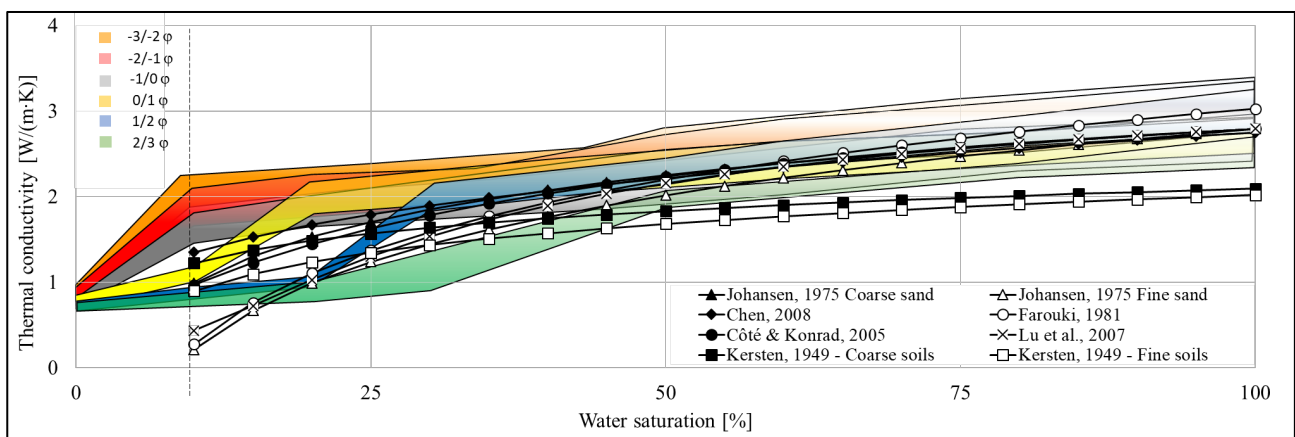


Figure 5-8: A comparison of empirical equations from the literature with our phi range test.

It should be noted that the validity of relationships derived from the literature is affected by conditions with saturations below 10%. Even a small percentage of water in the sample can cause substantial variations in thermal conductivity data, particularly between 5% and 40%. Our investigations have been specifically focused on the initial water saturation levels to identify distinct trends concerning grain size. The sieved materials were categorized into phi ranges, and the thermal conductivity was computed in relation to the variation in water content. This enabled us to identify positive trends associated with an increase in water saturation. Furthermore, we have confirmed a twofold increase in thermal conductivity as the experimental condition changes from 10% to 50% water saturation.

The influence of grain size on this positive trend is noteworthy, as coarse materials require a lower water content to generate an increase in thermal conductivity, in contrast to fine-grained materials. This effect can be attributed to pore size, which may impede water mobility. Smaller grain and pore diameters necessitate a greater amount of water to attain the same λ value. For instance, to achieve a value of approximately 2 W/m K , a 10% water content is required for material $-2/-1 \text{ phi}$, nearly 20% saturation for $0/1 \text{ phi}$, 30% for $1/2 \text{ phi}$, and up to 50% for $2/3 \text{ phi}$. The only anomaly lies in material $1/0 \text{ phi}$, which likely reflects peculiarities observed in the comparison between thermal conductivity and grain size. This trend has been corroborated, albeit in a broader context, by previous studies conducted by Barry-Macaulay et al., 2013; Côté and Konrad 2005; Johansen, 1977 and Kersten, 1949. It classified general materials into fine and coarse-grained categories.

Furthermore, it is clear that Kersten (1949) equations exhibit slight differences from the rest. The reason behind this disparity is that Kersten does not account for the porosity parameter. If we were to substitute a porosity value of 0,50 for all the other equations mentioned in the literature (instead of the average porosity of our samples, which is 0,41), all the equations would yield fictitious results with minimal error.

6. Concluding remarks

The doctoral research project began with the aim of uncovering in detail how petrophysical parameters influence thermal conductivity values. The observation of numerous feasibility studies for geothermal systems (low and medium enthalpy) that use approximate thermal conductivity values in engineering calculations and software for system design led to this purpose. While the Thermal Response Test (TRT) is the most commonly used technique worldwide, it provides an average value along the entire stratigraphic column of the drilled well, often composed of layers of sand, silt, clay, and bimodal or highly heterogeneous materials; therefore, the λ data is not very accurate.

Determining the thermal properties of soils is crucial for the future utilization of geothermal energy. Thermal properties are also significant in various engineering applications as well as in agricultural and meteorological applications. A new laboratory was designed and constructed to test different unconsolidated natural materials for thermal conductivity characterization. Water content, mineralogy, porosity, as well as bulk density are the fundamental petrophysical properties of the material that were considered to determine the effective thermal conductivity of soils in this research.

This thesis therefore begins with a brief chapter on the basics of thermophysics, including the Fourier equation and the physical principles behind the GHP method, as well as outlining the thesis objective of better understanding the causes that may have led to variable thermal conductivity results. Drawing inspiration from the literature, various authors, and scientific works, we created a laboratory from scratch that could be functional for directly calculating many factors necessary for a proper geological evaluation of the sample traversed by hypothetical geothermal probes. This laboratory was named GeoTh. The method of thermal cells is one of the best practical methods for determining the effective thermal conductivity of soils due to its simplicity of equipment, low cost, minimal sample requirement, and its applicability to soil samples obtained from routine surveys. Furthermore, we constructed it in a way to have 12 testers working simultaneously and with maximum accuracy in data, along with remote control and data storage in a cloud system. This allowed us to perform thousands of tests and improve the scientific literature, creating a rich dataset that can be continuously updated.

Having employed the same instrument and setup, the reasons for identifying different lambda values are to be sought in the samples and their characteristics. Whether only lithology influences or if there are other parameters that could play a role in varying the lambda value. In literature, it's believed that the contact zone between grains is a resistance to heat flow compared to the flow within the grain itself (Incorpera and DeWitt, 2001; Midttømme and Roaldset, 1998). So, the more grains there are, the more thermal resistances are present, resulting in decreased thermal conductivity (Hamuda et al., 2011). The effective thermal conductivity of the tested soils depends on the volumetric proportions of components, particle sizes and arrangements within the soil, as well as interface relationships. Although these values show a correlation between thermal conductivity and particle size of unconsolidated materials, they cannot be considered a definitive confirmation of the particle size effect on thermal conductivity since particle size influences other factors like pore size, permeability, mineralogy, and bulk density, which also affect thermal conductivity.

This doctoral research has allowed us, both in the data acquisition and processing phases, an unprecedented level of precision and accuracy on this type of samples. Additionally, we decided to test common subsurface materials but sieved into precise particle size ranges, a crucial innovative aspect of this project. Thermal and mineralogical analyses were carried out on these materials; hence, this thesis is certainly beneficial to the practical worlds of ceramics and construction engineering. It enabled us to observe significant variations in thermal conductivity values primarily with changes in water presence (λ : +300% difference between dry and fully saturated conditions), as well as in

relation to particle size distribution. This latter factor was thoroughly examined, making it one of the most innovative aspects of this project. It allowed us to confirm in high detail how λ decreases as grain size decreases, but this holds true for clayey, silty, and sandy materials up to the particle size of very coarse sand. Gravel tends to have a slightly lower thermal conductivity value than coarse sands, a finding also confirmed by Dalla Santa et al., 2020; Hamuda et al., 2011; Komle et al., 2010 and Gori et al., 2001.

This had been previously observed in other scientific works, but no one had ever observed these trends by conducting hydro-thermo-petro-physical tests on such well-selected materials. Moreover, we investigated the mineralogy of all our samples through XRD analysis, both for characterization purposes and to observe potential trends that could impact thermal results. The influence was observed, albeit not directly on thermal conductivity but on particle size distribution. In fact, the presence of certain minerals like quartz and carbonate minerals (primarily calcite and dolomite) clearly exhibits a percentage of occurrence in the material relative to the observed grain size. Therefore, we can say that mineralogy directly affects grain size (due to mineral hardness) and consequently influences thermal conductivity, albeit only indirectly (due to the thermal conductivity of minerals).

Under the same test boundary conditions and with the same mineralogy and porosity (as seen in tests with glass beads), the only parameter that continues to influence thermal conductivity is grain size. For this reason, we assert that grain size is extremely important as a factor influencing λ , with water saturation being the main parameter that causes it to vary.

To further validate the laboratory and the generated data, we compared the most significant thermal conductivity prediction equations with our specially calculated values for this purpose, observing them during different saturation phases. Moreover, some of these prediction equations demonstrate that by varying the grain size parameter, thermal conductivity changes (Chen, 2008; Lu et al., 2007; Côté and Konrad, 2005; Farouki, 1981; Johansen, 1977 and Kersten, 1949). Particularly, the thermal conductivity value decreases with grain size. We can confirm the excellent correlation with the literature data, but in this aspect as well, we can contribute an innovation to the scientific world, namely the need for a higher percentage of water as grain size decreases to achieve the same thermal conductivity value. This phenomenon can be observed between 10 and 50% of Water saturation.

In summary, the work in this thesis has led to the development and validation of a comprehensive hydro-thermo-petro-physical framework on unconsolidated natural materials. These samples were tested, taking into account all heat transfer mechanisms, including heat losses, which were

intentionally mitigated within the system. Using Fourier's law, the thermal conductivity value was calculated, and all other parameters were measured and studied to form a complete picture. Water remains the most influential parameter in thermal conductivity variation, with grain size firmly ranking second. We can confirm the change in lambda with varying grain size only for particle sizes equivalent to sand or with smaller grain diameters. For gravel, there is still high uncertainty in various aspects. Then, mineralogy indirectly, and porosity and bulk density according to literature, play an important but not determinative role in the range of values observed in this doctoral thesis.

Future steps could definitely involve testing bimodal materials or those with a mix of different percentages within the utilized ranges, as the influence of grain size distribution could have significant effects on thermal conductivity (Midttømme and Roaldset, 1998). Therefore, we aim to approach more realistic materials, and then compare them with materials actually drilled from geothermal wells. A comparison with other acquisition techniques could further validate the developed system, perhaps utilizing probe systems at different pressures.

Lastly, it would be intriguing, based on analyses performed on glass beads, specific ranges of natural materials, mixed materials, and drilled materials, to formulate a comprehensive equation that can predict a precise value of thermal conductivity and porosity by simply observing the particle size distribution curve and mineralogy of the material present in a hypothetical geothermal area. This factor could reduce costs and timelines for feasibility studies and enhance their accuracy.

References

Legislative Decree N°22, 22/2010, Article 1 comma 2.

Abu-Hamdeh N. and Reeder R. C. (2000): Soil Thermal Conductivity: Effects of Density, Moisture, Salt Concentration, and Organic Matter. *Soil Science Society of America Journal*, 64.

ASTM. - ASTM International, formerly the American Society for Testing and Materials (ASTM) is an international standards organization that develops and publishes voluntary consensus technical standards for a wide range of materials, products and systems.”

ASTM - C177-13. (2017): *Standard Test Method For Steady-State Heat Flux Measurements And Thermal Transmission Properties By Means Of The Guarded-Hot-Plate Apparatus*.

ASTM - D5334-08. (2014): *Standard Test Method for Determination of Thermal Conductivity of Soil and Soft Rock by Thermal Needle Probe Procedure*.

Barry-Macaulay D., Bouazza A., Singh R. M., Wang B. and Ranjith P. G. (2013): Thermal conductivity of soils and rocks from the Melbourne (Australia) region. *Engineering Geology*, 131 – 138, doi: 10.1016/j.enggeo.2013.06.014.

Beier R. A., Smith D. M. and Spitler J. D. (2011). Reference data sets for vertical borehole ground heat exchanger models and thermal response test analysis. *Geothermics (Elsevier)* 79 – 85, doi:10.1016/j.geothermics.2010.12.007.

Bergman T. L., Lavine A. S., Incropera F. P. and DeWitt D. P. (2011): *Fundamentals of Heat and Mass Transfer*. Seventh Edition. John Wiley & Sons, Inc. doi:ISBN 13 978-0470-50197-9.

Bertermann D., Muller J., Freitag S. and Schwarz H. (2018): Comparison between measured and calculated thermal conductivities within different grain size classes and their related depth ranges. *Soil Systems*, 2 (50). doi:doi:10.3390/soilsystems2030050.

Brigaud F., and Vasseur G. (1989): Mineralogy, porosity and fluid control on thermal conductivity of sedimentary rocks. *Geophysical Journal*, 98: 525-542.

BS 874-2.2. (1988): Methods for determining thermal insulating properties. Tests for thermal conductivity and related properties. Unguarded hot-plate method. 91.120.10 - Thermal insulation of buildings.

- Carslaw H.S. and Jaeger J.C. (1959): *Conduction of heat in solids*. Second edition. Oxford at the Clarendon press.
- Chen S.X. (2008): Thermal conductivity of sands. *Heat Mass Transfer* 44 (10): 1241. doi: 10.1007/s00231-007-0357-1.
- Cocchi A. (1998): *Elementi di termofisica generale e applicata*. Esculapio.
- Cortes D.D., Martin A.I., Yun T.S. and Fran F.M. (2009): *Thermal conductivity of hydrate-bearing sediments*. *Journal of Geophysical Research* 114 (11): 1–10. <https://doi.org/10.1029/2008JB006235>.
- Côté J. and Konrad J.M. (2005). A generalized thermal conductivity model for soils and construction materials. *Canadian. Geotech Journal.*, Vol. 42.
- Dai Y., Wei N., Yuan H., Zhan S., Shangguan W., Liu S., Lu X. and Xin Y. (2015): Effective Thermal Conductivity of Submicron Powders: A Numerical Study. *Applied Mechanics and Materials*. 846: 500–505. doi: 10.4028/www.scientific.net/AMM.846.500.
- Dalla Santa G., Peron F., Galgaro A. and Cultrera M. (2017): Laboratory Measurements of Gravel Thermal Conductivity An Update Methodological Approach. *Energy Procedia* 125: 671-677.
- Dalla Santa G., Galgaro A., Sassi R., Cultrera M., Scotton P., Meller J., Bertermann D. (2020): An updated ground thermal properties database for GSHP applications. *Geothermics*, 85. doi: 10.1016/j.geothermics.2019.101758.
- Daw J., Rempe J., Condie K., Knudson D. and Curtis W. (2010): Hot Wire Needle Probe for In-Pile Thermal Conductivity Detection. *Seventh American Nuclear Society International Topical Meeting on Nuclear Plant Instrumentation, Control and Human-Machine Interface Technologies*. Las Vegas, Nevada, November 7-11, 2010 (INL/CON-10-19633 NPIC&HMIT.).
- Di Sipio E., and Bertermann D. (2017): Thermal properties variations in unconsolidated material for very shallow geothermal application (ITER project). *Int. Agrophys*, 32: 149-164.
- Di Sipio E., and Bertermann D. (2017): Influence of Different Moisture and Load Conditions on Heat Transfer within Soils in Very Shallow Geothermal Application: An Overview of ITER Project. *42nd Workshop on Geothermal Reservoir Engineering. Stanford, California: SGP-TR-212*.
- Domenico P. A. and Schwartz F. W. (1990). *Physical and Chemical Hydrogeology*. Second edition. *John Wiley & Sons, Inc*.

Dong Y., McCartney J.S. and Lu. N. (2015): Critical Review of Thermal Conductivity Models for Unsaturated Soils. *Geotech Geol Eng.* doi: 10.1007/s10706-015-9843-2.

Dubois S., and Lebeau F. (2015): Design, construction and validation of a guarded hot plate apparatus for thermal conductivity measurement of high thickness crop-based specimens. *Materials and Structures* 48: 407 - 421. doi:DOI: 10.1617/s11527-013-0192-4.

Farouki (1981): *Evaluation of methods for calculating soil thermal conductivity.* Cold Regions Research and Engineering Laboratory Report - US Army Corps of Engineering, Hanover, New Hampshire. Vol. 82–8.

Gori F., Marino C. and Pietrafesa M. (2001): Experimental measurements and theoretical prediction of the thermal conductivity of two phases glass beads. *International Communications in Heat and Mass Transfer*, Elsevier Science Ltd. 28 (8): 1091 - 1102.

Haigh S.K. (2012): Thermal conductivity of sands. *Géotechnique* 62(7): 617–625. Doi:10.1680/geot.11.P.043.

Hamdhan I. N. and Clarke B. G. (2010): Determination of Thermal Conductivity of Coarse and Fine Sand Soils. *Proceedings World Geothermal Congress Bali, Indonesia.* 25-29.

Hamuda S. S., Rouainia M. and Clarke B. G. (2011): Effective thermal conductivity of partially saturated soils. *Unsaturated Soils* (Alonso & Gens (eds)). doi: 10.1201/b10526-102.

Haraisha S., Hamuda S. and Kinsheel A. (2019): Determination of effective thermal conductivity for Tripoli sand as influenced by changing water content. *International Conference on Technical Sciences (ICST2019).* Tripoli. doi:ICTS24632019-AC1048.

Horai K. I. (1971): Thermal conductivity of rock-forming minerals. *Journal Geophys Res.* 5: 1278 - 1308.

Inaba H. (1986): Measurement of the Effective Thermal Conductivity of Agricultural Products. *International Journal of Thermophysics* (Plenum Publishing Corporation) 7 (4). doi:0195-928X/86/0700-0773\$04.00/0.

Incorpera F. P. and DeWitt D. P. (2001). *Fundamentals of Heat and Mass Transfer.* 5th Ed. Wiley India Pvt. Limited.

ISO. n.d. International Organization for Standardization

- Johansen O. (1977): *Thermal conductivity of soils*. Ph.D. thesis, University of Trondheim, Trondheim, Norway. English Translation 637, US Army Corps of Engineers, Cold Regions Research and Engineering Laboratory, Hanover, New Hampshire.
- Katsura T., Kindaichi S. and Nagano K. (2006): Heat transfer experiment in the ground with ground water advection. <https://www.researchgate.net/publication/251299773>.
- Kersten (1949): *Thermal Properties of Soils*. Minnesota, University of Minnesota: Eng. Experiment Station.
- Komle N. I., Hutter E. S. and Feng W. J. (2010): Thermal conductivity measurements of coarse-grained gravel materials using a hollow cylindrical sensor. *Acta Geotechnica*, Springer. 5: 211 - 223. Doi: 10.1007/s11440-010-0126-z.
- Kramer A. C., Ghasemi-Fare O. and Basu P. (2014): Laboratory Thermal Performance Tests on a Model Heat Exchanger Pile in Sand. *Geotechnical and Geological Engineering*. doi: 10.1007/s10706-014-9786-z.
- Krumbein W. C. and Pettijohn F. I. (1961): Manual of Sedimentary Petrography. *Appleton-Century-Crofts*.
- Lee S.J., Choi J.C., Baek S., Kwon T. H., Ryu H. H. and Song K. I. (2016): Use of a Pre-Drilled Hole for Implementing Thermal Needle Probe Method for Soils and Rocks. *Energies*, 9: 846.
- Low E. J., Loveridge A. F., Powrie W. and Nicholson D. (2015): A comparison of laboratory and in situ methods to determine soil thermal conductivity for energy foundations and other ground heat exchanger applications. *Acta Geotechnica* (Springer-Verlag) 10: 209 - 218. doi:DOI 10.1007/s11440-014-0333-0.
- Low J. E., Loveridge F. A. and Powrie W. (2013): Measuring soil thermal properties for use in energy foundation design. *International society for soil mechanics and geotechnical engineering*.
- Lu S., Ren T., Gong Y. and Horton R. (2007): An improved model for predicting soil thermal conductivity from water content at room temperature. *Soil Science Society of America Journal*. 71(1), 8-14. doi: 10.2136/sssaj2006.0041.

- McManus J. (1988): Grain size determination and interpretation. *Techniques in Sedimentology*, Ed. Tucker M Blackwell, 63–85.
- Midttømme K. and Roaldset E. (1998): The effect of grain size on thermal conductivity of quartz sands and silts.” *Petroleum Geosciences* 4(2), 165 - 172. doi: 10.1144/petgeo.4.2.165.
- Missimer T.M. and Lopez O.M. (2018): Labortory measurement of thotal porosity in unconsolidated quartz sand by two integrated methods. *Journal Geol. Geophys*, 7:5. doi: 10.4172/2381-8719.1000448.
- Ramires M. L., Nieto de Castro C. A., Nagasaka Y., Nagashima A., Assael M. J. and Wakeham W. A. (1995). Standard reference data for thermal conductivity of water. *The Journal of Physical Chemistry*. 3: 1377 - 1381.
- Rapti D., Marchetti A., Andreotti M., Neri I. and Caputo R. (2022): GeoTh: An Experimental Laboratory Set-Up for the Measurement of the Thermal Conductivity of Granular Materials. *Soil Systems* 6(4),88. doi: 10.3390/soilsystems6040088.
- Roshankhah S., Garcia A. V. and Santamarina C. (2021): Thermal Conductivity of Sand–Silt Mixtures. *Journal of Geotechnical and Geoenvironmental Engineering*, doi: 10.1061/(ASCE)GT.1943-5606.0002425.
- Sass I. and Lehr C. (2011): Improvements on the thermal response test evaluation applying the cilinder source theroy. *Thirty-Sixth Workshop on Geothermal Reservoir Engineering*. Stanford, California. SGP-TR-191.
- Signorelli S., Bassetti S., Pahud D. and Kohl T. (2007). Numerical evaluation of thermal response tests. *Geothermics* (Elsevier) 141 - 166. doi: 10.1016/j.geothermics.2006.10.006.
- Smith S. D., Alzina A., Bourret J., Nait-Ali B., Pennec F. and Tessier-Doyen N. (2013): Thermal conductivity of porous materials. *Journal of Materials Research*, Vol. 28 (No. 17), doi: 10.1557/jmr.2013.179.
- Switzer A. D. (2013): Measuring and analysing particle size in a geomorphic context. *Treatise on Geomorphology*, Academic Press, San Diego, CA, 14: 224–242.
- Syvitski J. P. M. (1991): Principles, methods, and application of praticles size analysis. Cambridge: *Cambridge University press*.

Tanner W. F. and Balsillie J. H. (1995): Environmental Clastic Granulometry. Vol. 40. Florida: *Florida Geological Survey Special Publication*.

Tarnawski V. R., Momose T. and Leong W. H. (2011): Thermal Conductivity of Standard Sands II. Saturated Condition.” *International Journal of Thermophysics* 32: 984 - 1005. doi: 10.1007/s10765-011-0975-1.

Tavman I. H. (1996): Effective thermal conductivity of granular porous materials. *International Commission Heat Mass Transfer*, Elsevier Science Ltd, 23 (2): 169 - 176.

The American Geological Institute (1984). Dictionary of Geological Terms. Second. Robert L. Bates and Julia A. Jackson editors.

VDI. (2010): VDI-standard. VDI 4640 Blatt 1. Thermal Use of the Underground.

Wagner V., Bayer P., Bisch G., Kubert M. and Blum P. (2014): Hydraulic characterization of aquifers by thermal response testing : Validation by large-scale tank and field experiments. *Water resources research*. Vol. 50: 1-15. doi:10.1002/2013WR013939.

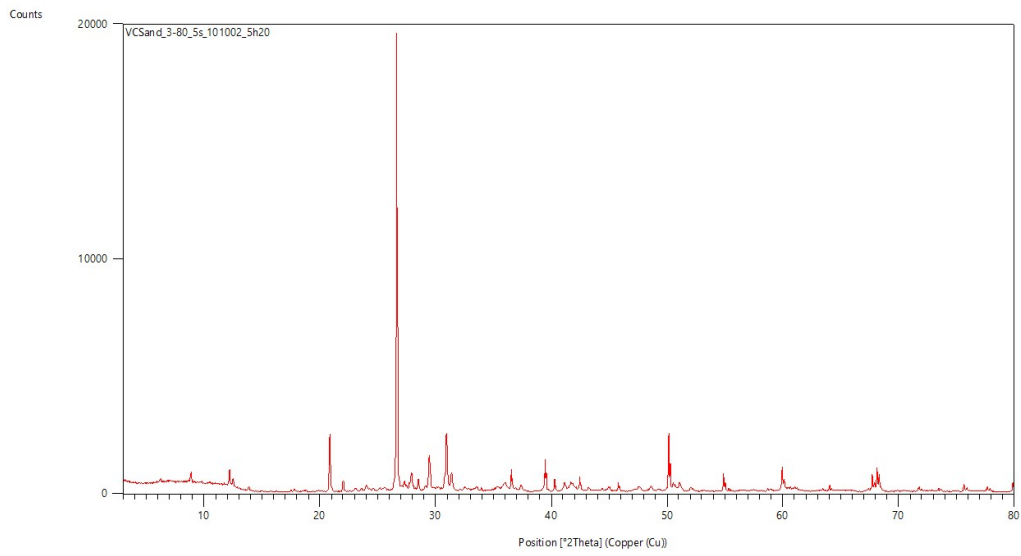
Wentworth C. K. (1922): A scale of grade and class terms for clastic sediments. Vol. 30. *Journal of Geology*.

Zhao D., Qian X., Gu X., Jajja S. A. and Yang R. (2016): Measurement techniques for thermal conductivity and interfacial thermal conductance of bulk and thin film materials. *Journal of Electronic Packaging* Vol. 138 / 040802-1. doi:DOI: 10.1115/1.4034605.

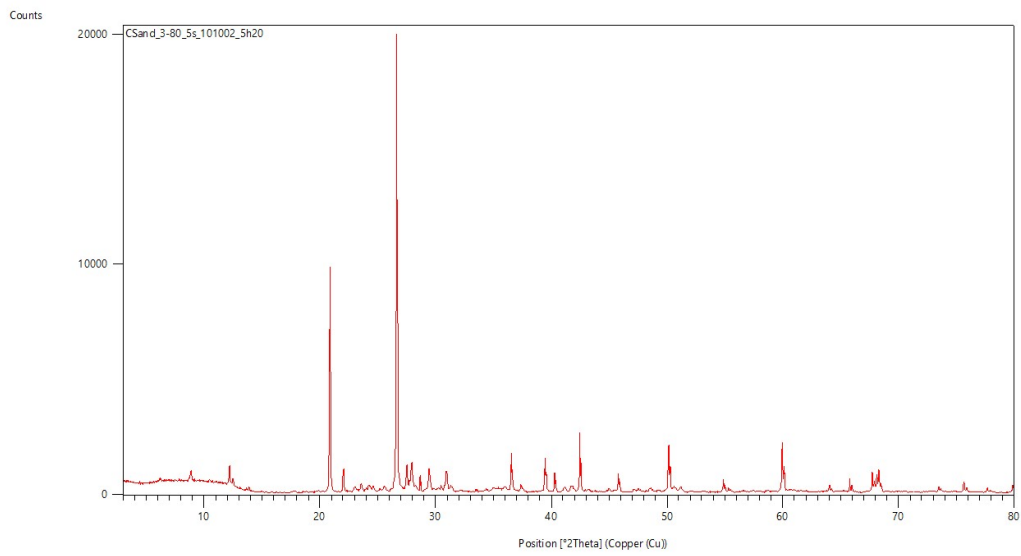
Zheng Q., Kaur S., Dames C. and Prasher S. R. (2020): Analysis and improvement of the hot disk transient plane source method for low thermal conductivity materials. *International Journal of Heat and Mass Transfer* (Elsevier) 151. doi: <https://doi.org/10.1016/j.ijheatmasstransfer.2020.119331>.

Appendix A

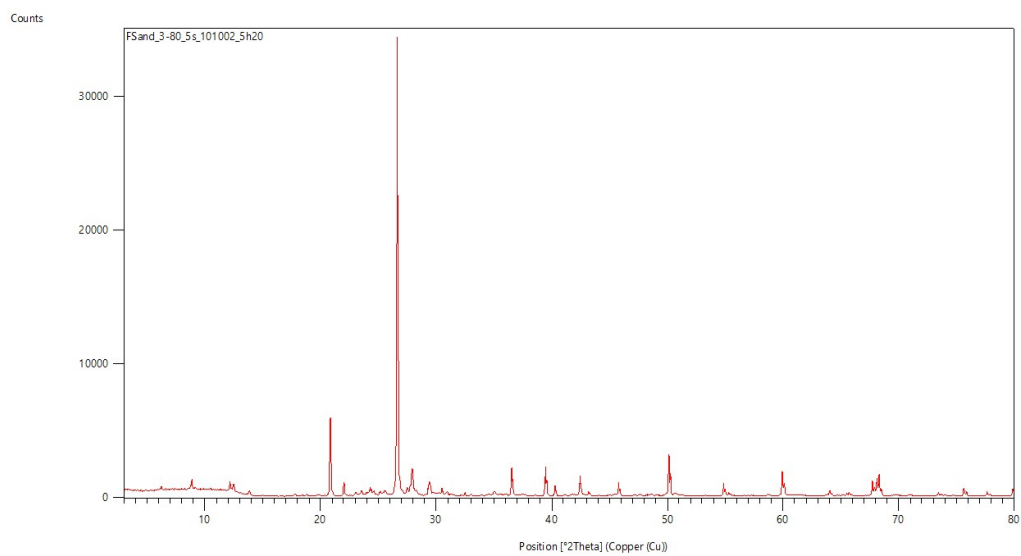
No-sieved samples, from Parma (Italy)



Appendix A - Figure 1: Very coarse sand



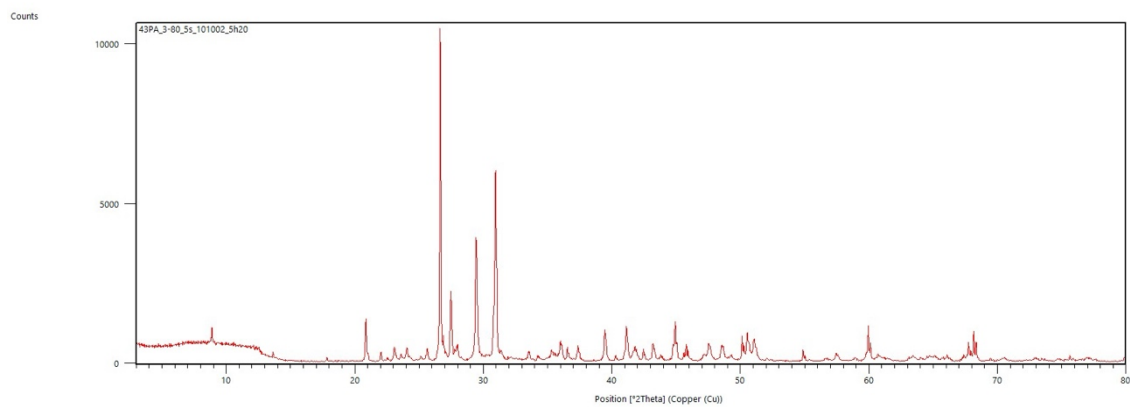
Appendix A - Figure 2: Coarse sand



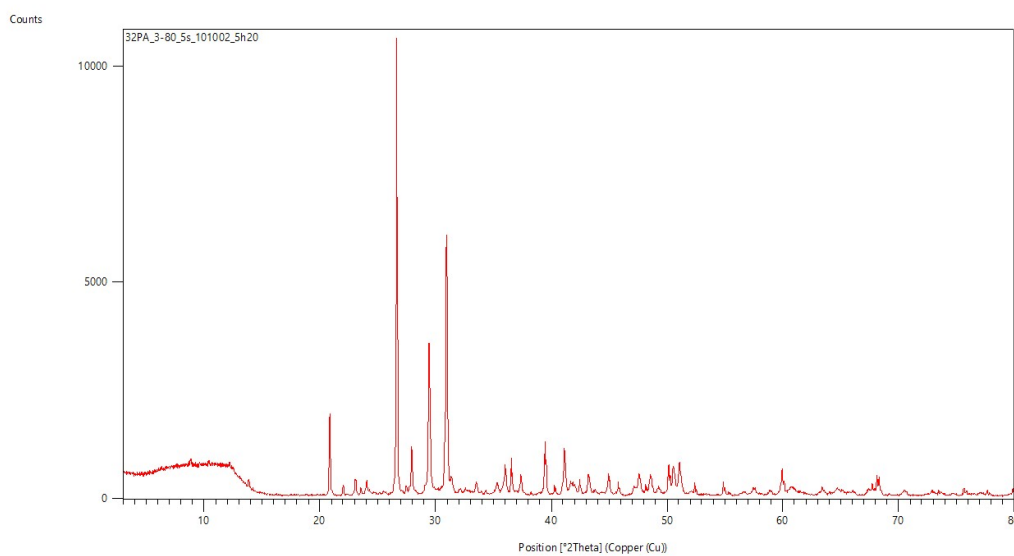
Appendix A - Figure 3: Fine sand

XRD Pattern

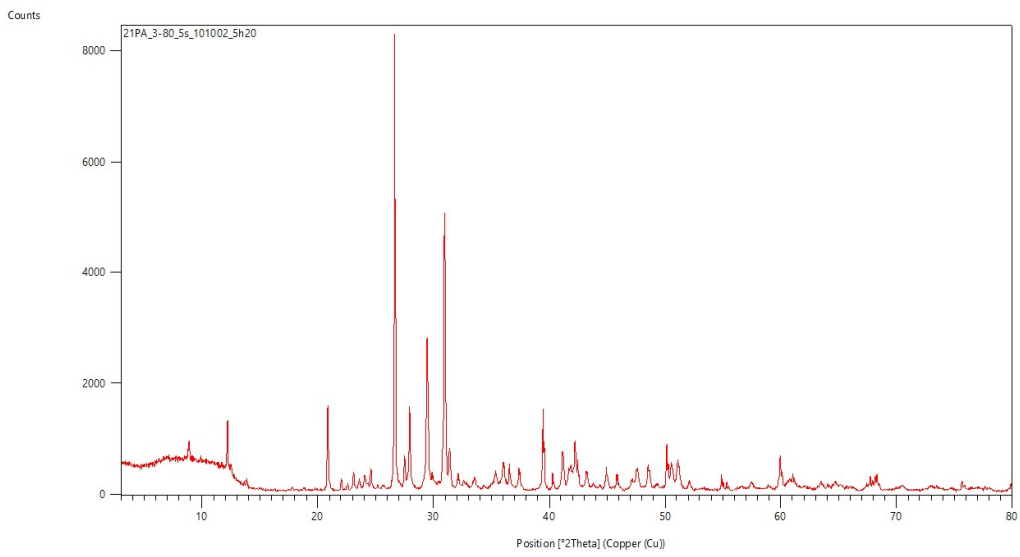
Parma samples



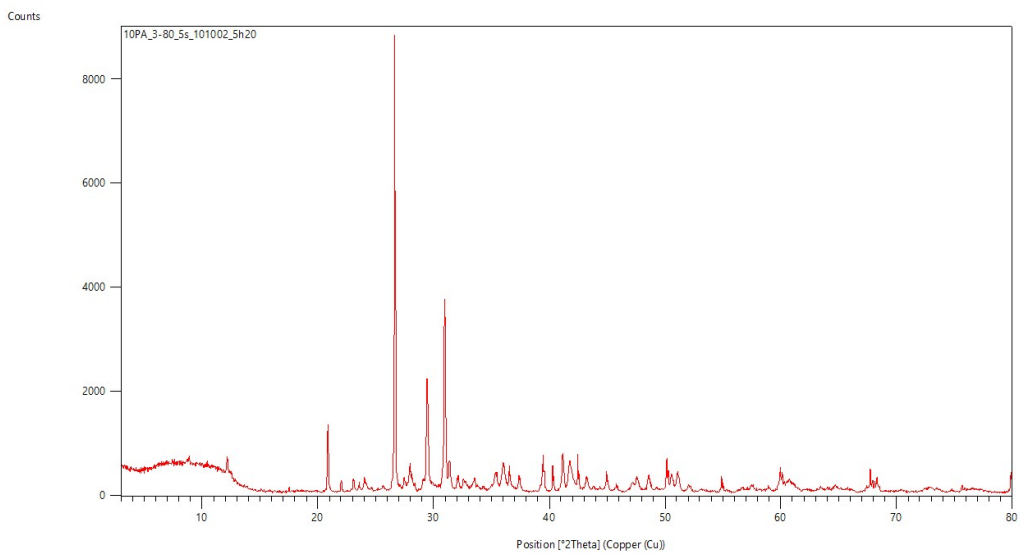
Appendix A - Figure 4: 43phi Parma



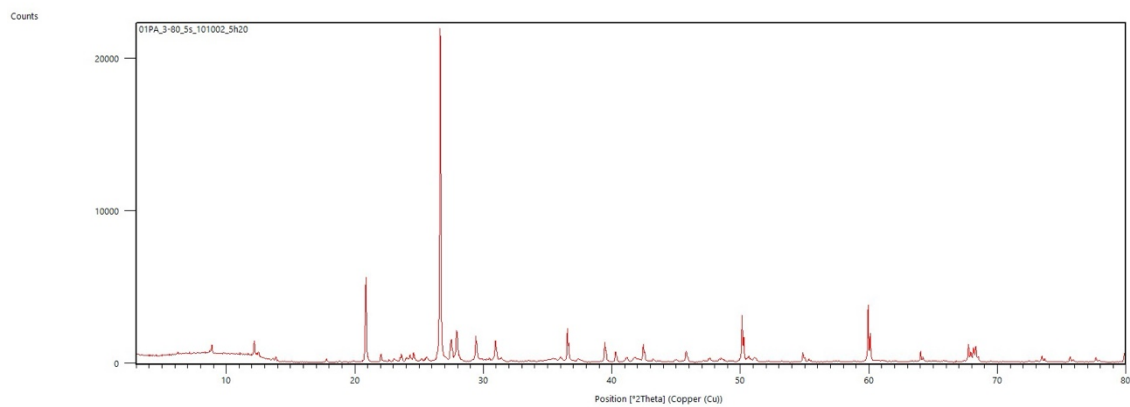
Appendix A - Figure 5: 32phi Parma



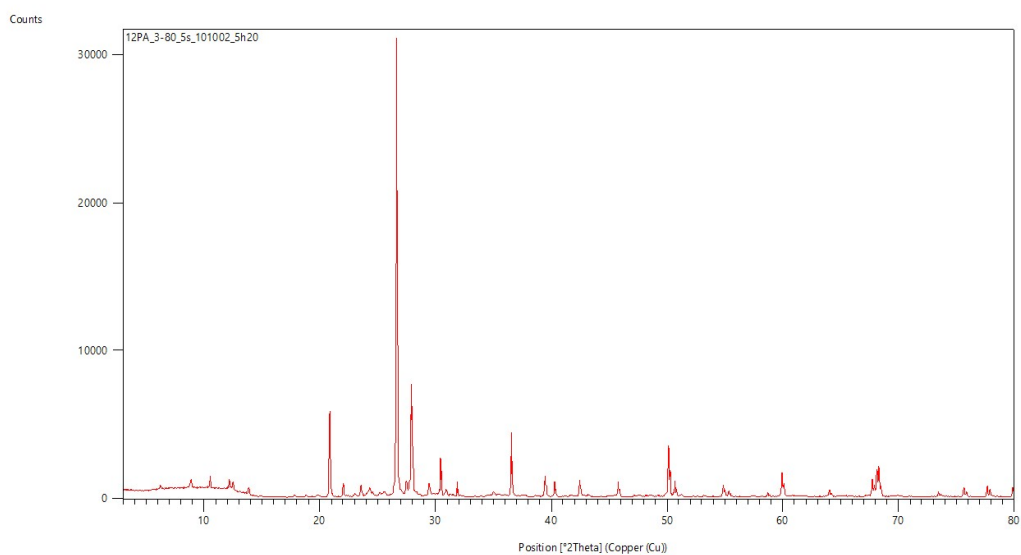
Appendix A - Figure 6: 21phi Parma



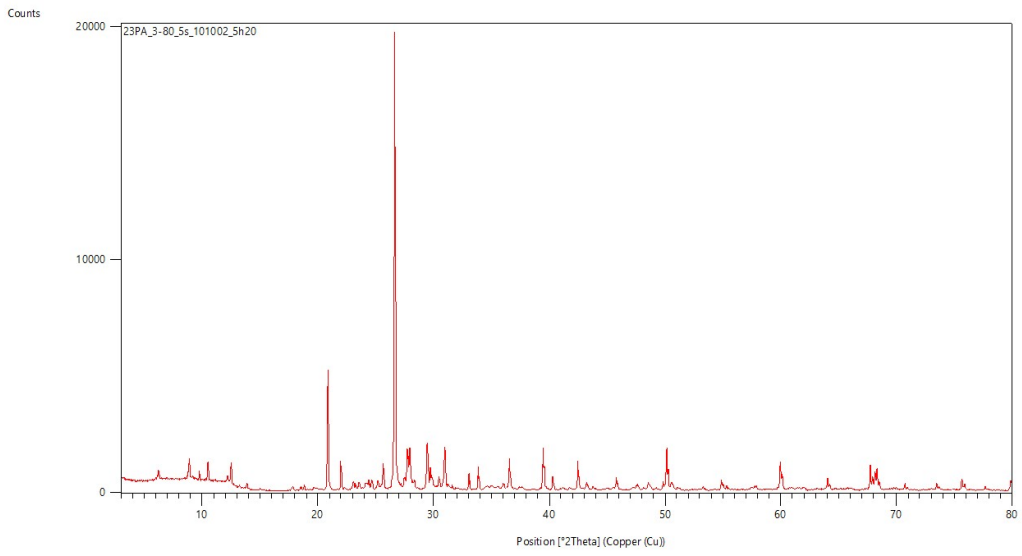
Appendix A - Figure 7: 10phi Parma



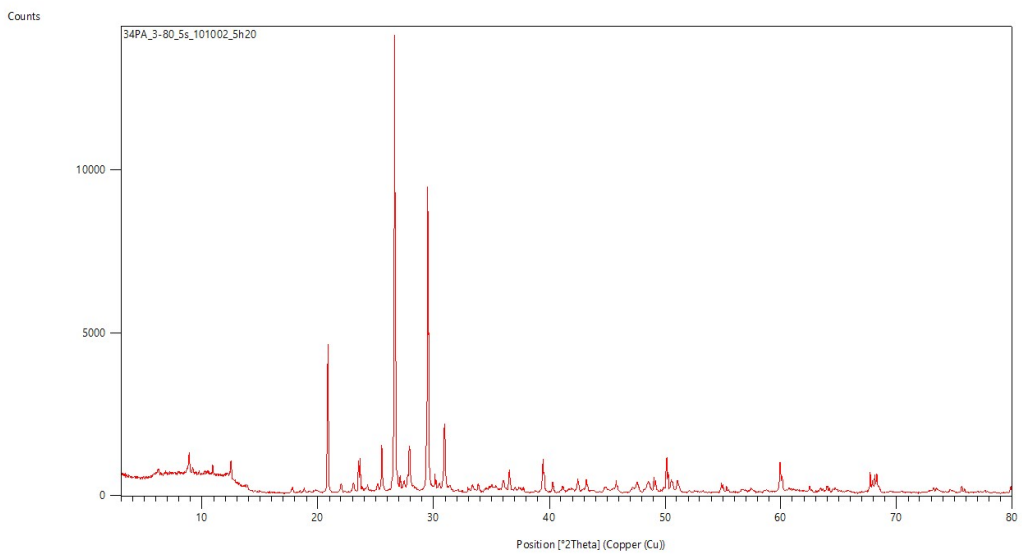
Appendix A - Figure 8: 01phi Parma



Appendix A - Figure 9: 12phi Parma



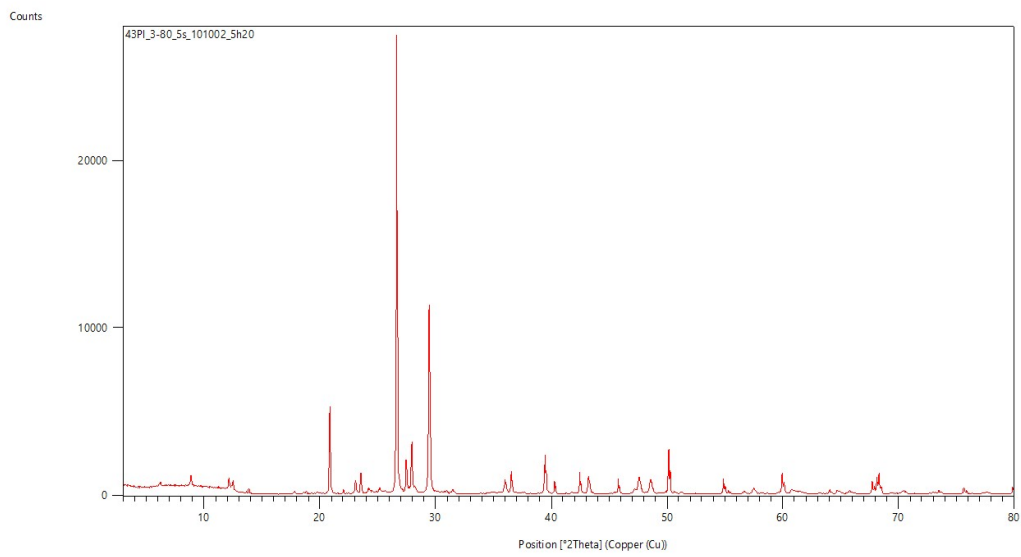
Appendix A - Figure 10: 23phi Parma



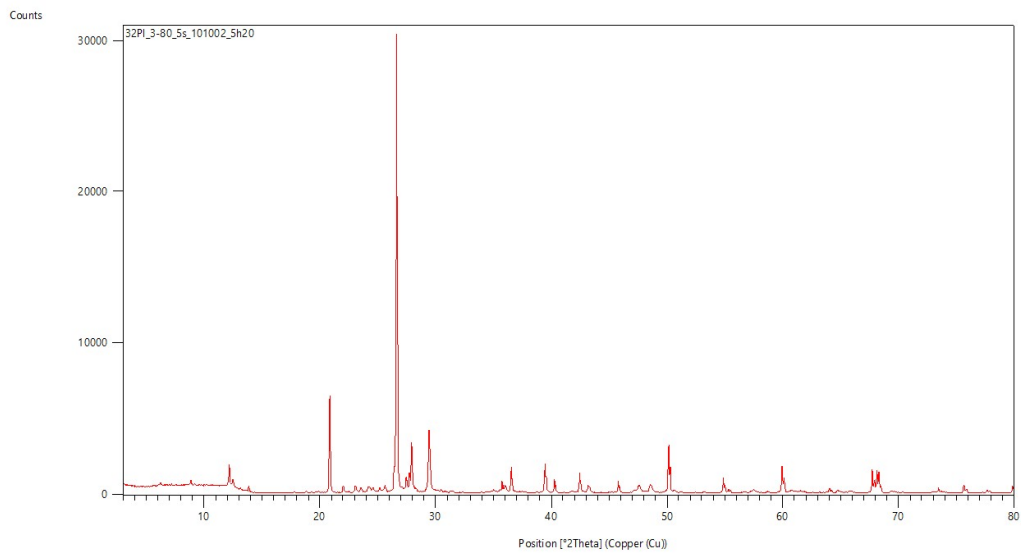
Appendix A - Figure 11: 34phi Parma

XRD Pattern

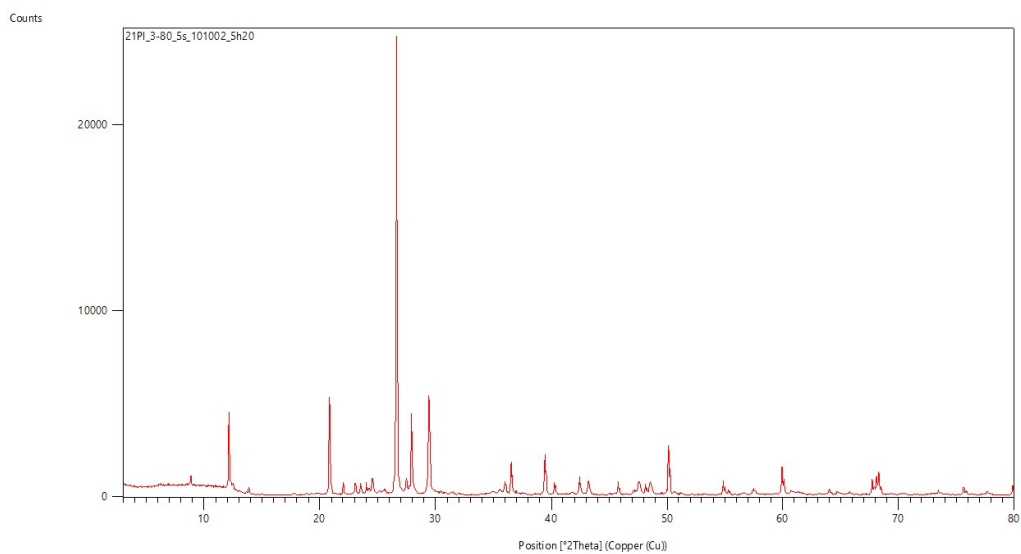
Piacenza samples (Italy)



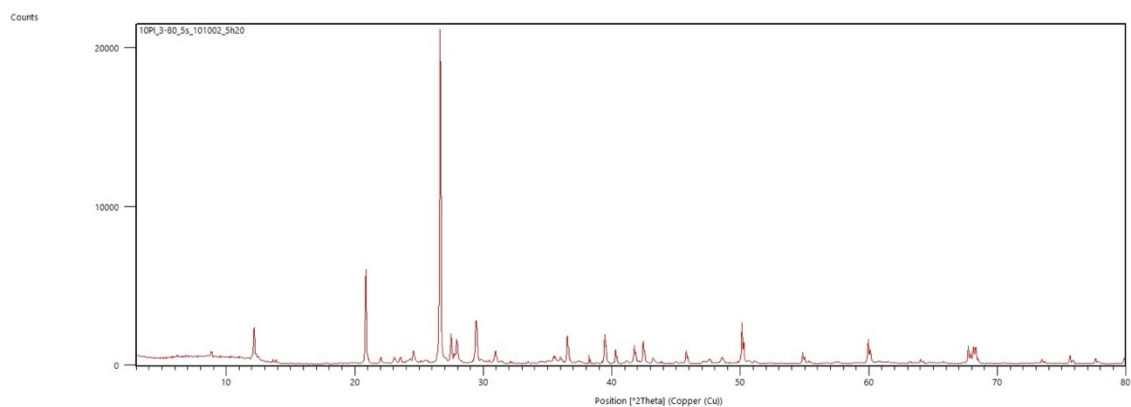
Appendix A - Figure 12: 43phi Piacenza



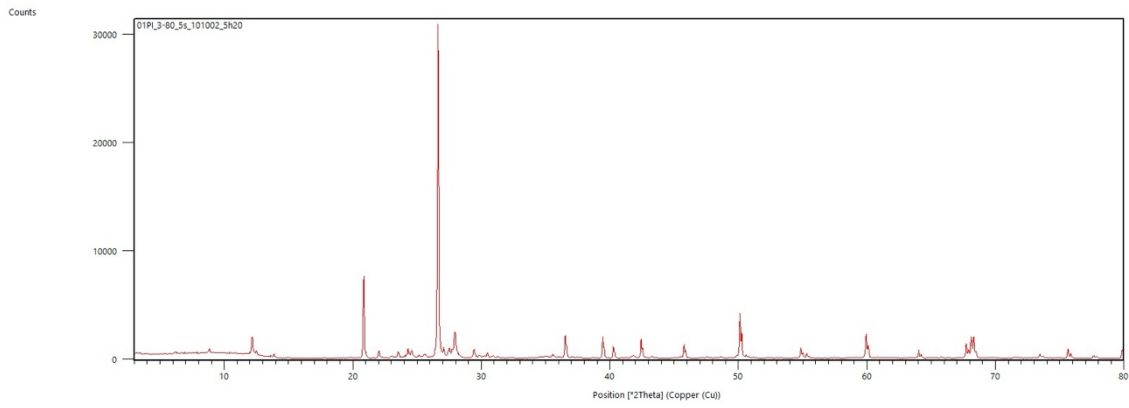
Appendix A - Figure 13: 32phi Piacenza



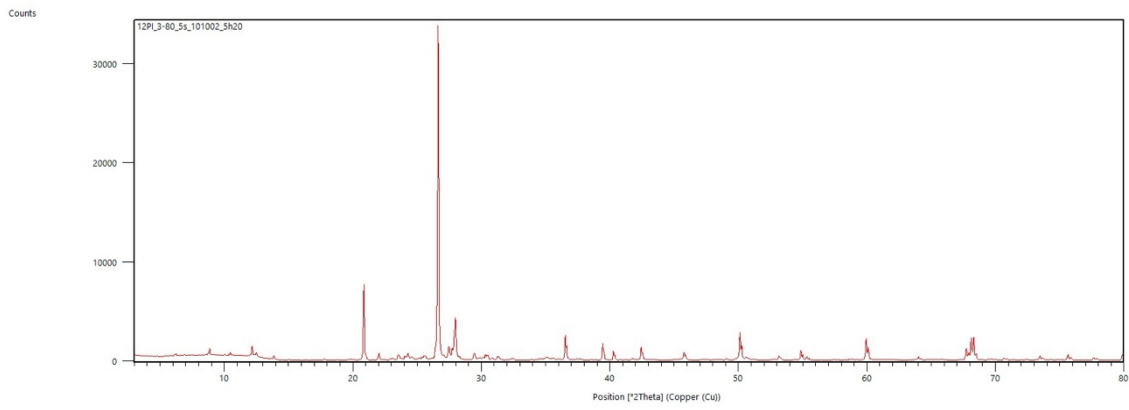
Appendix A - Figure 14: 21phi Piacenza



Appendix A - Figure 15: 10phi Piacenza



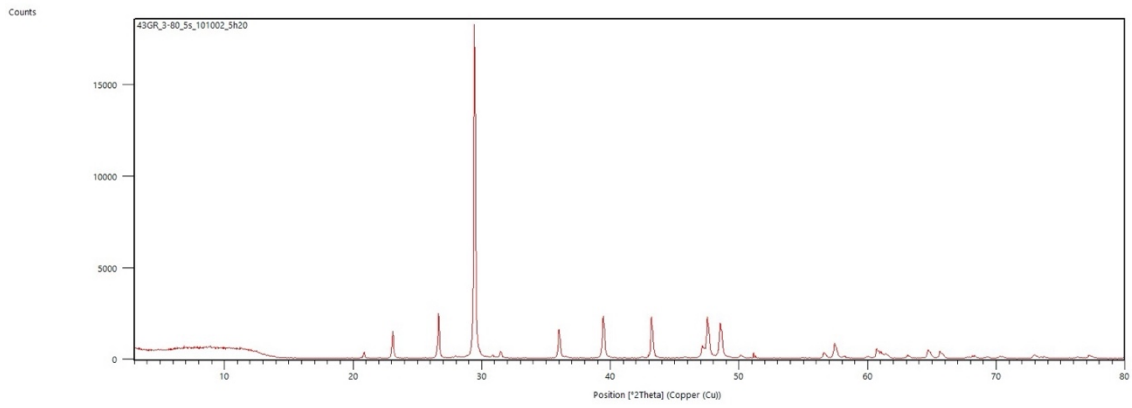
Appendix A - Figure 16: 01phi Parma



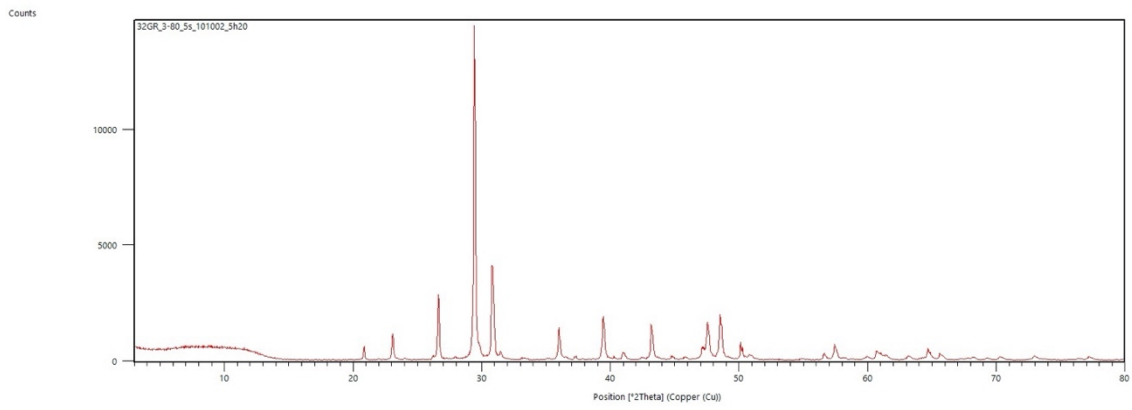
Appendix A - Figure 17: 12phi Piacenza

XRD Pattern

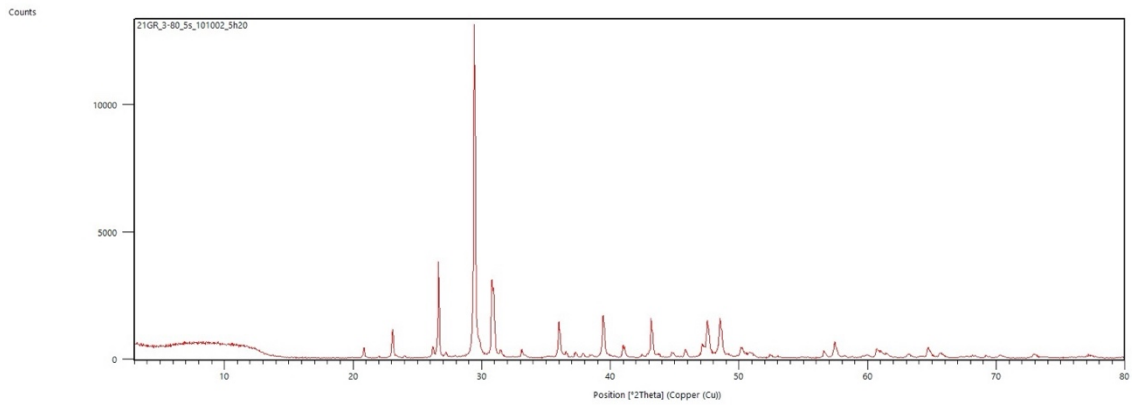
Preveza samples (Greece)



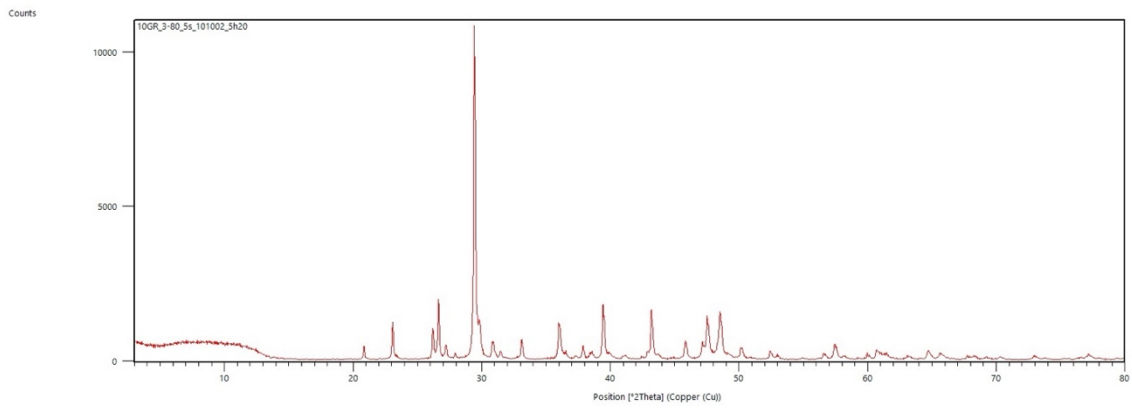
Appendix A - Figure 18: 43phi Preveza



Appendix A - Figure 19: 32phi Preveza



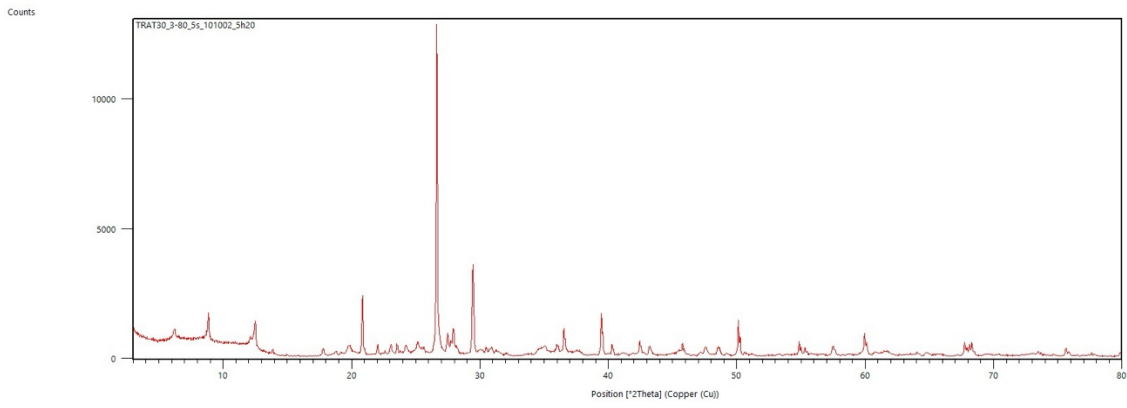
Appendix A - Figure 20: 21phi Preveza



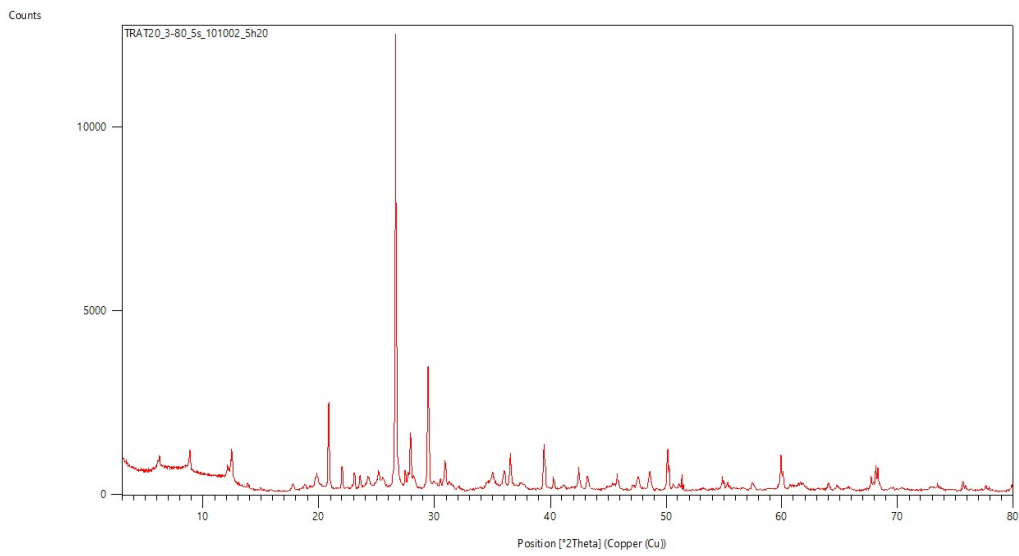
Appendix A - Figure 21: 10phi Preveza

XRD Pattern

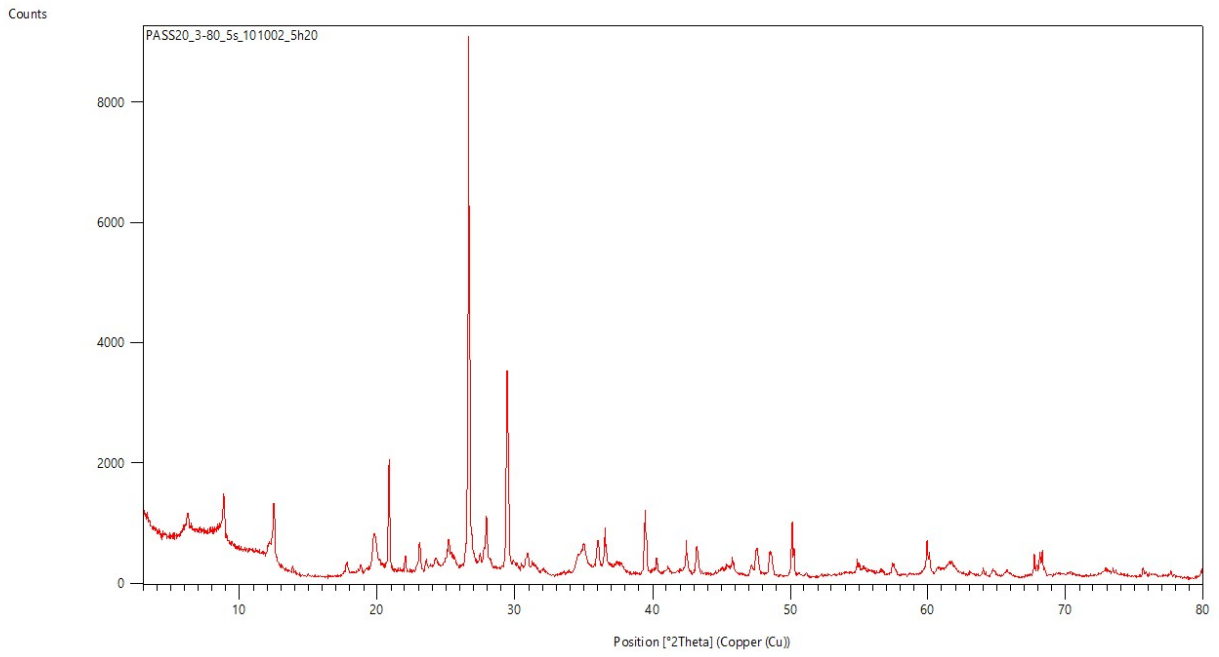
Reggio Emilia samples (Italy)



Appendix A - Figure 22: 45phi RE



Appendix A - Figure 23: 56phi RE



Appendix A - Figure 24: 610phi RE

Appendix B

Pattern fitting:



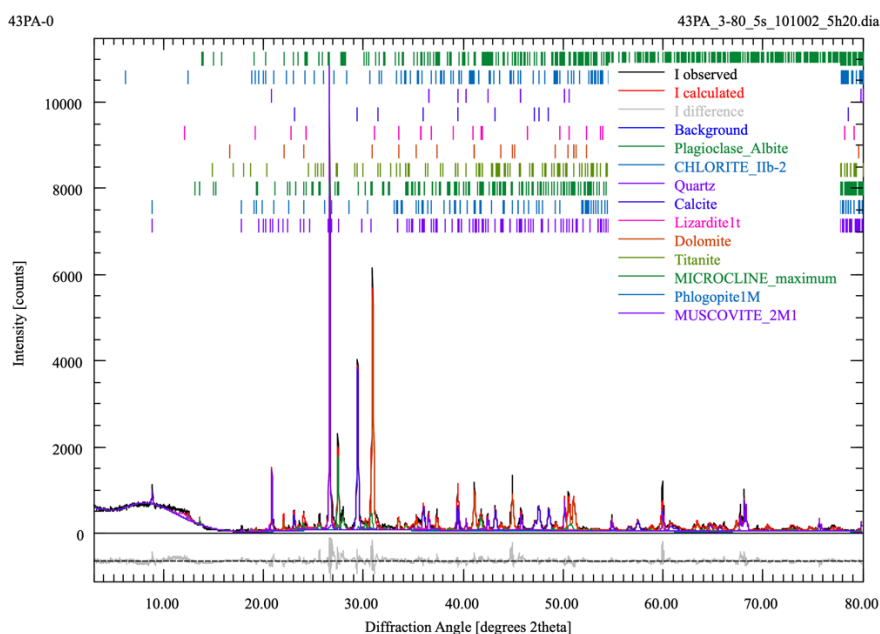
Sample Information

43PA-0				
File Name	43PA_3-80_5s_101002_5h20.dia			
Instrument configuration	Bruker_SOL-X_Unife.geq			
Wavelength	cu_berger86 (1.5406 Å)			
Directory	C:/Users/nicol/OneDrive/Desktop/RICERCHE E UNI/xrd marchetti/raffinamenti profex/PA/43PA			
Date of Refinement	mercoledì 29 marzo 2023			
Operator	nicol			
Statistics	$R_{wp} = 14.95$	$R_{exp} = 6.21$	$\chi^2 = 5.7956$	GoF = 2.4074

Global GOALS

Parameter	Value	ESD
Qalbite	0.038	0.002
Qchlorite2b	0.023	0.002
Qquartz	0.195	0.003
Qcalcite	0.211	0.003
Qlizardite1t	0.055	0.006
Qdolomite	0.322	0.004
Qtitanite	0.019	0.001
Qmicromax	0.091	0.003
QPhlogopite1M	0.000000	0.000000
Qmusc2m1	0.046	0.003

Diffraction Pattern



Appendix B - Figure 1: 43phi PA



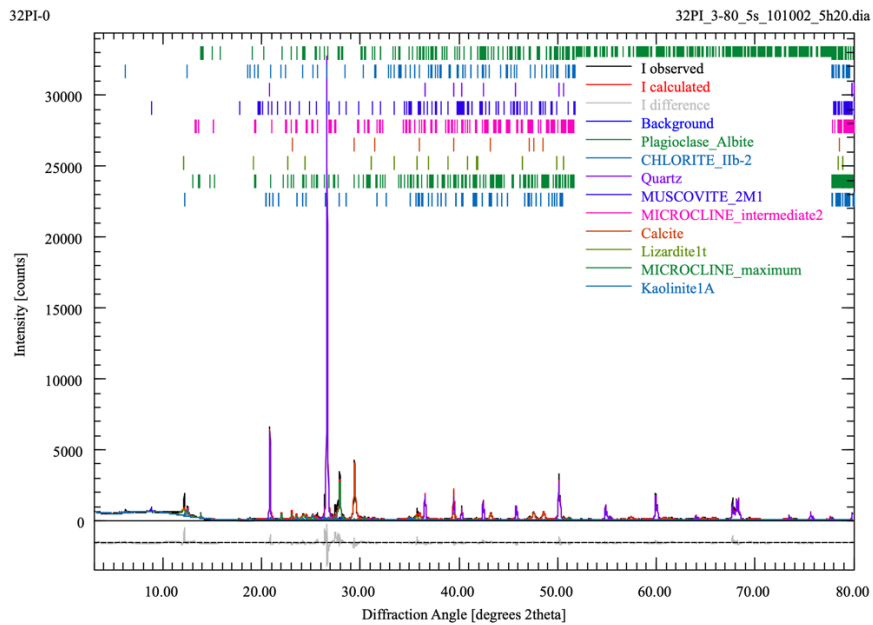
Sample Information

32PI-0				
File Name	32PI_3-80_5s_101002_5h20.dia			
Instrument configuration	Bruker_SOL-X_Unife.geq			
Wavelength	cu_berger86 (1.5406 Å)			
Directory	C:/Users/nicol/OneDrive/Desktop/RICERCHE E UNI/xrd marchetti/raffinamenti profex/PI/32PI			
Date of Refinement	venerdì 31 marzo 2023			
Operator	nicol			
Statistics	$R_{wp} = 12.52$	$R_{exp} = 5.83$	$\chi^2 = 4.6118$	GoF = 2.1475

Global GOALS

Parameter	Value	ESD
Qalbite	0.077	0.002
Qchlorite2b	0.105	0.008
Qquartz	0.553	0.006
Qmusc2m1	0.029	0.002
Qmicroint2	0.027	0.003
QCalcite	0.170	0.003
QLizardite1t	0.004	0.001
Qmicromax	0.021	0.003
QKaolinite1A	0.013	0.002

Diffraction Pattern



Appendix B - Figure 2: 32phi PI



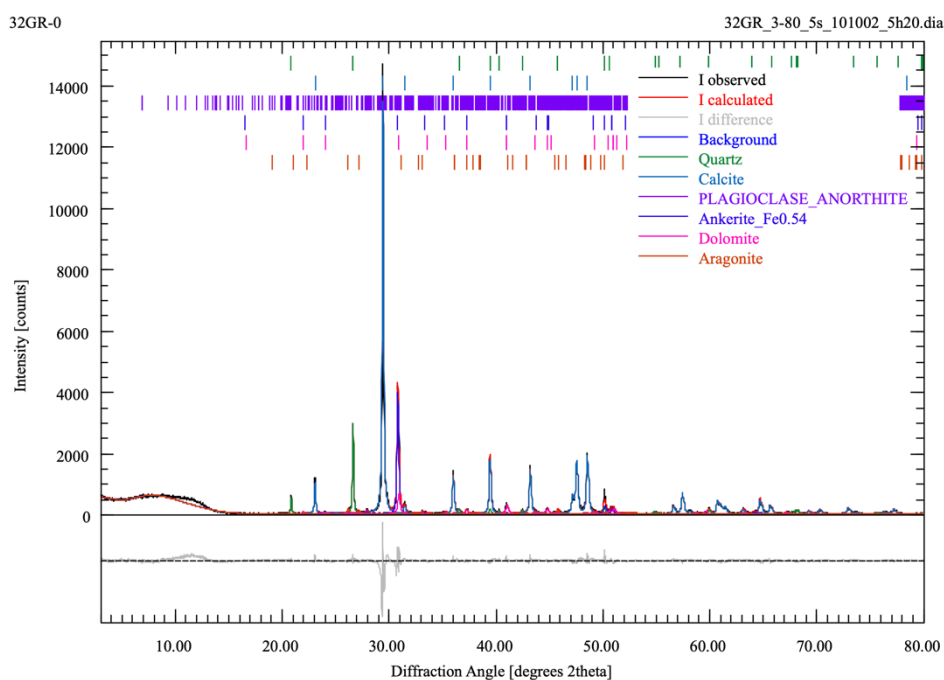
Sample Information

32GR-0				
File Name	32GR_3-80_5s_101002_5h20.dia			
Instrument configuration	Bruker_SOL-X_Unife.geq			
Wavelength	cu_berger86 (1.5406 Å)			
Directory	C:/Users/nicol/OneDrive/Desktop/RICERCHE E UNI/xrd marchetti/raffinamenti profex/GR/32GR			
Date of Refinement	martedì 4 aprile 2023			
Operator	nicol			
Statistics	$R_{wp} = 13.09$	$R_{exp} = 6.52$	$\chi^2 = 4.0307$	GoF = 2.0077

Global GOALS

Parameter	Value	ESD
Qquartz	0.096	0.002
QCalcite	0.708	0.004
Qanorthite	0.013	0.002
Qankerit05	0.067	0.004
Qdolomite	0.097	0.003
QAragonite	0.019	0.002

Diffraction Pattern



Appendix B - Figure 3: 32phi GR



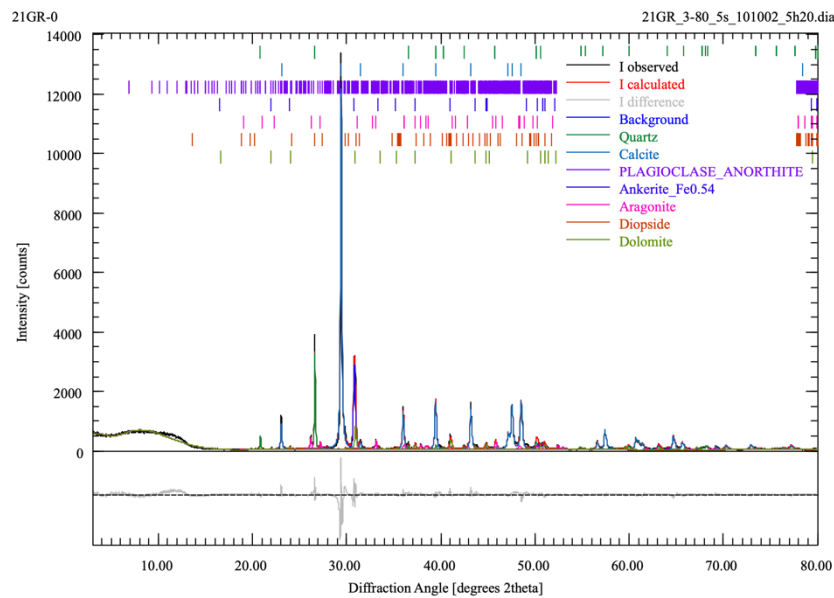
Sample Information

21GR-0				
File Name	21GR_3-80_5s_101002_5h20.dia			
Instrument configuration	Bruker_SOL-X_Unife.geq			
Wavelength	cu_berger86 (1.5406 Å)			
Directory	C:/Users/nicol/OneDrive/Desktop/RICERCH E UNI/xrd marchetti/raffinamenti profex/GR/21GR			
Date of Refinement	martedì 4 aprile 2023			
Operator	nicol			
Statistics	$R_{wp} = 13.20$	$R_{exp} = 6.49$	$\chi^2 = 4.1367$	GoF = 2.0339

Global GOALS

Parameter	Value	ESD
Qquartz	0.086	0.002
QCalcite	0.662	0.003
Qanorthite	0.0053	0.0009
Qankerit05	0.075	0.004
QAragonite	0.072	0.002
Qdiopside	0.006	0.002
QDolomite	0.095	0.005

Diffraction Pattern



Appendix B - Figure 4: 21phi GR



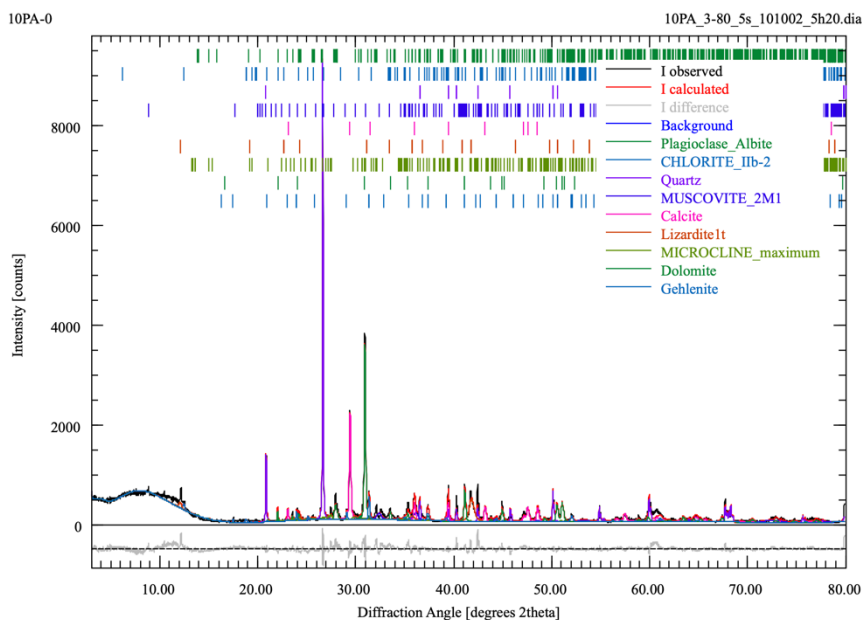
Sample Information

10PA-0				
File Name	10PA_3-80_5s_101002_5h20.dia			
Instrument configuration	Bruker_SOL-X_Unife.geq			
Wavelength	cu_berger86 (1.5406 Å)			
Directory	C:/Users/nicol/OneDrive/Desktop/RICERCH E UNI/xrd marchetti/raffinamenti profex/PA/10PA			
Date of Refinement	mercoledì 22 marzo 2023			
Operator	nicol			
Statistics	$R_{wp} = 16.26$	$R_{exp} = 6.62$	$\chi^2 = 6.0329$	GoF = 2.4562

Global GOALS

Parameter	Value	ESD
Qalbite	0.049	0.002
Qchlorite2b	0.030	0.002
Qquartz	0.209	0.005
Qmusc2m1	0.27	0.01
QCalcite	0.163	0.004
QLizardite1t	0.014	0.002
Qmicromax	0.025	0.004
Qdolomite	0.195	0.006
Qgehlenite	0.050	0.002

Diffraction Pattern



Appendix B - Figure 5: 10phi PA



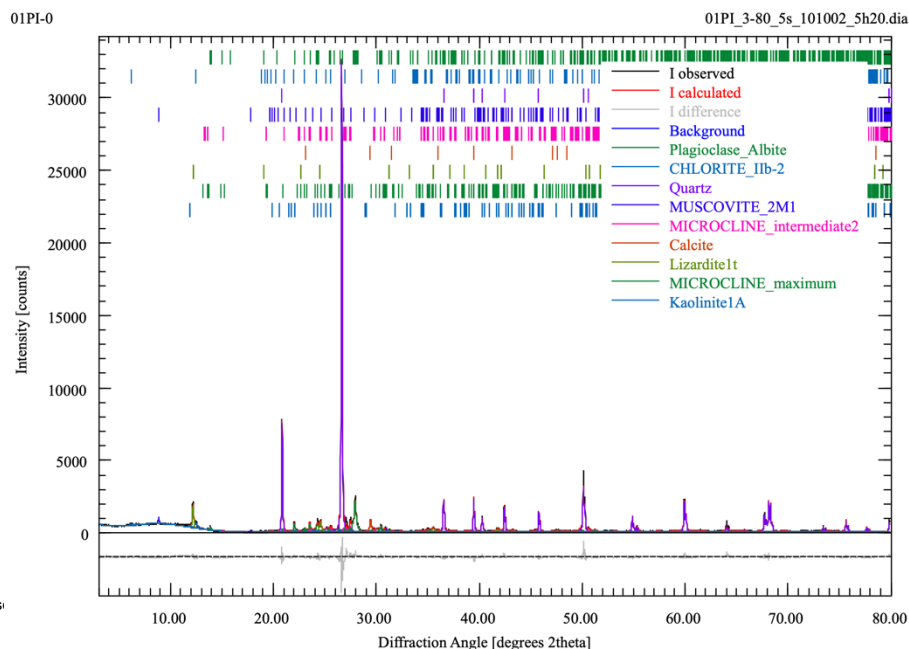
Sample Information

01PI-0				
File Name	01PI_3-80_5s_101002_5h20.dia			
Instrument configuration	Bruker_SOL-X_Unife.geq			
Wavelength	cu_berger86 (1.5406 Å)			
Directory	C:/Users/nicol/OneDrive/Desktop/RICERCHE E UNI/xrd marchetti/raffinamenti profex/PI/01PI			
Date of Refinement	venerdì 31 marzo 2023			
Operator	nicol			
Statistics	$R_{wp} = 11.17$	$R_{exp} = 5.76$	$\chi^2 = 3.7606$	GoF = 1.9392

Global GOALS

Parameter	Value	ESD
Qalbite	0.148	0.002
Qchlorite2b	0.065	0.004
Qquartz	0.638	0.004
Qmusc2m1	0.029	0.002
Qmicroint2	0.038	0.003
QCalcite	0.030	0.001
Qlizardite1t	0.005	0.001
Qmicromax	0.028	0.002
QKaolinite1A	0.021	0.002

Diffraction Pattern



Appendix B - Figure 6: 01phi PI